

# **A categorization and analysis of the ‘constant Lagrangian’ fits of the galaxy rotation curves of the complete SPARC database of 175 galaxies.**

E.P.J. de Haas<sup>1, a)</sup>

*Nijmegen, The Netherlands*

(Dated: May 18, 2018)

In this paper I categorize and analyze the ‘constant Lagrangian’ model fits I made of the complete SPARC database of 175 galaxies. Of the 175 galaxies, 45 allowed a single fit rotation curve, so about 26 percent. Another 9 galaxies could almost be plotted on a single fit. Then 30 galaxies could be fitted really nice on crossing dual curves. The reason for the appearance of this dual curve, in its two versions, could be given and related to the galactic constitution and dynamics. Another 25 galaxies could be fitted on parallel transition dual curves. This appearance could also be related to galactic dynamics and galactic mass distribution. Then there were the 19 multiple fit galaxies, complex extended galaxies, the complexities of which could be analyzed on the basis of the 4 types of dual fits. In total 128 of the 175 galaxies could be fitted and analyzed very well to reasonably well within the error margins. That is a 73 percent success rate. This amazing result rules out stochastic coincidence as an explanation of those fits. In my opinion, the success of the ‘constant Lagrangian’ approach indicates that the problem of the galaxy rotation curves can be solved on the basis of the principle of conservation of energy.

PACS numbers: 95.30.Sf, 95.35.+d

Keywords: Dark Matter, MOND, Schwarzschild, Galactic rotation curves

---

<sup>a)</sup>Electronic mail: [haas2u@gmail.com](mailto:haas2u@gmail.com)

# CONTENTS

<b>I. Introduction</b>	4
<b>II. The virial theorem in trouble on the galactic scale.</b>	4
<b>III. MOND</b>	6
<b>IV. Classical Lagrangian dynamics</b>	7
<b>V. A geodetic approach of gravitational orbits</b>	8
<b>VI. A completely syntonized model galaxy</b>	11
<b>VII. Galaxies with a single fit rotation curve</b>	16
<b>VIII. The non-single fit galaxies</b>	21
A. Almost single fit galaxies	21
B. Abrupt transition crossover dual fit galaxies	22
1. Upwards abrupt crossover transition	22
2. Right corner abrupt crossover transition	23
C. Non-crossover, parallel transition dual fit galaxies	25
1. Non-crossover upwards transition dual fit galaxies	25
2. Non-crossover downwards transition dual fit galaxies	26
D. Triple fit galaxies and beyond	27
E. The rest of the fitted galaxies (the almost no-fits)	28
<b>IX. Conclusion</b>	29
<b>References</b>	31
<b>A. The additional single fit selection.</b>	34
<b>B. The almost single fit selection.</b>	53
<b>C. Abrupt transition crossover dual fit galaxies</b>	57
1. Upwards abrupt crossover transition	57

2. Right corner abrupt crossover transition	68
<b>D. Non-crossover, parallel transition dual fit galaxies</b>	<b>73</b>
1. Non-crossover upwards transition dual fit galaxies	73
2. Non-crossover downwards transition dual fit galaxies	77
<b>E. Triple fit galaxies and beyond</b>	<b>85</b>
<b>F. Rest ‘dual’ fit galaxies</b>	<b>95</b>

## I. INTRODUCTION

In a recent preprint I introduced a ‘constant Lagrangian’ model for galactic dynamics (de Haas, 2018b). In a few sequential preprints I went from a qualitative attempt at fitting real rotational velocity curves using the proposed model, see (de Haas, 2018d,c), towards a quantitative analysis by including the error bars of the measured velocity, (de Haas, 2018e,a). In that last preprint I presented the analysis of the full set of 175 galaxies at the [SPARC database](#), as provided by (Lelli et al., 2016) in the file [Rotmod-LTG.zip](#). That rotation curve fitting result was presented in a non-categorized order, it just followed the order of the alphabetic-numerical list. I subsequently categorizes the fitting curves according to the fitting result. After having fit and categorized those 175 rotation curves, I realized that it allowed me to go from a rather weak deductive to a more robust inductive justification of the ‘constant Lagrangian’ model.

In this paper, after giving a somewhat renewed presentation of the ‘constant Lagrangian’ model, I present a further analysis of those 175 fits. I split the 175 galaxies in several categories. The most significant group is the single fit category, galaxies that directly fit to the model. Then there are four dual fit categories. Two with a crossover transition dual fit and two with a parallel transition dual fit. The galaxies with three or more fits can be analyzed using the four dual categories. At the end there is the rest category of galaxies that defy simple fits and subsequent categorization, 27 percent in total. That means that 73 percent of the galaxies allowed for perfect to moderate analysis and explanation on the basis of the constant Lagrangian model.

## II. THE VIRIAL THEOREM IN TROUBLE ON THE GALACTIC SCALE.

In 1932 the Dutch astronomer Oort observed that the stars in the galactic vicinity of the Sun are moving peculiarly fast, almost 8 times as fast as could be inferred from the calculated Newtonian acceleration. Oort assumed that dark matter would be the cause of this apparent difference, with ‘dark’ referring to ordinary matter not seen by us due to various reasons (Oort, 1932).

In 1933 Dark Matter was mentioned as “dunkle Materie” in a paper by Zwicky. Fritz Zwicky was studying the Coma Cluster of galaxies and found that his calculations for orbital

acceleration and stellar mass within it was off by a large factor. He concluded that there should be a much greater density of dark matter within the cluster than there was luminous matter. Zwicky concluded that this constituted an unsolved problem (Zwicky, 1933). In 1937 Zwicky regarded his study on the Coma Cluster a test of Newton's law of gravity on the largest cosmological scale possible, by applying the virial theorem on a cluster of galaxies. He also mentioned in his 1937 paper the possibility to test the virial theorem by applying it to the rotational velocities of the individual stars in the separate galaxies. But he concluded that this was technologically out of reach (Zwicky, 1937).

The breakthrough research of Rubin and Ford around 1970-1975 established beyond doubt the outer rotational velocity curves of individual galaxies, which turned out to be flat (Rubin et al., 1978). This was in conflict with velocity curves that resulted from the application of the virial theorem to the luminous mass of these galaxies. Rubin and Ford cited colleagues who suggested the existence of a large galactic halo of dark matter. In a 1980 paper presenting further research they concluded that the form of the rotation curves implied that significant non-luminous mass should be located at large distances beyond the optical galaxy. The total mass of a galaxy should, for large distances, increase at least as fast as the distance from the center (Rubin et al., 1980).

The third major evidence for Dark Matter was the gravitational lensing effect of clusters of galaxies. The mass of stars and hot gas in clusters who collectively act as a gravitational lens is too small to bend the light from the background galaxies as much as they actually do. A large density of dark matter in the center of these cluster is needed to explain the strength of the observed lensing effect (Koopmans et al., 2009).

In the course of decades it has become more and more clear that ordinary matter can't be the cause of those observed phenomena. That realization caused the term 'dark matter' to evolve into 'Dark Matter', with the capital letters indicating its elusive character. Today it has been predominantly, but not unanimously, been accepted that non-baryonic particles must exist in the calculated densities. A range of different astrophysical observations point in this direction (The ATLAS Collaboration, 2018).

### III. MOND

One of the few non-particle approaches to the problem of Dark Matter is MOND or MODified Newtonian Dynamics. MOND started in 1983 with two seminal paper of Milgrom. I quote from his papers:

*All determinations of dynamical mass within galaxies and galaxy systems make use of a virial relation of the form  $V^2 = MGr^{-1}$  where  $V$  is some typical velocity of particles in the system,  $r$  is of the order of the size of the system,  $M$  is the mass to be determined, and  $G$  is the gravitational constant. [...] It must have occurred to many that there may, in fact, not be much hidden mass in the universe and that the dynamical masses determined on the basis of the above virial relation are gross overestimates of the true gravitational masses. (Milgrom, 1983b)*

Instead of assuming the Newtonian theory to remain valid in and around galaxies, Milgrom modified Newton's second law by making inertia a function of acceleration (Milgrom, 1983b). Milgrom replaced  $m_g \mathbf{a} = \mathbf{F}$  by

$$m_g \mu \left( \frac{a}{a_0} \right) \mathbf{a} = \mathbf{F}. \quad (1)$$

With such a deviation only reveals itself for accelerations with  $a \approx a_0$ . When  $a \gg a_0$ ,  $\mu \approx 1$  and the Newtonian regime reasserts itself. This resulted in the capacity to reasonably fit most of the galaxy rotation curves and it led to an intrinsic connection to the baryonic Tully-Fisher relation as  $V_\infty^4 = a_0 GM$  (Milgrom, 1983a).

The original Tully-Fisher relation is a relation between the luminosity of a spiral galaxy and its, maximum, rotation velocity (Tully and Fisher, 1977). The physical basis of the Tully-Fisher relation is the relation between a galaxy's total baryonic mass and the velocity at the flat end of the rotation curve, the final velocity. According to McGaugh both stellar and gas mass of galaxies have to be taken into account in the relation that is referred to as the Baryonic Tully-Fisher (BTF) relation. In 2005 McGaugh determined the baryonic version of the LT relation as  $M_d = 50v_f^4$ , see (McGaugh, 2005). In this form,  $M_d$  is expressed in solar mass  $M_\odot = 1,99 \cdot 10^{30} \text{ kg}$  units and the final velocity of the galactic rotation velocity curve  $v_f$  is expressed in  $\text{km/s}$ . If we express the galactic mass in  $\text{kg}$  and the velocity in  $\text{m/s}$  we get the total baryonic mass, final velocity relations in SI unit values as  $M_b = 1,0 \cdot 10^{20} v_f^4$ .

In 1983, Milgrom interpreted the BTF relation as indicative of his proposed deviation from Newtonian gravity, justifying his modification of Newtonian dynamics or MOND (Milgrom, 1983b). Using McGaug’s 2005 values in SI units, Milgrom’s presentation of the BTF relation can be cast in the form  $v_f^4 = 1,0 \cdot 10^{-20} M_b = G a_0 M_b$ , resulting in an acceleration  $a_0 = 1,5 \cdot 10^{-10} \text{ m/s}^2$  in McGaug’s values. Milgrom hypothesized that this relation should hold exactly, thus interpreting it as an inductively found law of nature, instead of looking at it as just a coincidental empirical relation (Milgrom, 1983a). The resulting acceleration can be written as  $5 \cdot a_0 \approx c H_0$ , with the velocity of light  $c$  and the Hubble constant  $H_0$ . According to Milgrom, the deeper significance of this relation between this special galactic acceleration and the Hubble acceleration should be revealed by future cosmological insights (Milgrom, 1983b).

#### IV. CLASSICAL LAGRANGIAN DYNAMICS

One problem with Milgrom’s MOND is that is rather asynchronous to modify gravity by returning to Newton instead of starting by Einstein’s General Relativity. But in the standard cosmological General Relativity approach towards the galaxy rotation curve problem the existence of Dark Matter is presumed from the beginning. The ‘constant Lagrangian’ model can be seen as an intermediate approach: it uses General Relativity concepts without presuming from the start the existence of Dark Matter. This intermediate approach starts with Lagrangian mechanics.

The classical Lagrangian equation of motion reads

$$\frac{d}{dt} \left( \frac{\partial L}{\partial \dot{q}} \right) - \frac{\partial L}{\partial q} = 0. \quad (2)$$

In classical gravitational dynamics I assume circular orbits with  $\dot{q} = v$  and  $q = r$ . The Lagrangian itself is then given by  $L = K - V$ , with  $V$  the Newtonian potential gravitational energy and  $K$  the kinetic energy. One then gets

$$\frac{d}{dt} \left( \frac{\partial L}{\partial \dot{q}} \right) = \frac{dp}{dt} = F. \quad (3)$$

The other part gives

$$\frac{\partial L}{\partial q} = -\frac{dV}{dr}, \quad (4)$$

so one gets Newton's equation of motion in a central field of gravity

$$F_g = -\frac{dV}{dr}. \quad (5)$$

Further analysis of the context results in the identification of the Hamiltonian of the system,  $H = K + V$ , as being a constant of the orbital motion and the virial theorem as describing a relation between  $K$  and  $V$  in one single orbit but also between different orbits, given by the relation  $2K + V = 0$ .

The classical virial theorem has two main interpretations. The first one states that in circular orbits, the centripetal force equals the gravitational force. This leads directly to the scalar relation  $2K = -V$ . The second one states that masses in collapsing orbits have to dissipate half of the potential energy in order to resume a stable lower orbit because in such a collapse from a higher stable orbit to a lower stable orbit, only half of the freed potential energy can be transformed into kinetic energy.

On the galactic scale it is assumed that velocities are so low and gravitational fields are so weak, that Newtonian mechanics suffices and not much of relativity is needed. The problem with the rotational velocities of stars in galaxies and galaxies in cluster of galaxies is thus supposed to be a Newtonian physics issue that can be dealt with in the dynamics described above. The Dark Matter solution to the too fast rotational galactic velocities has two faces. On the one hand one tries to describe the density distribution of Dark Matter, needed in order to match the measurements with classical dynamics, specifically the virial theorem. On the other hand one tries to identify the Dark Matter constituents, usually seen as an out-of-the-box extension of the known Standard Model of particle physics.

## V. A GEODETIC APPROACH OF GRAVITATIONAL ORBITS

If one tries to apply the concepts of General Relativity to the galaxy rotation problem and related virial theorem, the notion of geodesic motion in General Relativity must be central. The analysis can start in a semi-relativistic approach, by applying the classical Lagrangian equation of motion to geodesic orbits. The most important aspect of geodesic motion in GR is that it requires no force to move on a geodesic. This has important implications for the Lagrangian equation of motion, because  $F_g = 0$  on a geodesic. One gets

$$\frac{d}{dt} \left( \frac{\partial L}{\partial \dot{q}} \right) = F_g = 0 \quad (6)$$

and as a consequence also

$$\frac{\partial L}{\partial q} = -\frac{dL}{dr} = 0. \quad (7)$$

As a result, one has

$$L = K - V = \text{constant} \quad (8)$$

on geodetic orbits. This is the theoretical core of the ‘constant Lagrangian’ model for galactic dynamics. The difference between the classical approach and this paper, the additional choice so to speak, is that I assume a model in which the Lagrangian is a constant for all orbits of my model galaxy. That’s all. The effort in presenting this model is in the sequence of introduction, interpretation, application and implication of this core ad-hoc assumption of a constant  $L$  for all  $r$  on a model galaxy rotation curve.

The first observation is that I do not use the Einstein Equations but the classical Lagrangian equations on geodetic orbits. This choice has to be interpreted as an in between approximation. Newton’s law of gravity follows from the Einstein Equations in case of a weak field: Newton is the weak field limit of Einstein. But in Einstein’s time, the planetary solar system was already assumed to be a weak gravitational field. More essentially is the observation that an axiomatic theory of gravity that states that in geodetic motion, no forces of gravity exist, only local curvature of space-time, will not magically transform into an axiomatic theory that is all about forces of gravity in orbits around central masses, just by slowly weakening the potential. The use of the classical Lagrangian has to be interpreted as an in between these two conflicting axiomatic systems. I use Lagrange as the diplomatic mediator between Newton and Einstein. The theoretical core of my model is breathtakingly simple. The rest, it’s introduction, interpretation, application and implication, isn’t simple at all.

Although the requirement that the force of gravity is zero on a geodetic orbit seems obvious from a GR perspective, there is still dispute among the experts relative to this issue. Relative to the geodetic precession or the de Sitter precession, discussion and opposite views remain as to the role of the force of gravity in this effect. Some claim that the force of gravity cannot have any role in it, others describe the geodetic precession as the sum of a time-like Thomas precession due to the force of gravity and a Schouten precession due to the curvature of three dimensional space (de Haas, 2014). Given this paradoxical situation relative to a well established effect of General Relativity, it is by no means settled how

to handle the requirement of having no gravitational force on a geodesic motion relative to satellites orbiting the earth. So let alone relative to galactic orbits, where General Relativity too had to presume the existence of Dark Matter.

The Lagrangian of the system as being the constant of the geodesic motion is used on a daily basis by many of us because it is applied by GNSS systems for the relativistic correction of atomic clocks in satellites. Let's elaborate this a bit further. In General Relativity, the proper time-rate  $d\tau$  is defined through the metric distance  $ds$  as  $ds \equiv cd\tau$ . The square metric distance is defined through

$$ds^2 \equiv g_{\mu\nu} dx^\mu dx^\nu. \quad (9)$$

Given coordinate world time-rate  $dt$ , which is the time-rate of a standard clock at a position where  $d\tau = dt$  (in GR-Schwarzschild this implies a clock at rest at infinity), we get the general

$$\frac{ds^2}{dt^2} = \frac{c^2 d\tau^2}{dt^2} = g_{\mu\nu} \frac{dx^\mu}{dt} \frac{dx^\nu}{dt} = g_{\mu\nu} V^\mu V^\nu, \quad (10)$$

with the geodesic four-vector velocity  $V^\mu$ . In this equation,  $d\tau$  stands for the local proper clock-rate of a clock in a geodesic orbit in a field of gravity and  $dt$  is the universal clock-rate. Because of this interpretation of  $dt$ , the velocity  $V^\mu$  is the velocity as seen from a position where  $d\tau = dt$ . See for example (Singer, 1956), (Weinberg, 1972, p. 79), (Misner et al., 1973, p. 1054-1055), (Straumann, 1984, p. 97), (Ohanian and Ruffini, 2013, p. 119).

In case of the Schwarzschild metric in polar coordinates, we have (Ruggiero et al., 2008)

$$ds^2 = \left(1 + \frac{2\Phi}{c^2}\right) c^2 dt^2 - \left(1 + \frac{2\Phi}{c^2}\right)^{-1} dr^2 - r^2 d\theta^2 - r^2 \sin^2 \theta d\phi^2. \quad (11)$$

In case of a clock on a circular geodesic on the equator of a central non-rotating mass  $M$  we have  $\frac{dr}{dt} = 0$ ,  $\frac{d\theta}{dt} = 0$ ,  $\sin\theta = 1$  and  $\frac{d\phi}{dt} = \omega$ . We thus get

$$\frac{ds^2}{dt^2} = \frac{c^2 d\tau^2}{dt^2} = \left(1 + \frac{2\Phi}{c^2}\right) c^2 - r^2 \omega^2 \quad (12)$$

and

$$\frac{d\tau^2}{dt^2} = 1 + \frac{2\Phi}{c^2} - \frac{r^2 \omega^2}{c^2}. \quad (13)$$

With  $v_{orbit} = r\omega$  we have

$$\frac{d\tau^2}{dt^2} = 1 + \frac{2\Phi}{c^2} - \frac{v_{orbit}^2}{c^2}. \quad (14)$$

So finally we get the GR result

$$\frac{d\tau}{dt} = \sqrt{1 + \frac{2\Phi}{c^2} - \frac{v_{orbit}^2}{c^2}} \quad (15)$$

with  $d\tau$  as the clock-rate of a standard clock A in a geodetic orbit and  $dt$  as the ‘universal’ clock-rate G of a standard clock at rest in infinity, the only condition for which  $d\tau = dt$ . The result of Eqn. (15) is the basic relativistic correction used in GNSS clock frequencies, with the first usually presented as the gravity effect or gravitational potential correction and the second as the velocity effect or the correction due to Special Relativity (Ashby, 2002; Hećimović, 2013; Delva and Lodewyck, 2013).

Given the classical definitions of  $K = \frac{1}{2}mv_{orbit}^2$  and  $V = m\Phi$ , we get

$$\frac{d\tau}{dt} = \sqrt{1 - \frac{2L}{U_0}}. \quad (16)$$

All the satellites of a GNSS system are being installed on a similar orbit and thus syntonized relative to one another because they share the same high and velocity and have constant  $L$  and  $\frac{dr}{dt}$  on those orbits. But different GNSS systems, as for example GPS compared to GALILEO, are functioning on different orbits with different velocities and those systems aren’t syntonized relative to one another. This non-syntonization between satellites on orbits with different heights and virial theorem connected velocities is an all to real technical obstacle for the effort towards realizing an integration of the different GNSS systems into one single global network. For satellites for which the virial theorem holds, the Lagrangian isn’t a constant on orbits with different radii. Thus, with  $\frac{\Delta L}{\Delta r} \neq 0$ , atomic clocks moving in free fall on those different radii aren’t syntonized. For GNSS systems, the virial theorem constitutes a problem, not an asset.

## VI. A COMPLETELY SYNTONIZED MODEL GALAXY

Fundamental in the approach of this paper is to analyze gravity using relative frequency shifts, and thus  $\frac{dr}{dt}$ , as one of the basic experimental inputs. Such a method is looming in today’s geodesy. In modern gravitational geodesy scientists are investigating the relativistic frequency shift as a new observable type for gravity field recovery (Mayrhofer and Pail, 2012). Driven by this development, modern geodesy is about to go through a change from the Newtonian paradigm to Einstein’s theory of general relativity (Kopeikin et al., 2017). A new

generation of atomic clock is the game changer for this new domain of chronometric geodesy, and requires additional new techniques to be developed in the field of frequency transfer and comparison (Delva and Lodewyck, 2013). The paradigm shift towards gravitational divergence recovery is based on the principle of frequency comparison between two clocks on different space-time locations in order to measure the frequency shift between them (Delva and Lodewyck, 2013). The knowledge of the Earth’s gravitational field has often been used to predict frequency shifts between distant clocks. In relativistic geodesy, the problem is reversed and the measurement of frequency shifts between distant clocks now provides knowledge of the gravitational field (Delva and Lodewyck, 2013). This reversal is also present in my postulate of the ‘constant Lagrangian’ model. A constant Lagrangian implies a zero divergence in the syntonization of atomic oscillators and thus an absence of gravitational stress. A divergence in the Lagrangian implies a divergence in the time dilation factor  $\frac{d\tau}{dt}$  and thus a non-zero gravitational stress.

The key to this paper’s approach is to extend this clock frequency perspective towards gravity from geodesy to galaxies. When I connected

$$\frac{d\tau^2}{dt^2} = 1 + \frac{2\Phi}{c^2} - \frac{v_{orbit}^2}{c^2} = 1 - \frac{2L}{U_0} \quad (17)$$

to the problem of the galactic rotation curve, I realized that the flat rotation curve implies atomic clock syntonization in those areas. In those outer regions, the gravitational potential can be assumed to be approximately zero and the velocity constant. This made me curious as to the clock-rate status in the inner regions. It is intriguing to realize that you can jump from orbit to orbit and still encounter a constant clock-rate on all the orbiting satellites you encounter on an imaginary voyage through the outer regions of galaxies. Those flat rotation rate zones are the GNSS engineer’s dream come true. This implies that precisely in those regions where the classical virial theorem seems in trouble,  $L \simeq constant$ , not just in one single orbit *but also between different orbits*.

It should be clear that for those geodetic orbits, the classical virial theorem, which in its most essential form states that  $F_{gravity} = F_{centripetal}$ , becomes meaningless because on circular geodetics this reduces to the empty expression  $0 = 0$ . From the energy perspective, by what mechanism should masses in orbital collapse in the outer region of galaxies dissipate half of the potential energy? It seems that the virial theorem isn’t fundamental, but in need of a dissipative mechanism in order to assert itself. Without such a (thermo)dynamics,

conservation of mechanical energy in orbital collapse could well be the rule, with as a consequence that all the potential gravitational energy is transformed into orbital kinetic energy: a ‘constant Lagrangian’ model.

In order to study the relativistic clock-rate behavior in the inner regions of galaxies, I had to construct a model galaxy. My model galaxy is build of a model bulge with mass  $M$  and radius  $R$  and a Schwarzschild metric emptiness around it. The model bulge has constant density  $\rho_0 = \frac{M}{V} = \frac{3M}{4\pi R^3}$  and its composing stars rotate on geodetics in a quasi-solid way. So all those stars in the bulge have equal angular velocity on their geodetic orbits, with  $v = \omega r$ . On the boundary between the quasi solid spherical bulge and the emptiness outside of it, the orbital velocities are behaving smoothly. So the last star in the bulge and the first star in the Schwarzschild region have equal velocities and potentials. I also assume that the Newtonian potential itself is unchanged and unchallenged, remains classical in the whole galaxy and its surroundings. Such a model galaxy doesn’t, for the moment, have a SMBH in the center of its bulge and it only has some very lonely stars in the space outside the bulge.

The gravitational potential in such a case is well known, see Fig.(1). If this sphere would be in a quasi solid condition for which the classical virial theorem would hold, so  $2K = -V$ , then on the boundary  $r = R$  we would have  $K = \frac{GM}{2R}$  and  $L = K - V = \frac{3GM}{2R}$ . At the center of the rotating sphere,  $K = 0$  and we also have  $L = \frac{3GM}{2R}$ .

From  $r = 0$  to  $r = R$ , the potential  $\Phi$  increased as  $r^2$ . The kinetic energy does the same because  $v^2 = \omega^2 r^2$ . One can conclude that they increase identical and that  $L = K - V$  is a constant inside the quasi-solid sphere. We can write for the region from  $r = 0$  to  $r = R$

$$\frac{L}{m} = \frac{v_{orbit}^2}{2} + \frac{GM}{r} = \frac{3GM}{2R} = constant. \quad (18)$$

As a result, inside such a model bulge,  $L$  is a constant of the motion, not only in one orbit but also between orbits. All the clocks inside such a model bulge would be syntonized.

Thus, in the model galaxy that I am about to construct, we have  $L = constant$  inside the model bulge and we have  $L = constant$  in the outer regions where the rotational velocity curve flattens and the Newtonian potential turns negligibly small. So let’s be bold and declare  $L = K - V = constant$  in the entire galaxy, without changing the Newtonian potential. What would be the implications?

Point	Relation	Expression
Outside the <b>bulge</b>	$r > R$	$-\frac{GM}{r}$
On the Surface	$r = R$	$-\frac{GM}{R}$
Inside the <b>bulge</b>	$r < R$	$-GM \left[ \frac{3R^2 - r^2}{2R^3} \right]$
At the centre	$r = 0$	$-\frac{3}{2} \left( \frac{GM}{R} \right)$

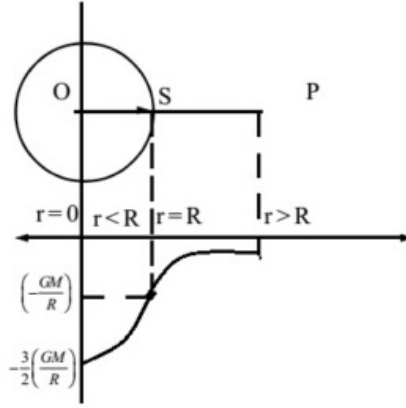


FIG. 1. The potential inside and out of a model bulge

We would get  $K = L + V$  and  $L = V(r = 0)$  so for the region  $0 \leq r \leq R$  we get

$$v_{orbit}^2 = \frac{GM}{R} \cdot \frac{r}{R} \quad (19)$$

and outside the model bulge, where  $R \leq r \leq \infty$ , we have

$$v_{orbit}^2 = \frac{3GM}{R} - \frac{GM}{r}. \quad (20)$$

In Fig.(2) I sketched the result, with  $-V = +K_{escape}$ .

From the perspective of a free fall Einstein elevator observer, the free fall on a radial geodesic from infinity towards the center of the bulge, the other free fall tangential geodesics seem to abide the law of conservation of energy, because the escape kinetic energy plus the orbital kinetic energy is a constant on my model galaxy with galactic constant  $L$ . An Einstein elevator system with test mass  $m$  that would be put in an orbital collapse situation, magically descending from orbit to orbit in a process in thermodynamic equilibrium, would have constant total kinetic energy, from the radial free fall perspective. This can be expressed as  $L = K_{orbit} - V = K_{orbit} + K_{escape} = K_{final}$ .

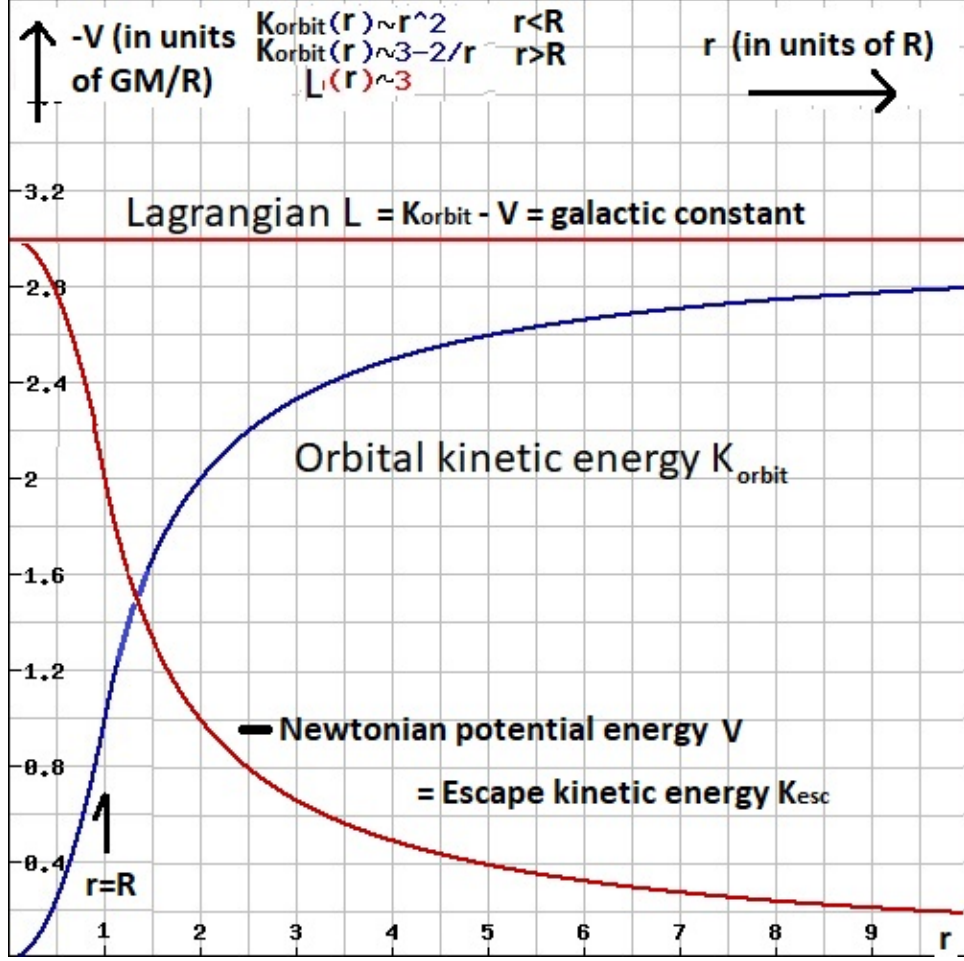


FIG. 2. The square of the orbital velocity profile in the model galaxy with  $L = \text{constant}$ .

Such a model galaxy would also be a GNSS engineer's dream come true because the whole model galaxy is in one single synchronized mode, a clock-rate halo or time-bubble, defined by

$$\frac{d\tau}{dt} = \sqrt{1 - \frac{2L}{U_0}}. \quad (21)$$

Given the Baryonic Tully-Fisher relation in Milgrom's version  $v_{final}^4 = Ga_0M$  with  $2\pi a_0 \approx cH_0$ , with  $a_0$  as Milgrom's galactic minimum acceleration and  $H_0$  as the Hubble constant, we get as a galactic clock-rate fix

$$\frac{d\tau}{dt} = \sqrt{1 - \frac{2L}{U_0}} = \sqrt{1 - \frac{v_{final}^2}{c^2}} = \sqrt{1 - \sqrt{\frac{v_{final}^4}{c^4}}} = \quad (22)$$

$$\sqrt{1 - \sqrt{\frac{Ga_0M}{c^4}}} = \sqrt{1 - \sqrt{\frac{GH_0M}{2\pi c^3}}} = \sqrt{1 - \sqrt{\frac{M}{2\pi M_U}}}, \quad (23)$$

in which I used  $L = 3GM/R = K_{final} = \frac{1}{2}mv_{final}^2$  and  $M_U = \frac{c^3}{GH_0}$ . This last constant can

be referred to as an apparent mass of the Universe, a purely theoretical number constant, see (Mercier, 2015).

In a model Universe, this would imply that my model galaxy would realize a proper time bubble with clock-rate  $d\tau$  relative to the universal clock-rate  $dt$  in proportion to the masses of galaxy  $M$  and Universe  $M_U$ . In the theoretical environment of my model galaxy, the Baryonic Tully-Fisher relationship implies that the galactic clock-rate is fixed through the mass of my model galaxy and that this fix is a cosmological one. So what is a universal acceleration minimum  $a_0$  in MOND can be interpreted as a universally correlated (through  $M_U$ ) but still local (through  $M$ ) clock-rate syntonization in my model galaxy geodetic environment.

## VII. GALAXIES WITH A SINGLE FIT ROTATION CURVE

Having determined the model galactic velocity rotation curve based on the Lagrangian as a galactic constant of orbital motion, the question is to what extent real galaxies can be modeled in this way. In my Lagrangian approach I analyze the plot of  $v_{orb}^2$ , in  $(km/s)^2$  against  $r$ , in  $kpc$ . This in contrast to the usual rotation curves where  $v_{orb}$ , in  $(km/s)$  is plotted against  $r$ , in  $kpc$ . In the Lagrangian approach, the energies, not the velocities, are primary.

In each plot the experimental values are given in red stars with vertical error bars and the theoretical model values in black circles. The fitting plot is with one single fit for  $M$ , in units of  $10^{10} Msolar$ , and  $R$ , in units of  $kpc$ . The most important cut in the model is the change from the model bulge to the model empty space around it, which happens at the chosen value for  $R$ . In the model bulge,  $V_{orb}^2 \propto r^2$ , outside the model bulge  $V_{orb}^2 \propto -r^{-1}$ .

In this section, I use the [SPARC database](#), including the error margins, as provided by (Lelli et al., 2016). This database functions as a random set relative to my model. I analyzed, fitted, the full set of 175 galaxies at the [SPARC database](#), as provided by (Lelli et al., 2016) in the file [Rotmod-LTG.zip](#). The SPARC website also provides a luminosity and mass distribution analysis of those 175 galaxies. It is to the reader to compare the results of my fits with the surface brightness and mass distribution graphs of SPARC (from the [MassModels-LTG.zip](#) file). As an inductive first indication, the fits of this database shows that, at least, huge stretches of almost all galaxy rotation curves can be plotted on a constant Lagrangian curve.

Of the 175 galaxies, 45 allowed a single fit rotation curve, so about 25 percent. This amazing result rules out stochastic coincidence as an explanation of those fits. Relative to the model, those 175 galaxies were a random set. The restrictions for a single fit (of almost all measurements) within the error margins are such that a 25 percent positive match rules out the possibility of a coincidental correlation without any causation. In the next pages I present 8 selected galaxies of the 45 with a nice single fit. In Appendix A, the rest of the 45 single fits are given. All the plots are produced in Microsoft Excel, which for a High School teacher is the standard available software.

In the results of Fig.(3) and Fig.(4) the three aspects of the model curve are clearly present. First the model bulge patten is clearly present in the ascending parabolic part of the curve. This part of the model is classical because it combines the virial theorem and the constant Lagrangian. In my model, there shouldn't be need for any Dark Matter inside the bulge, because the behavior is purely classical. Then secondly the shift from bulge to free space as a continuous increasing function instead of the abrupt decrease as would be expected classically with the virial theorem. Thirdly is the type of ascending towards a maximum. This part of the graph is more clearly visible in Fig.(6).

Whatever the theory applied, these single fit galaxies have realized a constant Lagrangian structure and are syntonized over the entire rotation curve. This result is a consequence of the fit and independent of my justifications of the model. One should realize the consequence: if we were able to launch GNSS satellites in orbit over the entire rotation curve of those galaxies, all the atomic clocks in those standard satellites would be syntonized. If we could express the degree of syntonization on a galactic velocity curve in terms of entropy, these single fit galaxies reach the lowest possible time-like entropy because they achieve the highest order as to the syntonization of their clocks.

If we examen the surface brightness and mass distribution graphs of these galaxies, (from the [MassModels-LTG.zip](#) file), there is one dominant denominator: with a few exceptions, the measured rotation curves of these galaxies do not extend beyond the measured range of the surface brightness. The four exceptions are D564-8, UGC04483, UGC00634 and UGC08490.

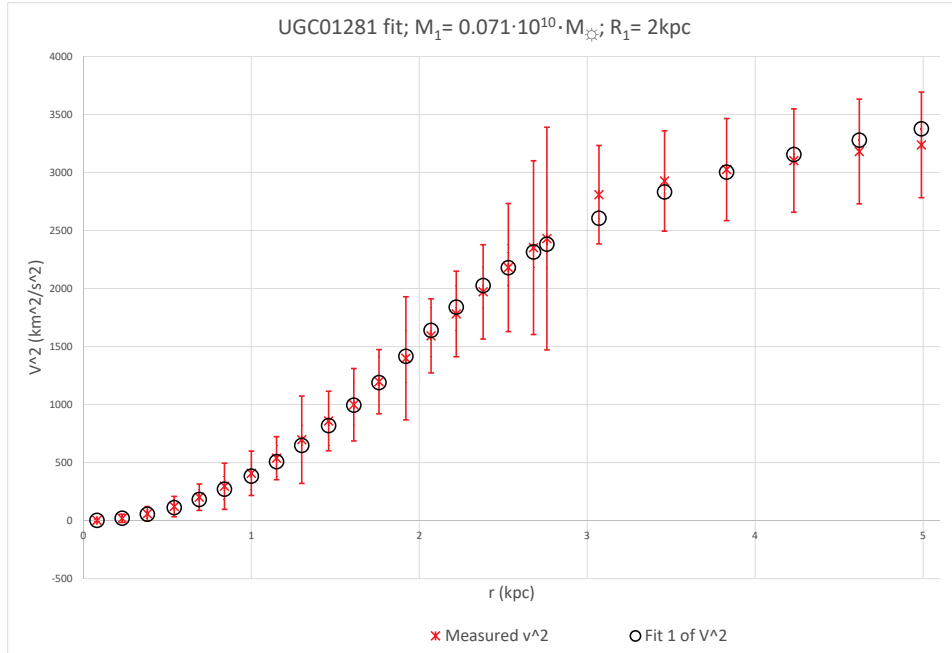


FIG. 3. UGC01281

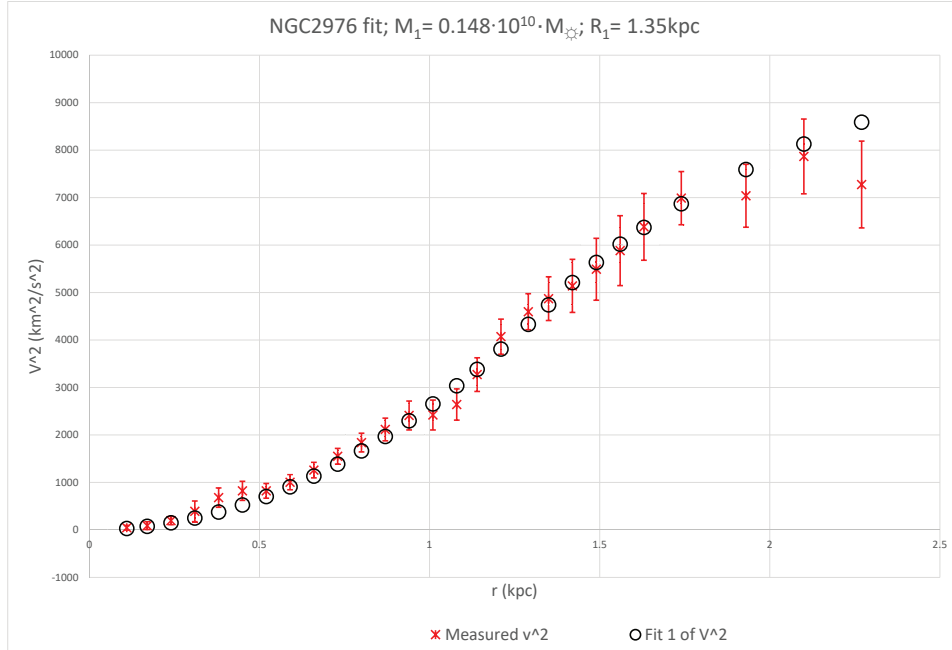


FIG. 4. NGC2976

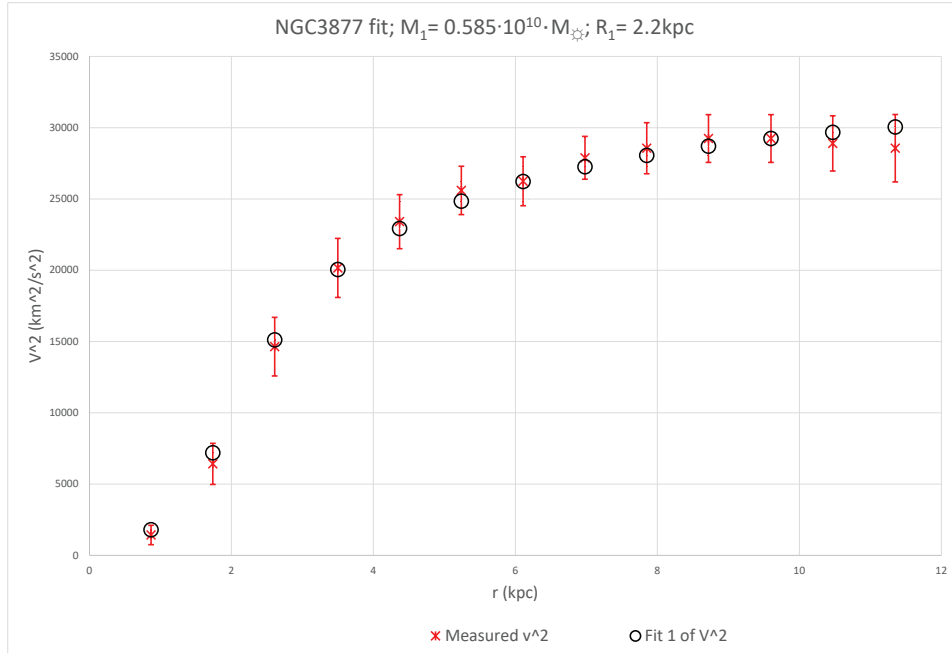


FIG. 5. NGC3877

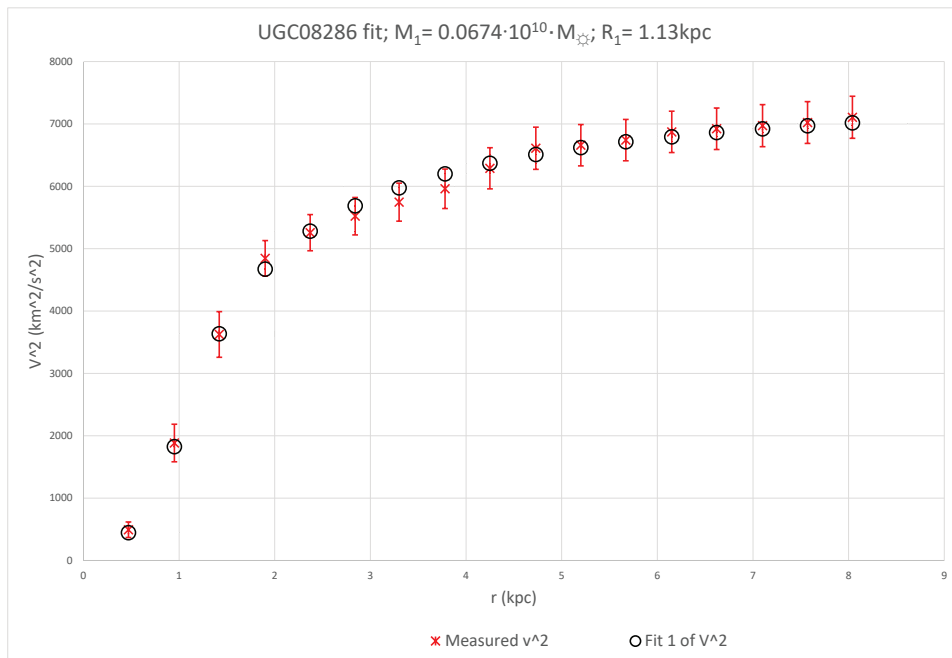


FIG. 6. UGC08286

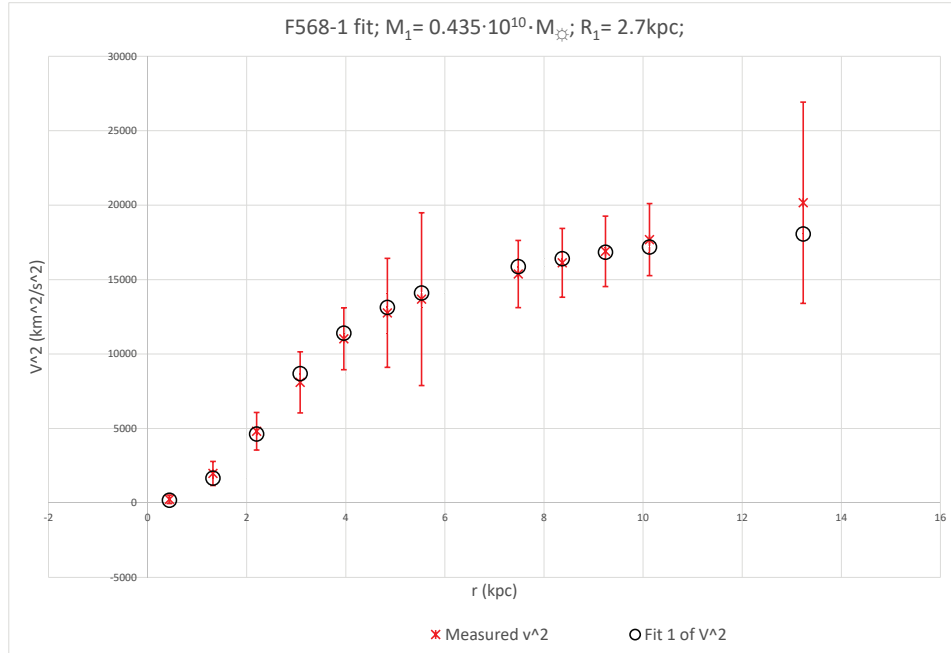


FIG. 7. F568-1

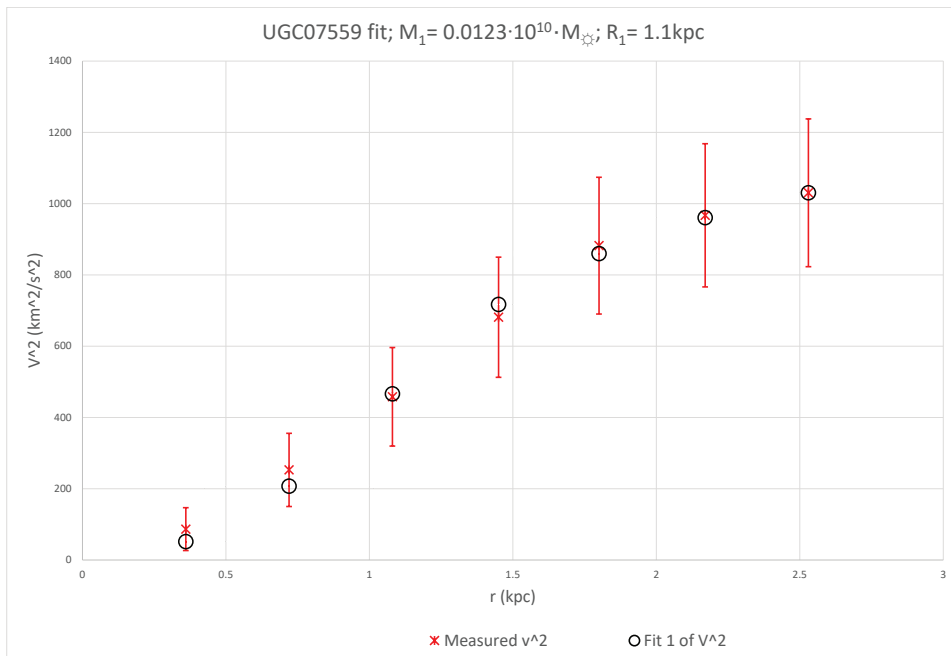


FIG. 8. UGC07559

## VIII. THE NON-SINGLE FIT GALAXIES

Some 116 galaxies of the 175 could be categorized as ‘dual fit’, with the remark that it also contains a rest category with a rotation ‘curve’ that was actually too chaotic or too partial to be fit at all.

### A. Almost single fit galaxies

The first category in the dual fit galaxies are the ones that almost allowed a single fit, but where the error margins prevented such a decision. These ‘deviations’ from a single model curve presented itself at the bulge part closest to the center of those galaxies. See Fig.(9) as an example. There are 9 galaxies in this category. See Appendix B.

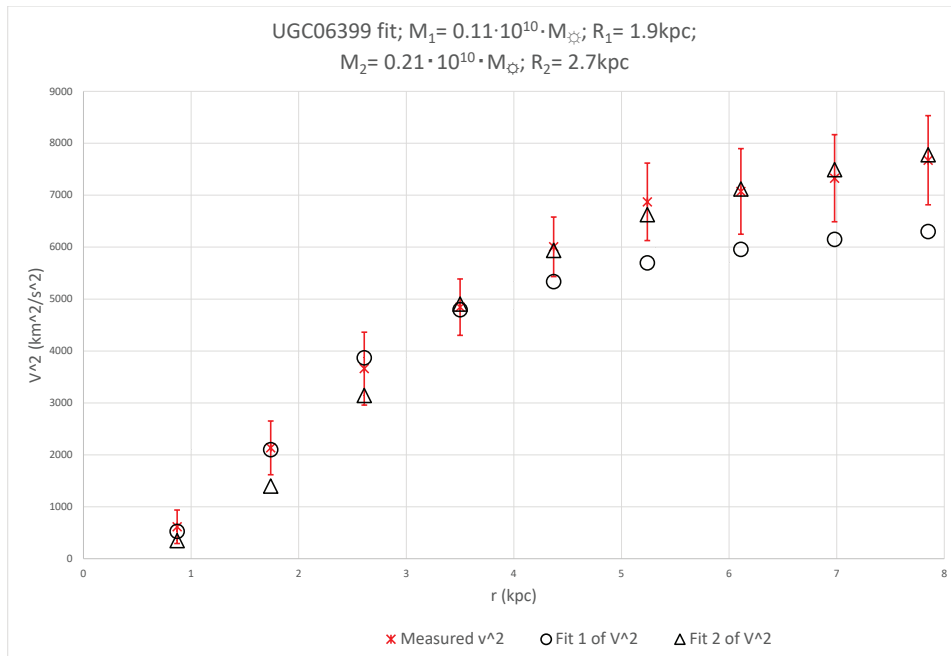


FIG. 9. UGC06399

## B. Abrupt transition crossover dual fit galaxies

The second category in the dual fit galaxies are the ones that have an abrupt transition from one fit to the next. These abrupt transitions from a one model curve to the next model curve mostly occurred. See Fig.(67) as an example. There are 30 galaxies in this category. See Appendix C. In many cases, the abrupt transition is corresponding to a change in the composition of the galaxy. For example the ending of a strong surface brightness and the beginning of the gas filled outer regions of the galaxy.

The abrupt transitions mainly come in two types, upwards crossing over from below as in Fig.(67) or right corner crossing over from the left as in Fig.(84). In the first case, the galaxy's time-rate shifts to a higher frequency, in the second case it shifts to a lower frequency. The frequency shifts are rather abrupt, effectively splitting these galaxies in two clock-rate time zones.

### 1. *Upwards abrupt crossover transition*

In the example of Fig.(67), the crossover coincides with the new  $R_2$ , so it marks a new end of the 'bulge' or the beginning of a new 'outside the bulge' area. The additional 21 galaxy fits of this type can be found in Appendix C1. In the velocity rotation curves of SPARC, the two zones are also recognizable, but not so distinctly as in the squared velocity rotation curves, especially when fitted along constant Lagrangian curves.

In the upwards abrupt transition, the rotation curve starts of as a model galaxy including a model bulge ending at  $R_1$  with inside mass  $M_1$  and an outside area where the virial theorem seems invalidated and the constant Lagrangian alone determines the shape of the curve. In the model galaxy there is by definition only an insignificant amount of mass outside the model bulge but in real galaxies the mass outside the bulge can be much more than the mass of the bulge, as is the case for galaxies with a substantial disk.

My interpretation of the upwards abrupt transition is that the galaxies dynamics allowed for or favored a sudden reset because the upward crossover happens to coincide with the new bulge radius  $R_2$ , identifying a higher mass  $M_2$  inside  $R_2$ . The additional mass outside  $R_1$  first follows the model curve beyond  $R_1$  but eventually the accumulated new mass disrupts the initial 'constant Lagrangian' curve. But the model curve doesn't break down, it just

resets itself by defining a new bulge with radius  $R_2$  which includes all the additional mass into  $M_2$ . It is as if a thin spherical shell with a high density mass  $M_2 - M_1$  appears at  $R_2$ , causing this abrupt transition.

Because the two constant Lagrangian curves co-define atomic clock-rate frequencies, this crossover partitions the galaxy in two distinct clock-rate zones or ‘time bubbles’. It results in a lower atomic frequency or clock-rate time-bubble inside a higher atomic frequency or clock-rate time-bubble.

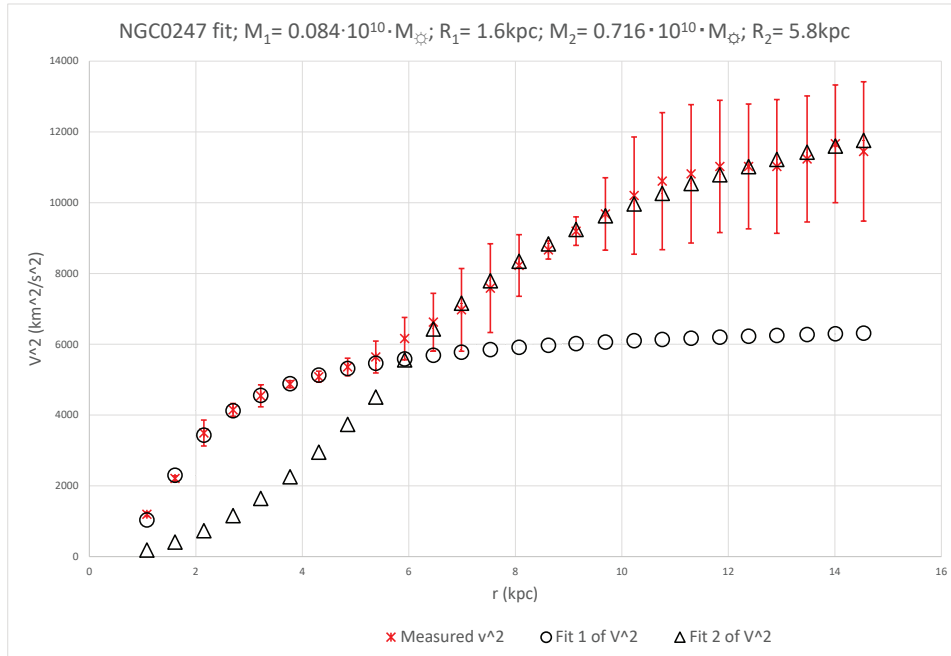


FIG. 10. NGC0247

## 2. Right corner abrupt crossover transition

In the example of Fig.(11), the crossover coincides with the end of the model bulge at  $R_1$ . The additional 7 galaxy fits of this type can be found in Appendix C 2. What seems to happen here is that the initial model bulge is being build up but then proves incapable of installing its own ‘constant Lagrangian’ curve or clock-rate time bubble outside its bulge defined by  $M_1$  and  $R_1$ . That failure doesn’t result in a recourse to the virial rotation curve but to a ‘constant Lagrangian’ curve defined by a smaller model bulge inside the original model bulge. This smaller model bulge has radius  $R_2$  and mass  $M_2$ . So in this case the bulge is abruptly reset to a smaller version.

This type of crossover also partitions the galaxy in two distinct clock-rate zones or ‘time bubbles’. Now it results in a higher atomic frequency or clock-rate time-bubble inside a lower atomic frequency or clock-rate time-bubble.

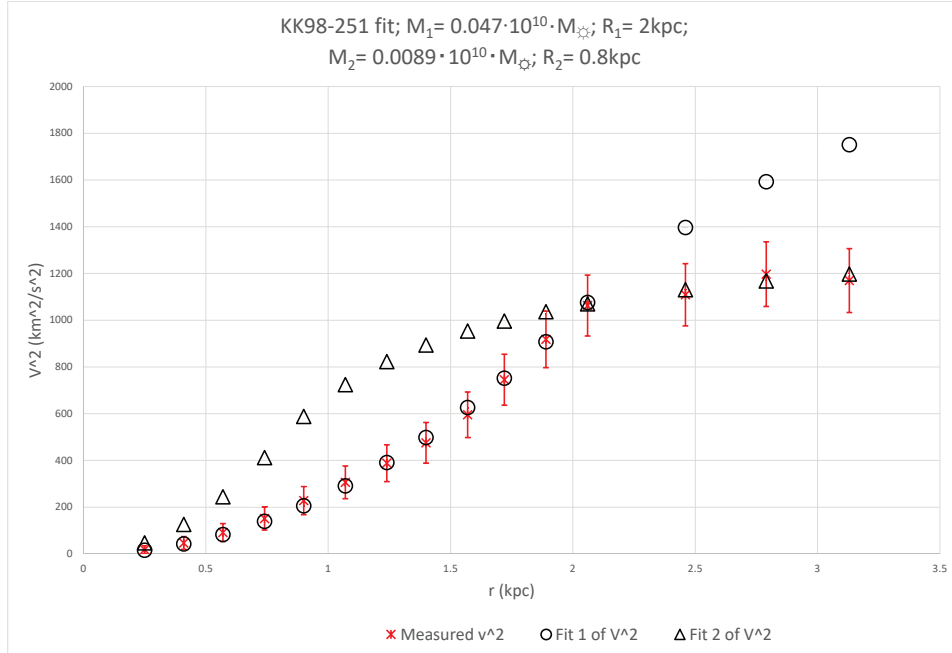


FIG. 11. KK98-251

### C. Non-crossover, parallel transition dual fit galaxies

This subsection contains 25 galaxies. It can be divided in two very different subsections.

#### 1. Non-crossover upwards transition dual fit galaxies

This subsection contains 9 galaxies. In the example of Fig.(12), a typical galaxy for this category is given. See Appendix D 1 for the remaining 8 galaxies of this subsection. It is as if the galaxy is drifting towards a higher frequency on a higher constant Lagrangian before settling for a new constant curve. This might be related to the appearance of extra mass in the transition zone. In these zones of these galaxies, the transition to a higher constant Lagrangian model curve seems to follow the addition of mass instead of a sudden shift. The settlement of the measured velocity curve on a new and higher model curve might then happen when no significant amount of mass is added any longer. This transition should then be read as indicating a continuous and substantial increase of the amount of galactic mass that is added to the effective model bulge.

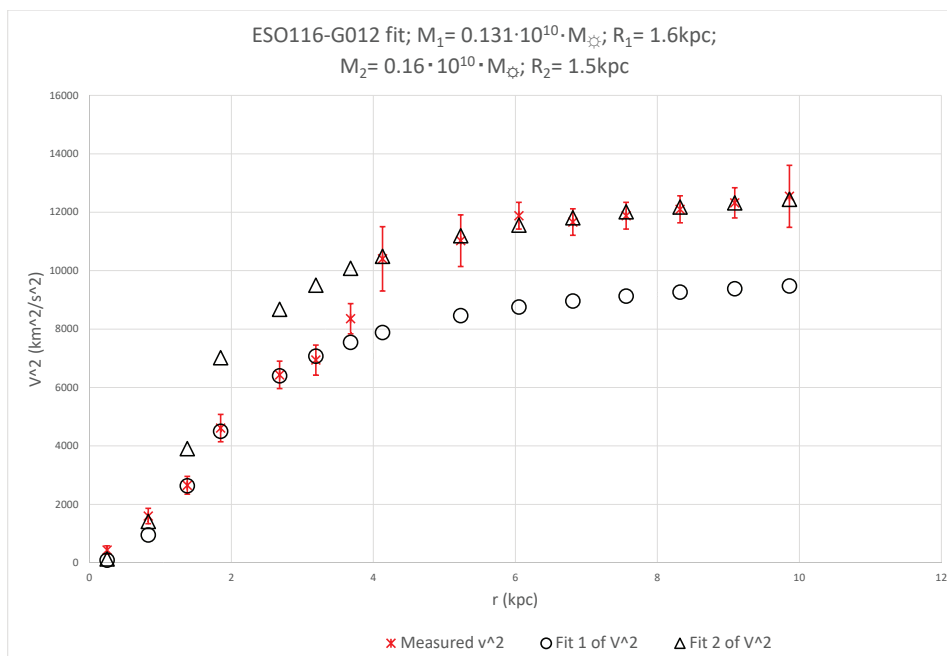


FIG. 12. ESO116-G012

## 2. *Non-crossover downwards transition dual fit galaxies*

This subsection contains 16 galaxies. In the example of Fig.(13) a typical example is given. The characteristic of this subtype is that is mainly occurs in the larger scale velocity curves, roughly in between  $10kpc$  and  $100kpc$ . See Appendix D2 for the remaining 15 galaxies of this subsection. The galaxies of this category drift slowly on a large scale,  $\simeq 10kpc$ , dimension downwards until a new upwards moving constant Lagrangian curve is found. The direction of the drift implies that from orbit to orbit energy is being or has been dissipated in a virial like way. These downward drift zones should therefore show a thermodynamically higher activity than the surrounding constant Lagrangian zones. Those zones should be the more turbulent zones of those galaxies because with a non-zero  $\frac{\Delta L}{\Delta r}$ , the Newtonian force of gravity  $F_g$  should also be non-zero in that zone and matter should not be moving on geodetic orbits. It should be a zone with non-zero gravitational stress between orbits. But because the galaxies almost always achieve to return to a non-virial constant Lagrangian curve, a purely Newtonian regime should not be expected in such zones. Those zones might be characterized as drifting in between an Einsteinian dynamics and a Newtonian dynamics, because the Lagrangian isn't a constant so gravitational stresses should be expected but the drifting down seems too slow for a full reaffirmation of the virial theorem.

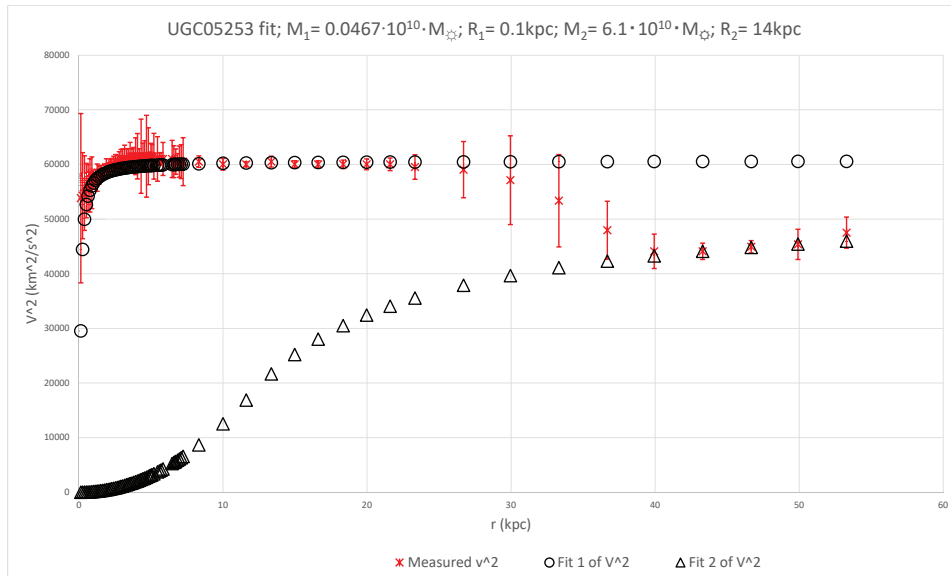


FIG. 13. UGC05253

## D. Triple fit galaxies and beyond

This subsection contains 19 galaxies. In the example of Fig.(14) a typical galaxy in this category is given. See Appendix E for the remaining 18 galaxies of this subsection. The galaxy NGC5371 is chosen because of its small error margins. Those small margins greatly reduce the freedom of interpretation while fitting the experimental curve. Most of these galaxies have rotation curves that reach beyond  $50kpc$ . The characteristic of this subtype is that the rotation curves can be analyzed as a row of dual rotation curves. As such, these rotation curves do not need additional interpretation beyond the conclusion that they are extended and complicated but still possess large stretches that can be fitted on constant Lagrangian curves. The shift from one curve to another is not a failure of the ‘constant Lagrangian’ model but instead reveals internal dynamics of the galaxy. That is similar to how paradigm shifts work. One can see from the first fit that this galaxy has a strong small bulge that dominates the rotation curve up to  $7.5kpc$ . Then the additional mass of the disk that was building up disrupts this first fit and a second fit is installed, dominated by the mass of bulge and disk. This fit loses its grip after  $20kpc$ , when the luminosity fades and at the same time a lot of H1 gas is added. In between  $25kpc$  and  $30kpc$ , this galaxy is probably gravitationally and thermodynamically highly active because the measured rotation curve is dropping, which implies that in that region, gravitational energy has been and/or is being dissipated. Then from  $35kpc$  and beyond, the gas clouds in that region should be less active again, allowing them to remain on a constant Lagrangian curve again. Interesting in this galaxy is the interrelation between the first shift and the third fit, they have the same  $R$ . Another observation is the fact that the description of the subsequent curves, their justification, can be entirely formulated using the baryonic, observable mass of that galaxy. If the ‘constant Lagrangian’ postulate could be formulated as being nothing but the conservation of energy in disguise, active in those situations where virial dissipation of gravitational energy during orbital collapse isn’t possible or opportunistic, then a ‘Dark Matter’ hypothesis would be completely superfluous for the explanation of galaxy rotation curves. In the analysis of the fit of galaxy NGC5371 I made extensive use of the surface brightness and mass model of the SPARC database.

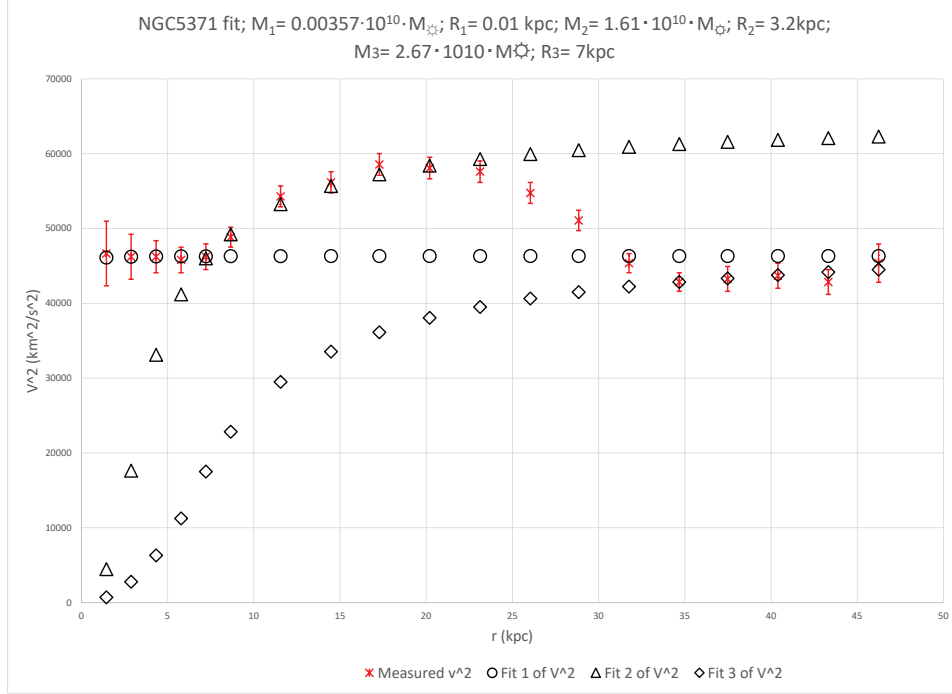


FIG. 14. NGC5371

### E. The rest of the fitted galaxies (the almost no-fits)

This category contains 47 galaxies. For these 47 galaxies, a partial fit was almost always possible. For UGC08286 it might have been better not to present a fit at all, see Fig.(15). See the appendix for the rest of the galaxies of this category. Most of the galaxies in this section could be appointed to one of the previous categories but not without the cost of seeming over eager to impose order, even when disorder dominates. This means that 27 percent of the galaxies couldn't be easily put into one of the proposed categories.

Only 16 of these galaxies were so chaotic that any fit might seem appropriate. At least 25 of them could without too much imagination, but at the cost of significantly less error margin rigor, be categorized into one of the previous sections. The scientific integrity demands that when the SPARC database of 175 galaxies are subjected to an independent model, that the 'failures' and the difficulties to model reality will be recognized as such. Thus, the rest category of about 47 galaxies has about the same weight as the single fit category of about 45 galaxies. That doesn't change the fact that statistically these two numbers should be vastly different if the 'constant Lagrangian' model had no connection to reality whatsoever. All the galaxies of this category are presented in the appendix with proposed best fit. It is

up to the reader to decide to what extent these fits are product of my imagination and to what extent forced by the measured velocities with their respective error margins.

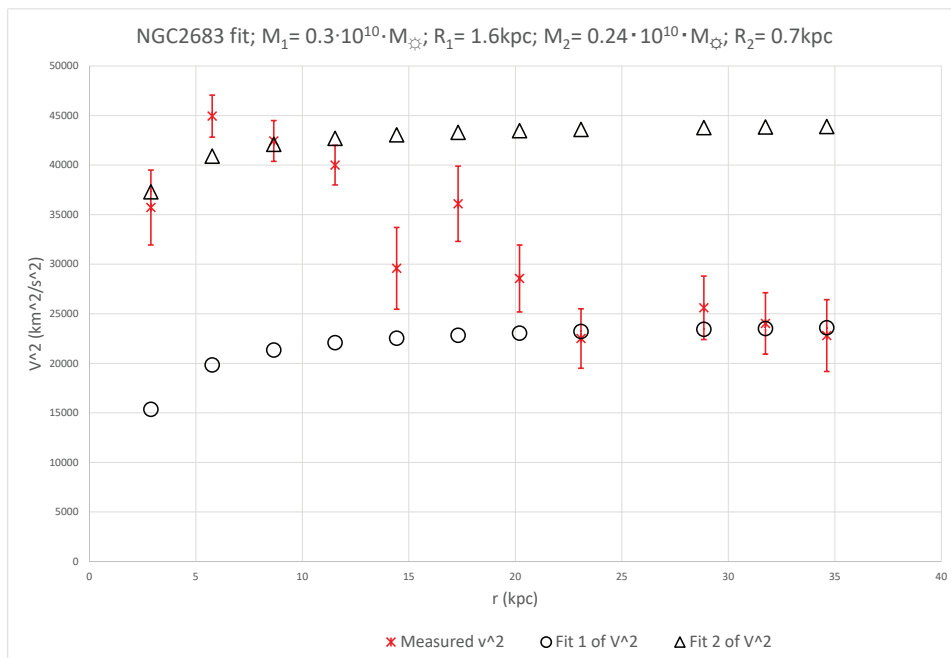


FIG. 15. NGC2683

## IX. CONCLUSION

The least daring conclusion of this paper is that complete to huge stretches of galaxy rotation curves can be effectively plotted on constant Lagrangian curves. On these stretches atomic clocks are highly synchronized, creating effective time-rate zones and bubbles.

Of the 175 galaxies, 45 allowed a single fit rotation curve, so about 26 percent. Another 9 galaxies could almost be plotted on a single fit. Then 30 galaxies could be fitted really nice on crossing dual curves. The reason for the appearance of this dual curve, in its two versions, could be given and related to the galactic constitution and dynamics. Another 25 galaxies could be fitted on parallel transition dual curves. This appearance could also be related to galactic dynamics and galactic mass distribution. Then there were the 19 multiple fit galaxies, complex extended galaxies, the complexities of which could be analyzed on the basis of the 4 types of dual fits. In total 128 of the 175 galaxies could be fitted and analyzed very well to reasonably well within the error margins. That is a 73 percent success rate.

This amazing result rules out stochastic coincidence as an explanation of those fits. Relative to the model, those 175 galaxies were a random set.

In my opinion, the success of the ‘constant Lagrangian’ approach indicates that the problem of the galaxy rotation curves can be solved on the basis of the principle of conservation of energy. Inside a model bulge, thermodynamic and stellar processes allow for a side by side existence of the virial theorem and the constant Lagrangian condition. Outside the model bulge, orbital collapse conditions are mostly such that these conditions do not allow the collapsing matter to dissipate half of the gravitational energy. This invalidates the virial theorem, which is then replaced by the constant Lagrangian condition. From a radial free fall perspective, the last condition is just a conservation of energy expression. From a General Relativity perspective, a constant Lagrangian condition implies a zero force of gravity and that in turn means that a metric approach is allowed and needed. But on stretches of galactic curves where the Lagrangian isn’t a constant from orbit to orbit, gravitational stresses are present and the application of General Relativity should be expected to meet its limitations. Those regions can be seen as intermediates between Newton and Einstein. That might also be the reason for the partial successes of MOND.

## REFERENCES

- Ashby, N. (2002, May). Relativity and the global positioning system. *Physics Today* 55(5), 41–47.
- de Haas, E. P. J. (2014). The geodetic precession as a 3d schouten precession and a gravitational thomas precession. *Canadian Journal of Physics* 92(10), 1082–1093.
- de Haas, E. P. J. (2018a). A ‘constant lagrangian’ fit of the galaxy rotation curves of the ‘f-series’ from the sparc database. *Preprint on viXra.org: Astrophysics*. [vixra:1805.0168](https://arxiv.org/abs/1805.0168).
- de Haas, E. P. J. (2018b). A ‘constant lagrangian’ model for galactic dynamics in a geodetic approach towards the galactic rotation dark matter issue. *Preprint on viXra.org: Astrophysics*. [vixra:1804.0298](https://arxiv.org/abs/1804.0298).
- de Haas, E. P. J. (2018c). Fitting some galaxy rotation curves using the ‘constant lagrangian’ model for galactic dynamics. *Preprint on viXra.org: Astrophysics*. [vixra:1804.0386](https://arxiv.org/abs/1804.0386).
- de Haas, E. P. J. (2018d). Fitting the ngc 1560 rotation curve and other galaxies in the ‘constant lagrangian’ model for galactic dynamics. *Preprint on viXra.org: Astrophysics*. [vixra:1804.0328](https://arxiv.org/abs/1804.0328).
- de Haas, E. P. J. (2018e). A stars-gas dual fit result in the ‘constant lagrangian’ model for galactic dynamics when applied to the sparc database. *Preprint on viXra.org: Astrophysics*. [vixra:1805.0047](https://arxiv.org/abs/1805.0047).
- Delva, P. and J. Lodewyck (2013). Atomic clocks: new prospects in metrology and geodesy. In *Workshop on Relativistic Positioning Systems and their Scientific Applications Brdo, Slovenia, September 19-21, 2012*. arXiv:1308.6766 [physics.atom-ph].
- Hećimović, Ž. (2013). Relativistic effects on satellite navigation. *Tehnički vjesnik* 20(1), 195–203.
- Koopmans, L. et al. (2009). Strong gravitational lensing as a probe of gravity, dark-matter and super-massive black holes. *Astrophysical Journal*. [arXiv:astro-ph/0902.3186v2](https://arxiv.org/abs/0902.3186v2).
- Kopeikin, S. M., I. Y. Vlasov, and W. B. Han (2017). The normal gravity field in relativistic geodesy. *ArXiv e-prints*. arXiv:1708.09456 [gr-qc].
- Lelli, F., S. S. McGaugh, and J. M. Schombert (2016, December). SPARC: Mass Models for 175 Disk Galaxies with Spitzer Photometry and Accurate Rotation Curves. *The Astronomical Journal* 152, 157.
- Mayrhofer, R. and R. Pail (2012). Future satellite gravity field missions: Feasibility study

- of post-newtonian method. In S. Kenyon (Ed.), *Geodesy for Planet Earth*, Volume 136 of *International Association of Geodesy Symposia*, pp. 231–238. Springer International Publishing. Switzerland.
- McGaugh, S. S. (2005). The baryonic tully-fisher relation of galaxies with extended rotation curves and the stellar mass of rotating galaxies. *The Astrophysical Journal* 632, 859–871. [arXiv:astro-ph/0506750v2](#).
- Mercier, C. (2015). Calculation of the apparent mass of the universe. [Website access](#) (accessed on April, 14, 2018).
- Milgrom, M. (1983a). A modification of the newtonian dynamics - implications for galaxies. *The Astrophysical Journal* 270, 371–387. [Astronomy Abstract Service pdf](#).
- Milgrom, M. (1983b). A modification of the newtonian dynamics as a possible alternative to the hidden mass hypothesis. *The Astrophysical Journal* 270, 365–370. [Astronomy Abstract Service](#).
- Misner, C., K. Thorne, and J. Wheeler (1973). *Gravitation*. San Francisco: Freeman and Company.
- Ohanian, H. and R. Ruffini (2013). *Gravitation and Spacetime* (3 ed.). New York: Cambridge University Press.
- Oort, J. H. (1932). The force exerted by the stellar system in the direction perpendicular to the galactic plane and some related problems. *Bulletin of the Astronomical Institutes of the Netherlands* 6, 249–287.
- Rubin, V., N. Thonnard, and W. J. Ford (1978). Extended rotation curves of high-luminosity spiral galaxies. iv - systematic dynamical properties, sa through sc. *Astrophysical Journal, Part 2 - Letters to the Editor* 225, L107–L111.
- Rubin, V., N. Thonnard, and W. J. Ford (1980). Rotational properties of 21 sc galaxies with a large range of luminosities and radii from ngc 4605 ( $r=4\text{kpc}$ ) to ugc 2885 ( $r=122\text{kpc}$ ). *Astrophysical Journal* 238, 471–487.
- Ruggiero, M. L., D. Bini, A. Gericco, and A. Tartaglia (2008). Emission versus fermi coordinates: applications to relativistic positioning systems. *Classical and Quantum Gravity* 25(20), 205011. [arXiv:0809.0998 \[gr-qc\]](#).
- Singer, S. F. (1956). Application of an artificial satellite to the measurement of the general relativistic "red shift". *Phys. Rev.* 104, 11–14.
- Straumann, N. (1984). *General Relativity and Relativistic Astrophysics*. Berlin: Springer-

Verlag.

The ATLAS Collaboration (2018). Search for dark matter produced in association with bottom or top quarks in  $\sqrt{s} = 13\text{TeV}$  collisions with the atlas detector. *The European Physical Journal C* 78(1), 18.

Tully, R. B. and J. R. Fisher (1977). A new method of determining distances to galaxies. *Astronomy and Astrophysics* 54, 661–673.

Weinberg, S. (1972). *Gravitation and cosmology: principles and applications of the general theory of relativity*. New York: Wiley & Sons.

Zwicky, F. (1933). Die rotverschiebung von extragalaktischen nebeln. *Helvetica Physica Acta* 6, 110–127.

Zwicky, F. (1937). On the masses of nebulae and of clusters of nebulae. *Astrophysical Journal* 86, 217–247.

Appendix A: The additional single fit selection.

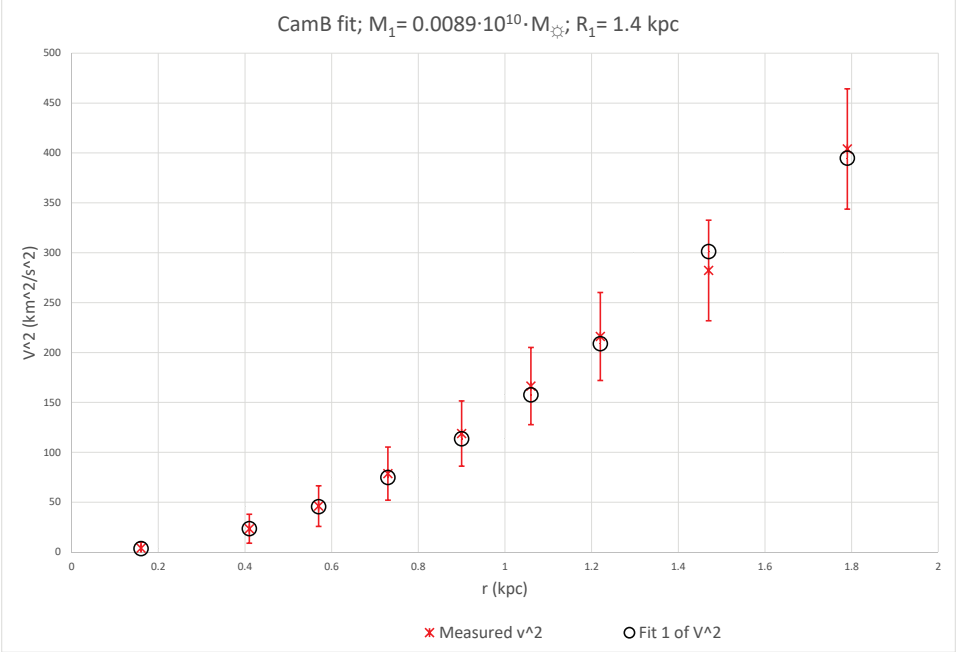


FIG. 16. CamB

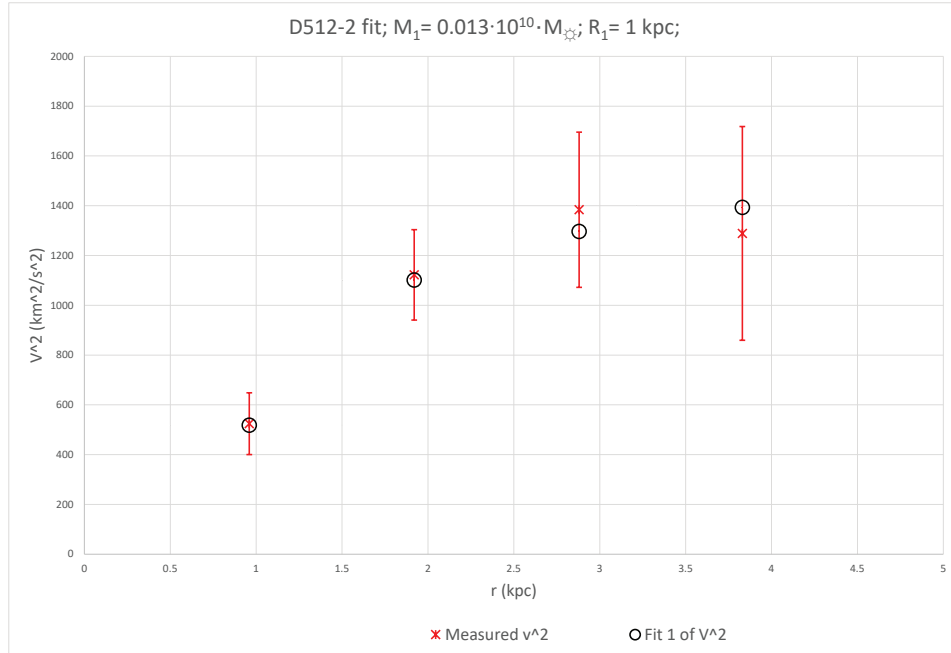


FIG. 17. D512-2

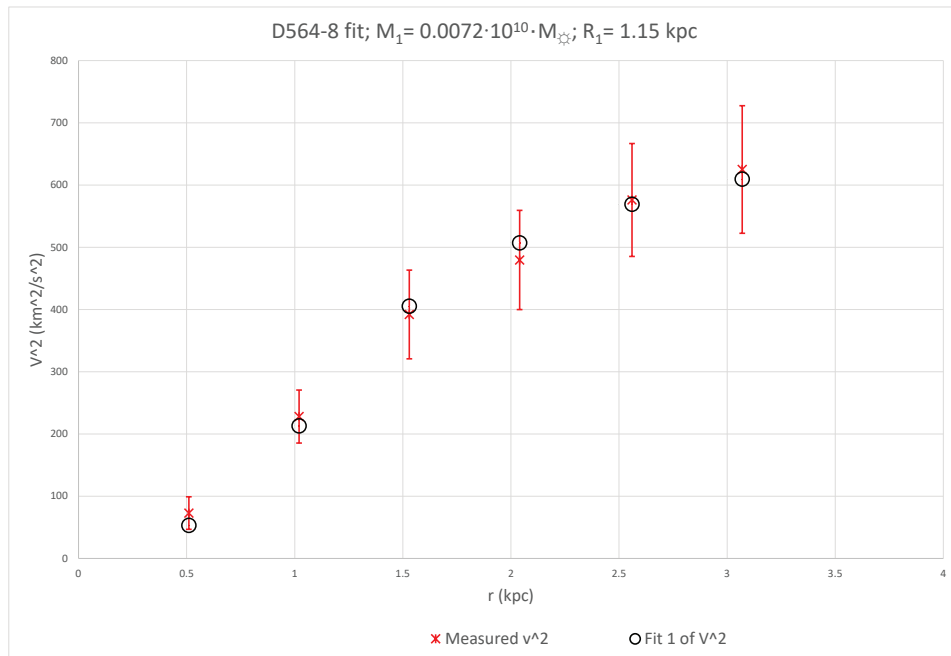


FIG. 18. D564-8

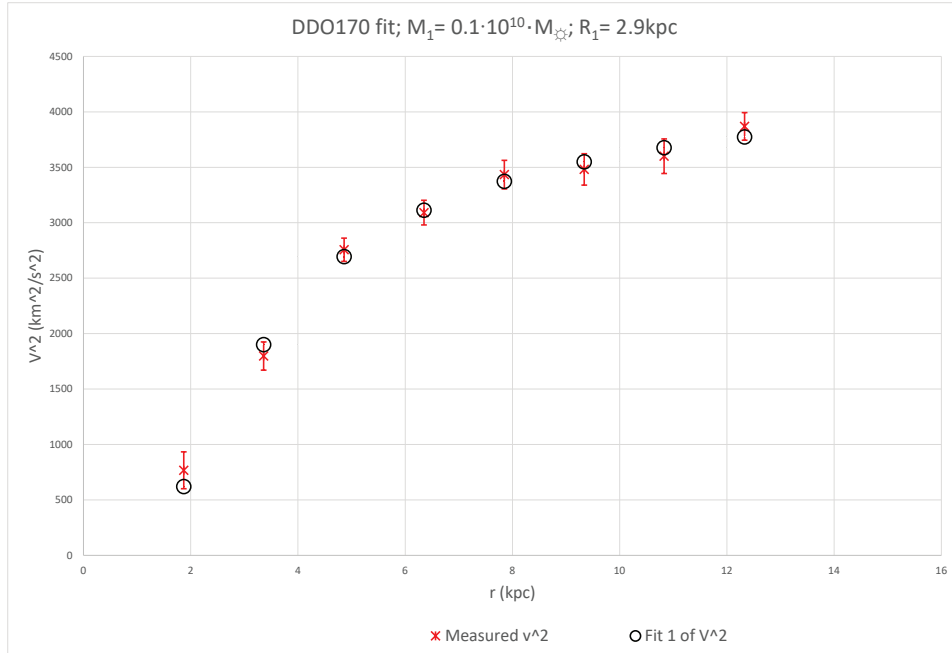


FIG. 19. DDO170

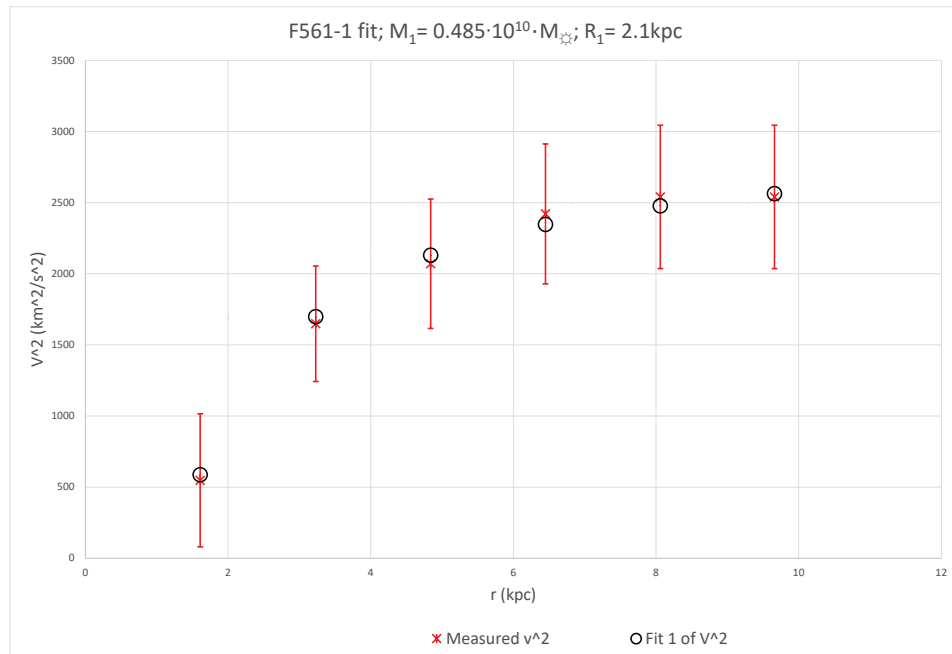


FIG. 20. F561-1

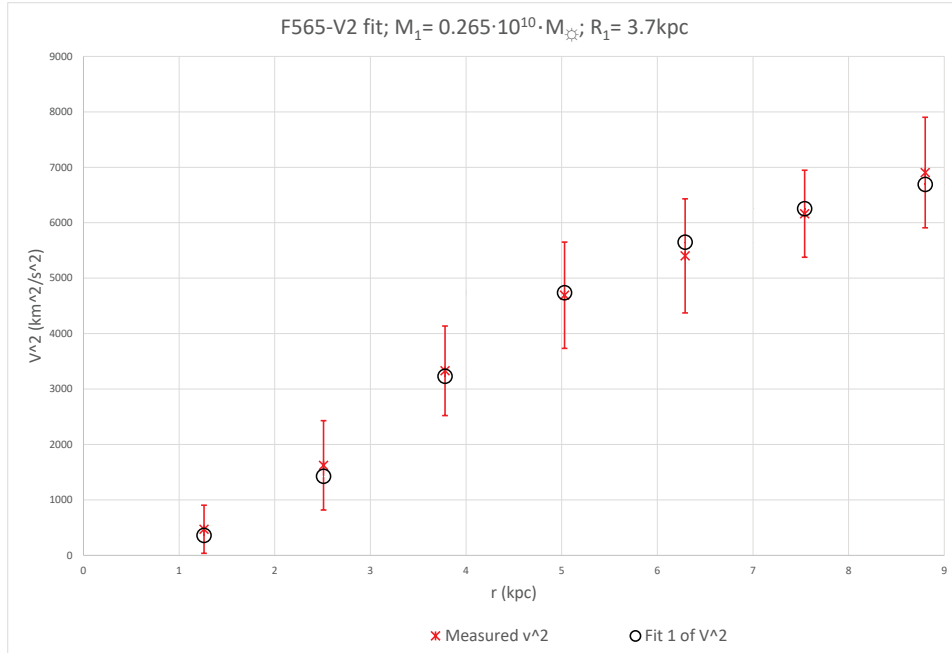


FIG. 21. F565-V2

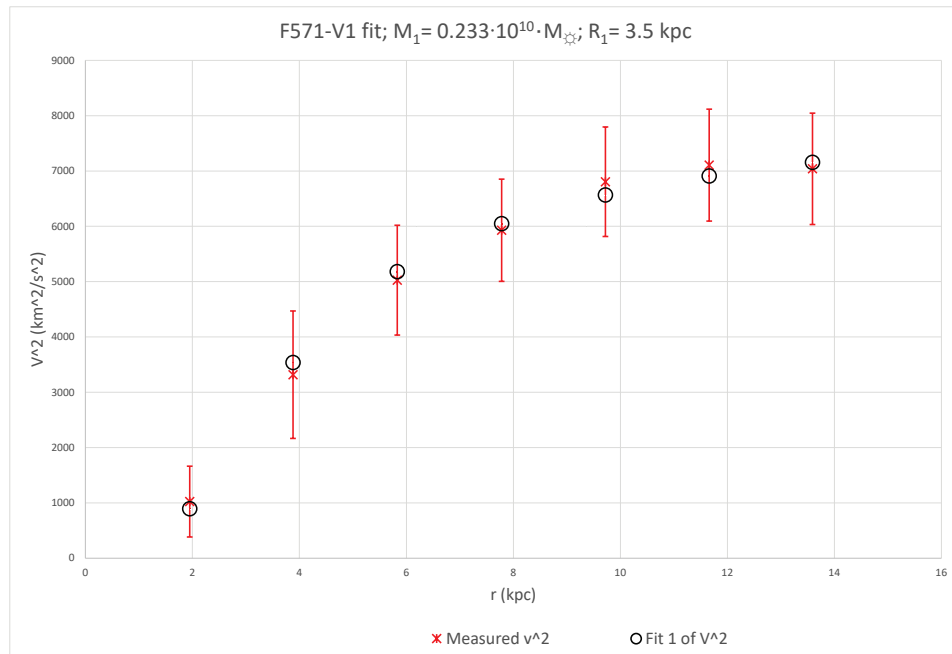


FIG. 22. F571-V1

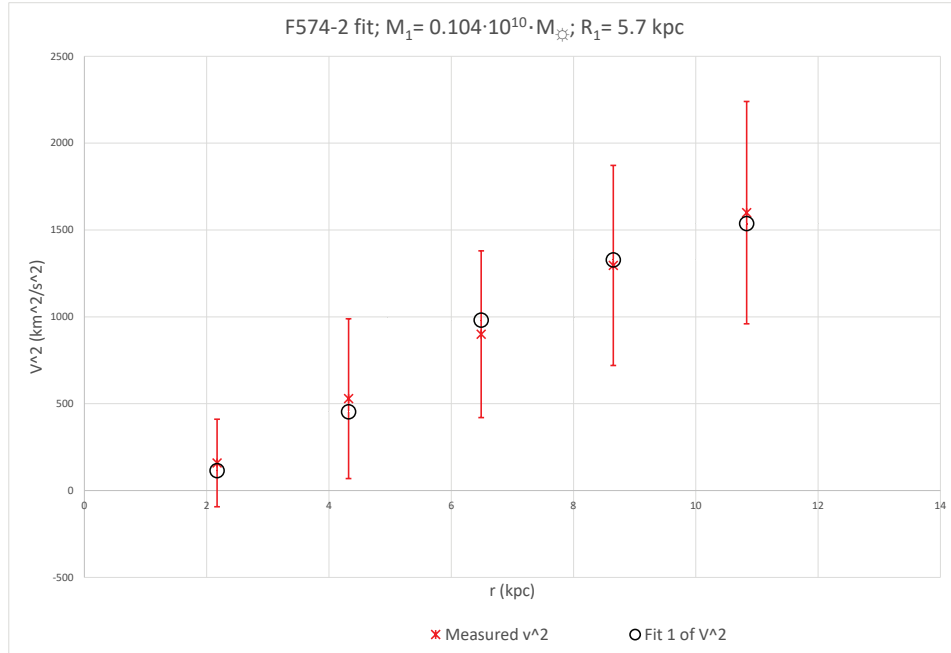


FIG. 23. F574-2

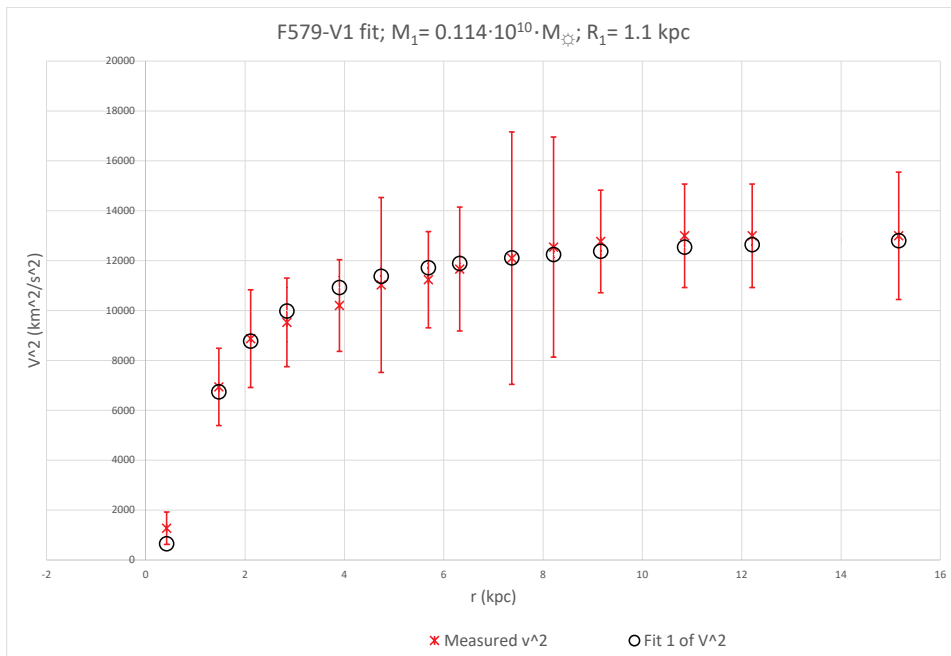


FIG. 24. F579-V1

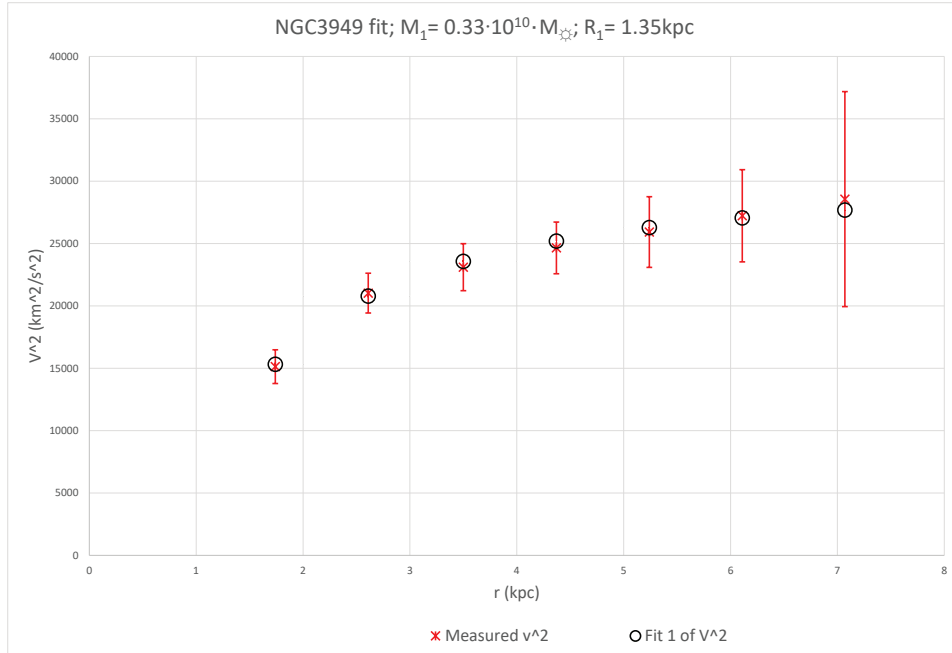


FIG. 25. NGC3949

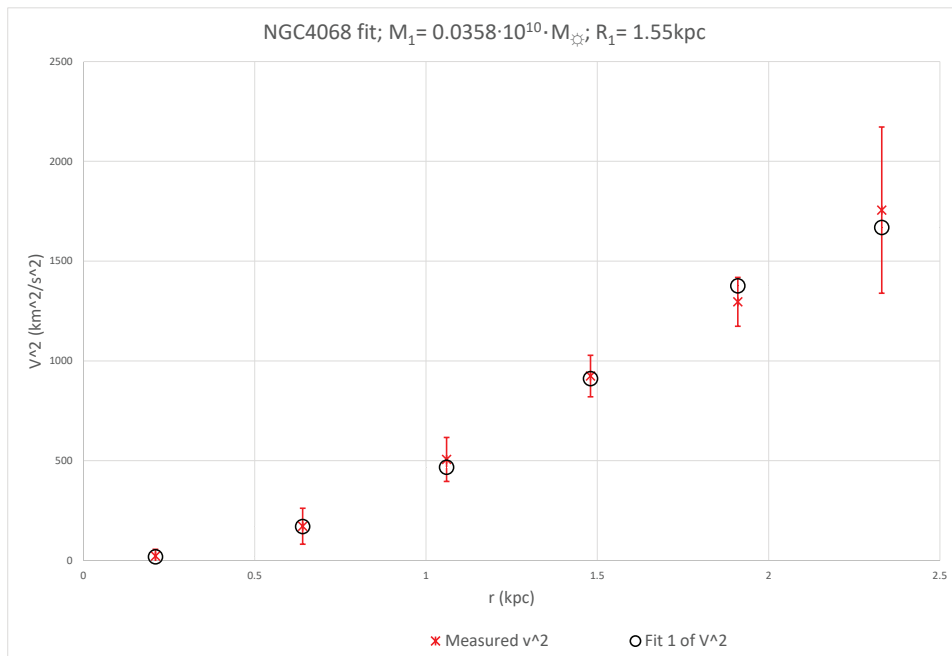


FIG. 26. NGC4068

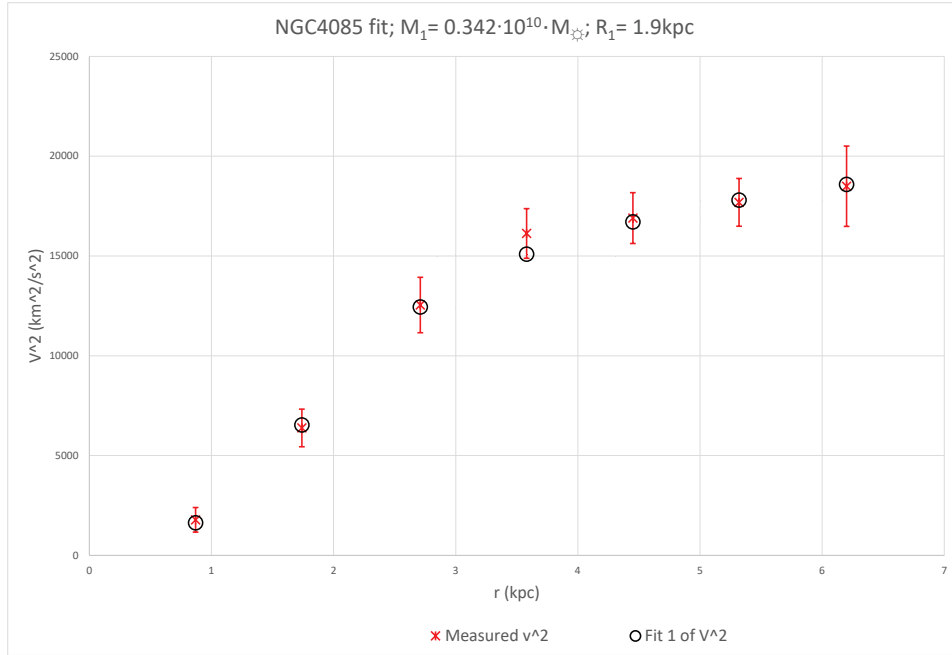


FIG. 27. NGC4085

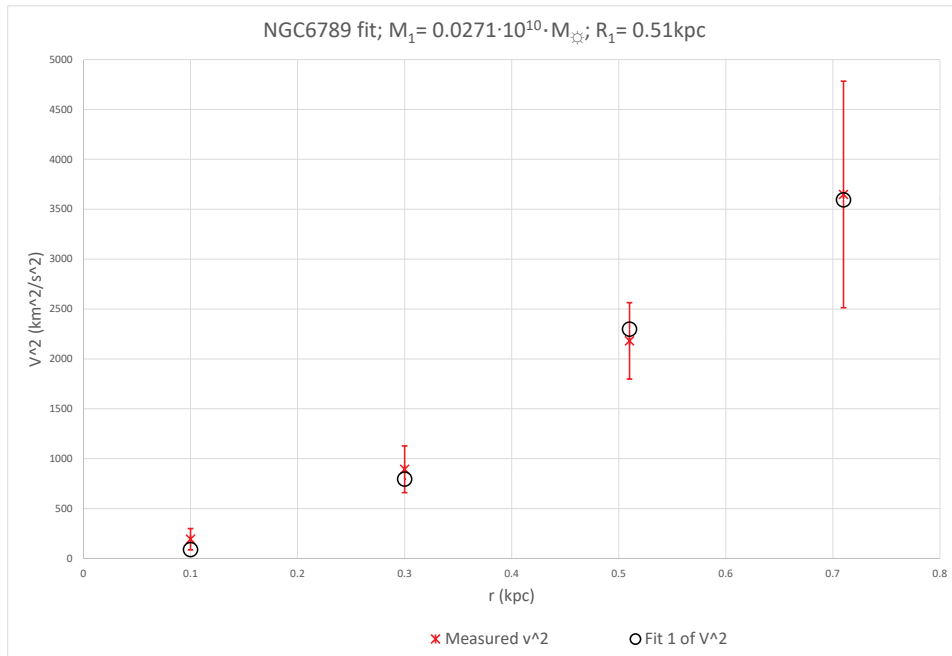


FIG. 28. NGC6789

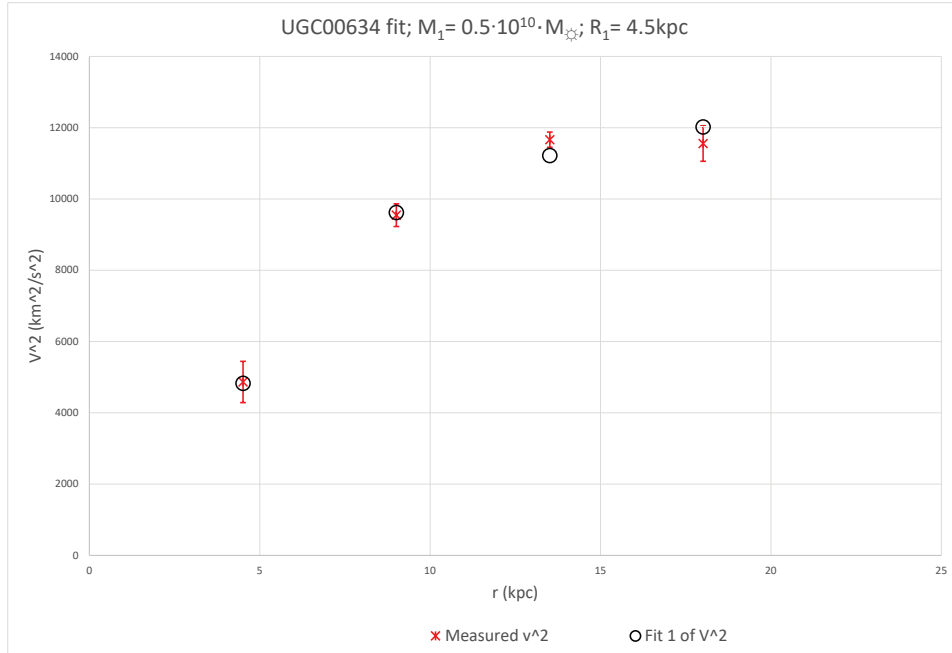


FIG. 29. UGC00634

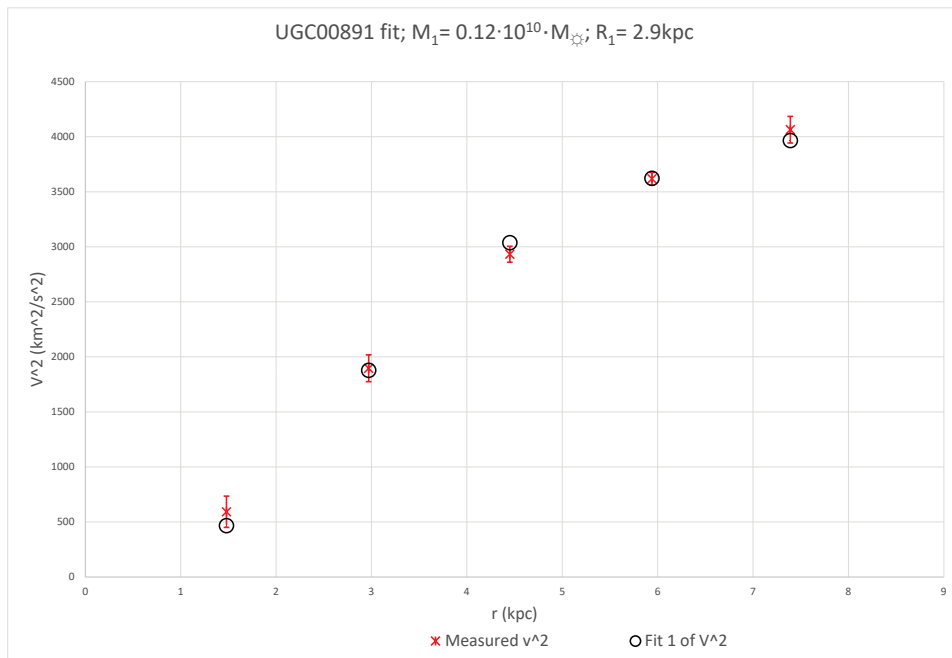


FIG. 30. UGC00891

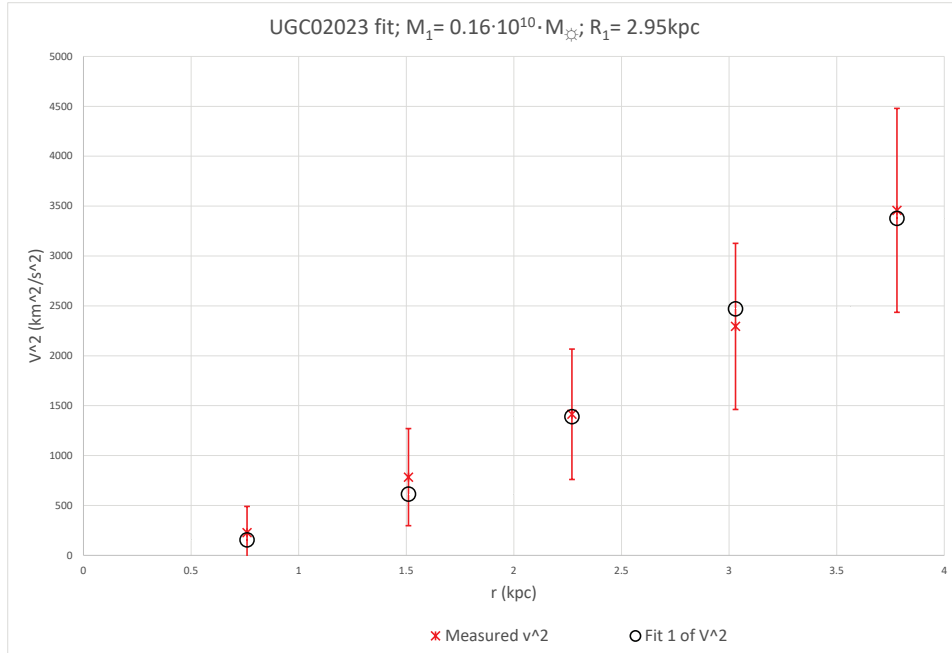


FIG. 31. UGC02023

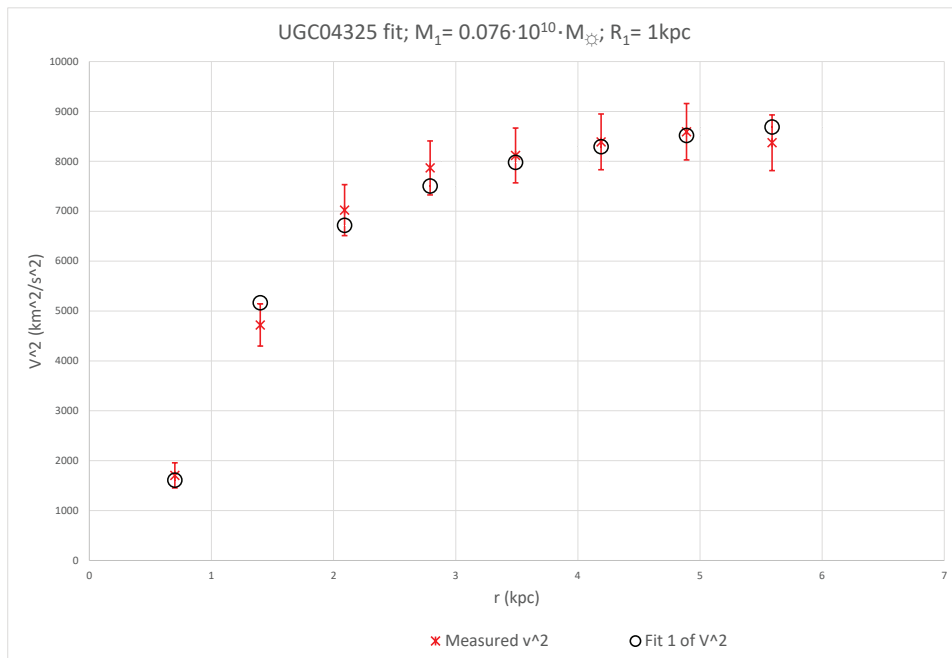


FIG. 32. UGC04325

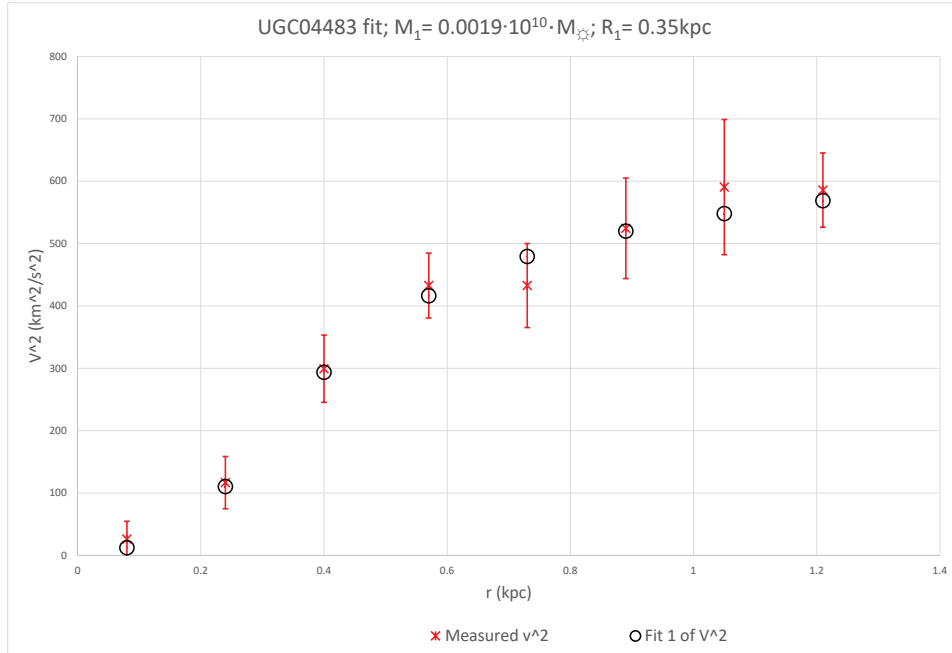


FIG. 33. UGC04483

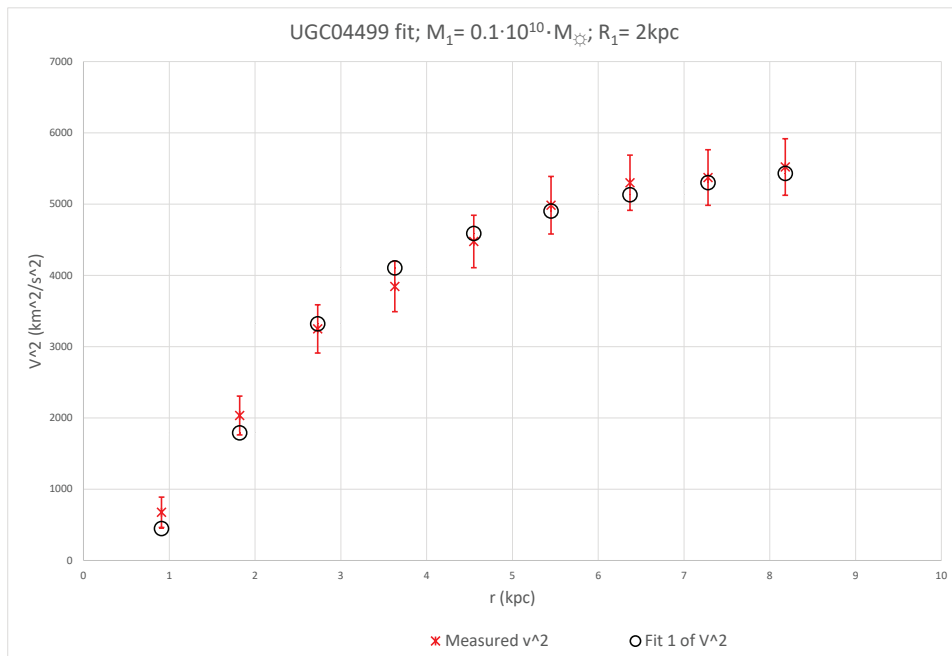


FIG. 34. UGC04499

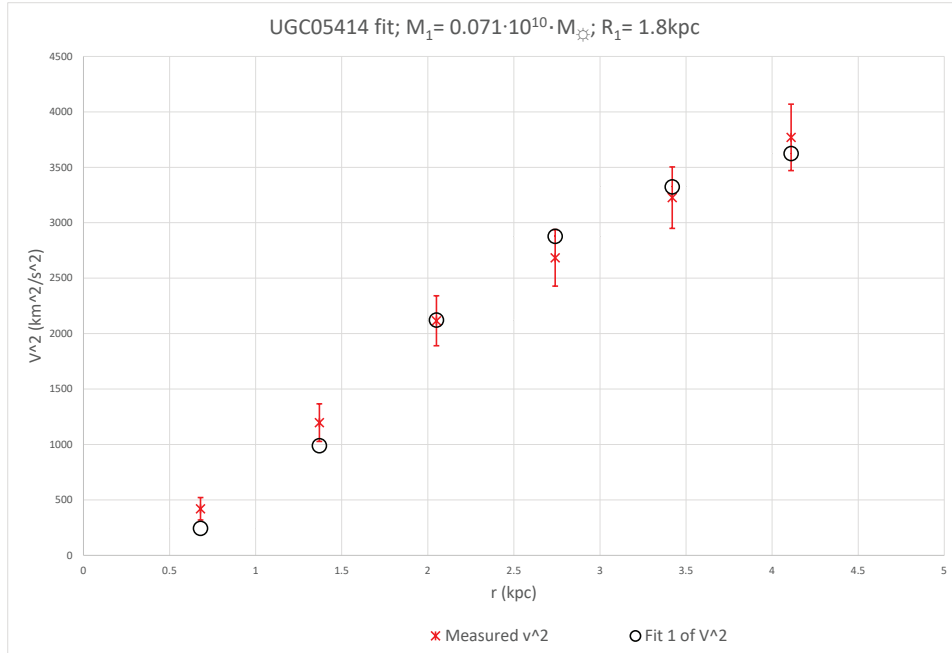


FIG. 35. UGC05414

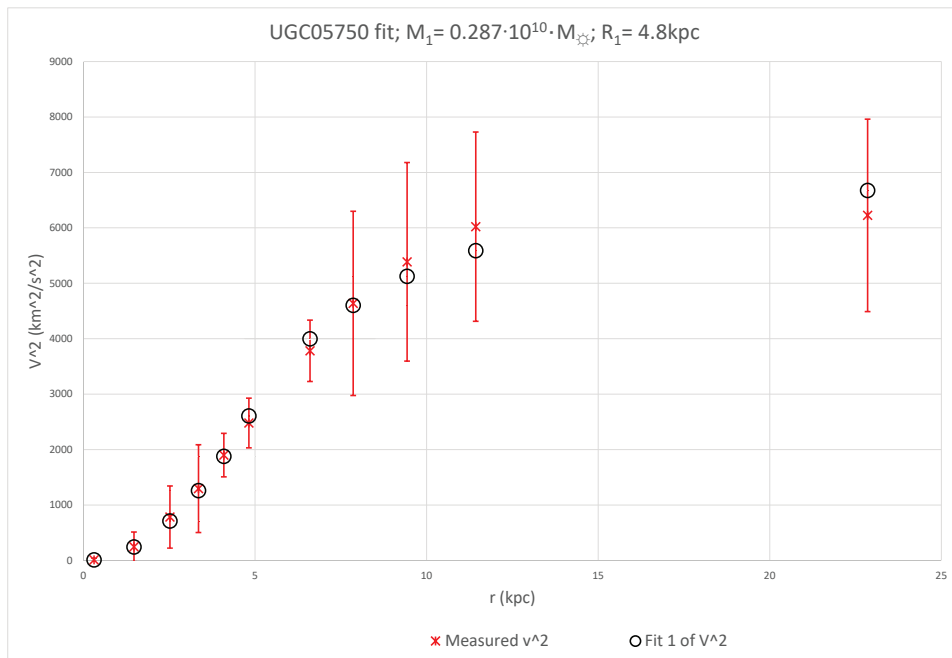


FIG. 36. UGC05750

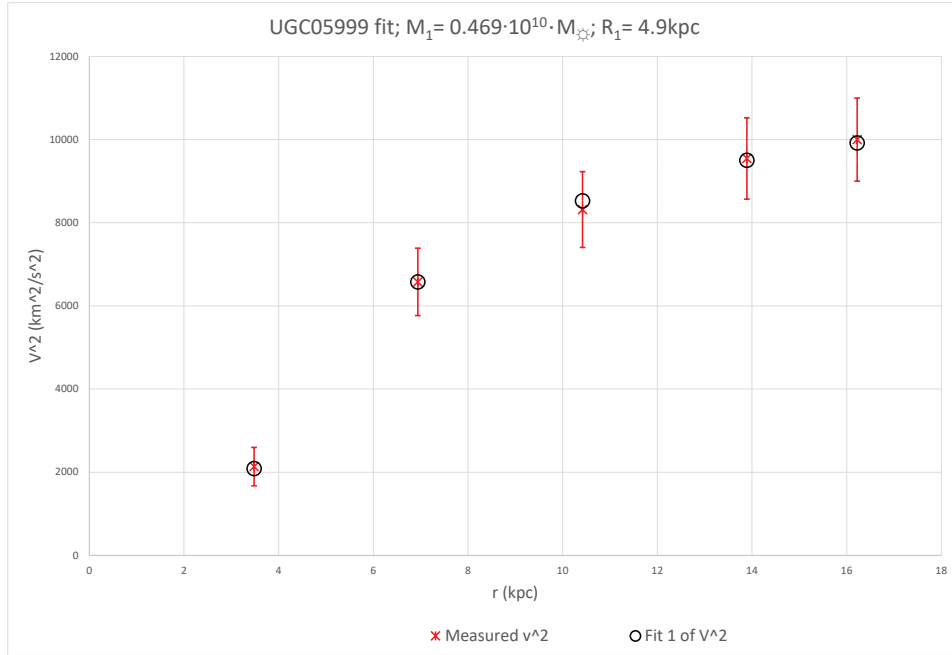


FIG. 37. UGC05999

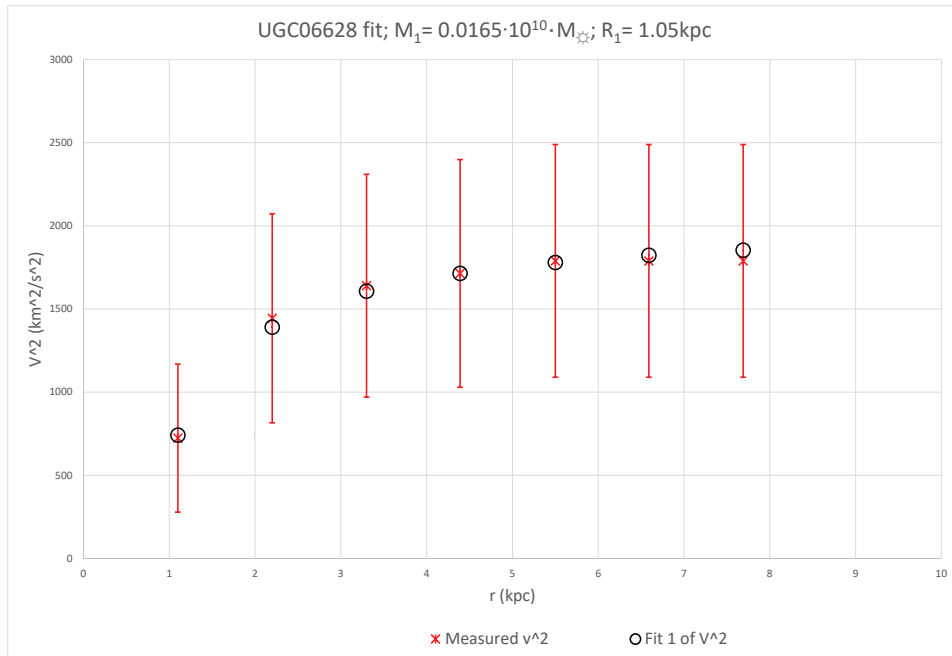


FIG. 38. UGC06628

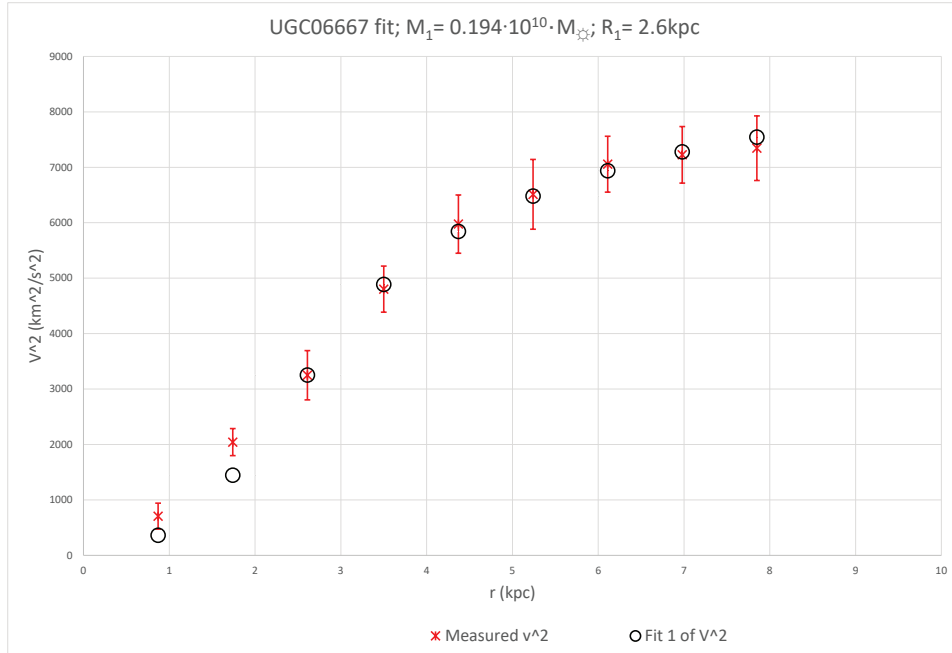


FIG. 39. UGC06667

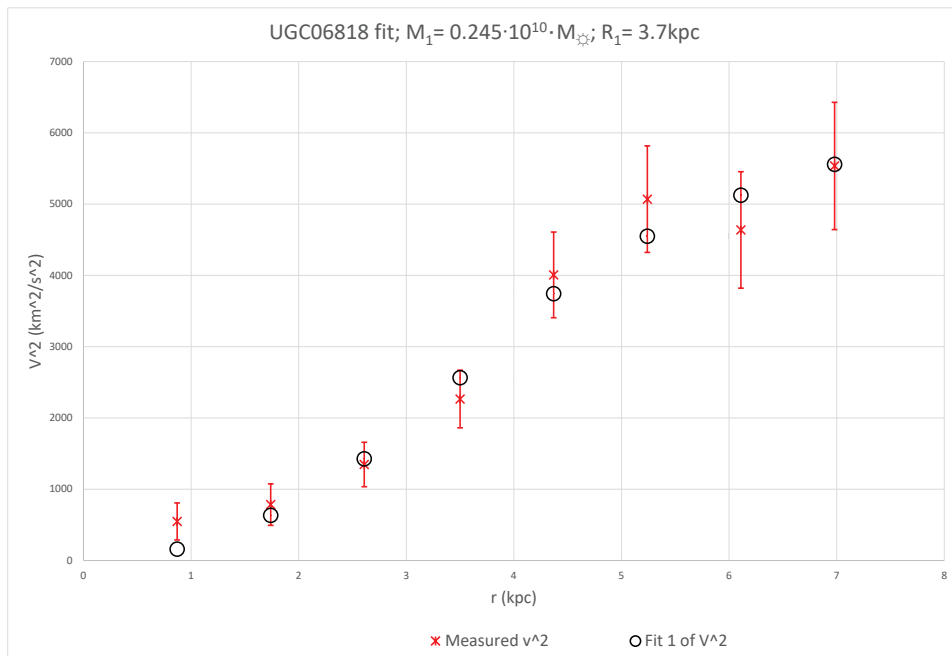


FIG. 40. UGC06818

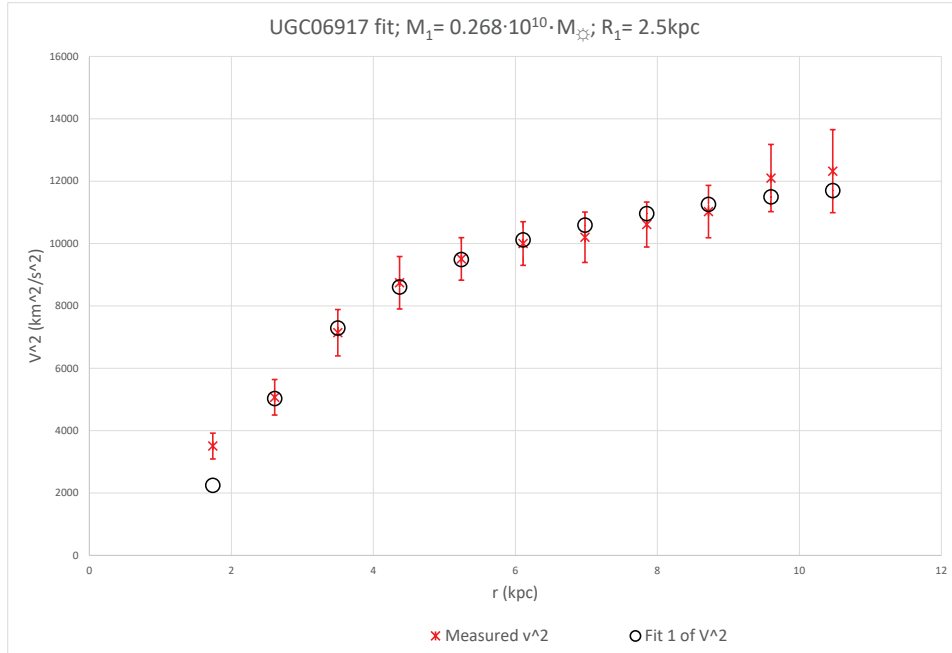


FIG. 41. UGC06917

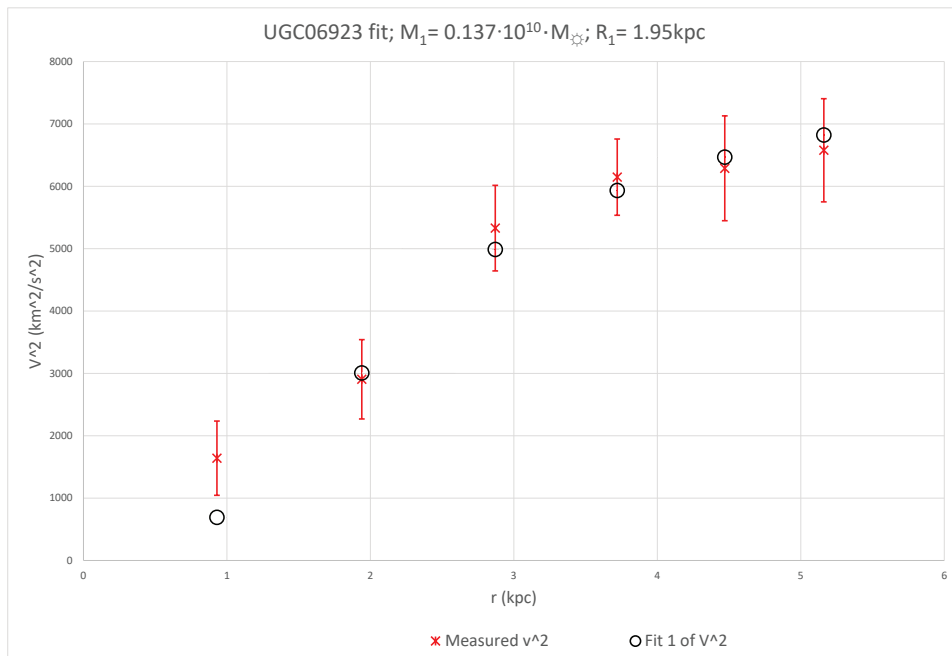


FIG. 42. UGC06923

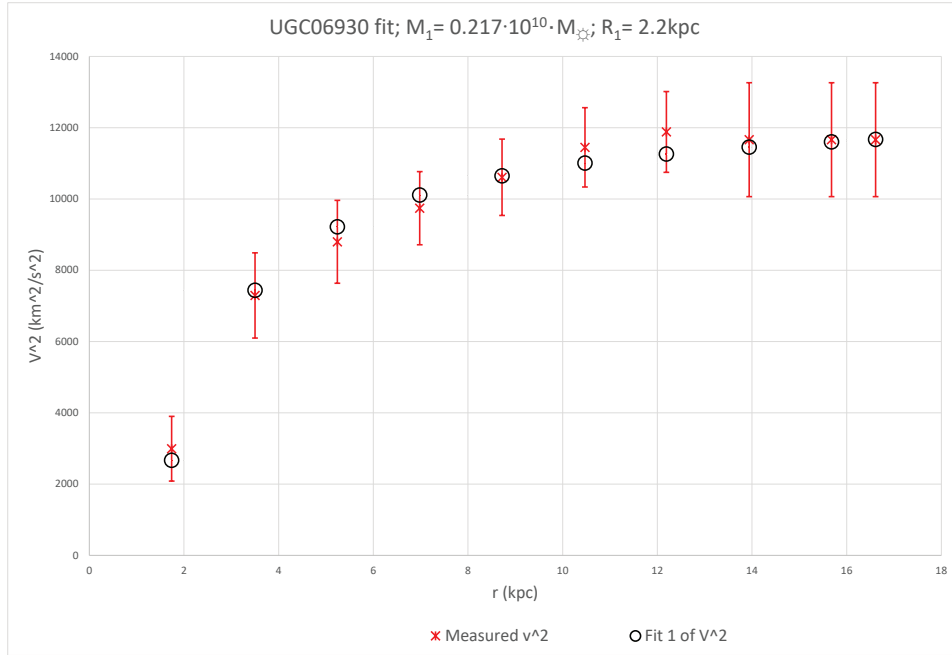


FIG. 43. UGC06930

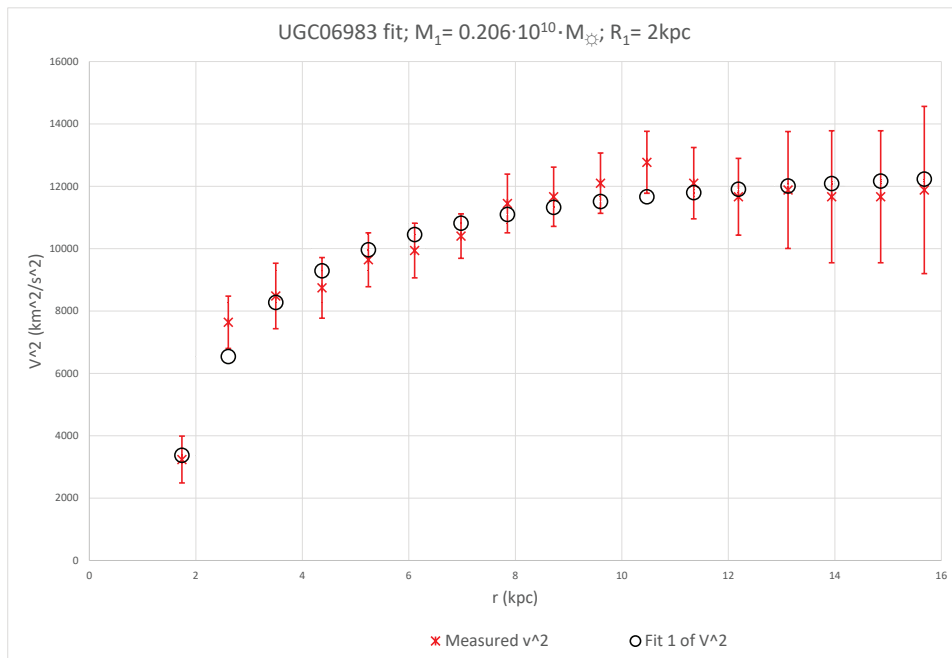


FIG. 44. UGC06983

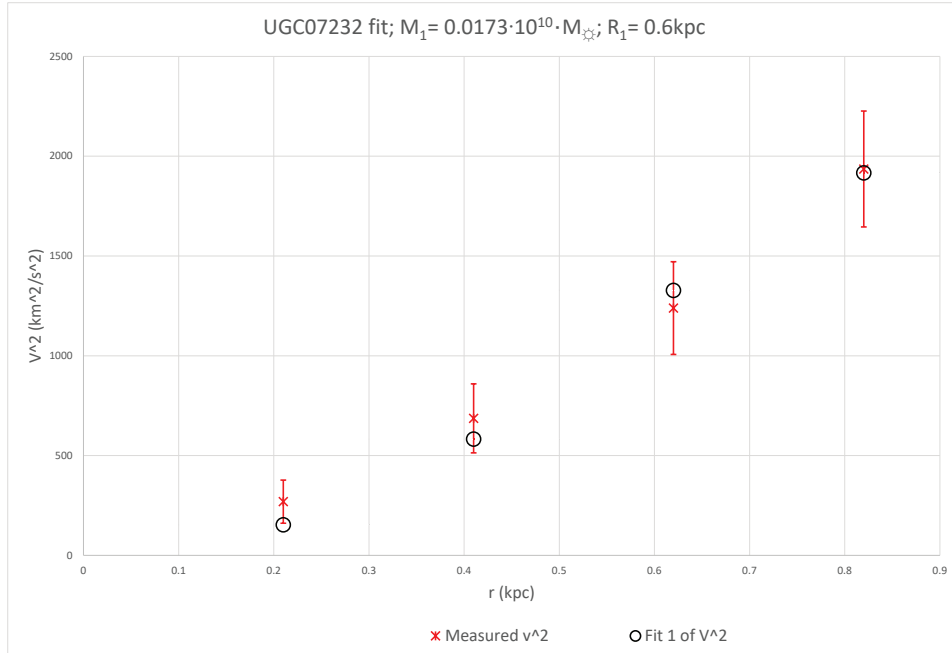


FIG. 45. UGC07232

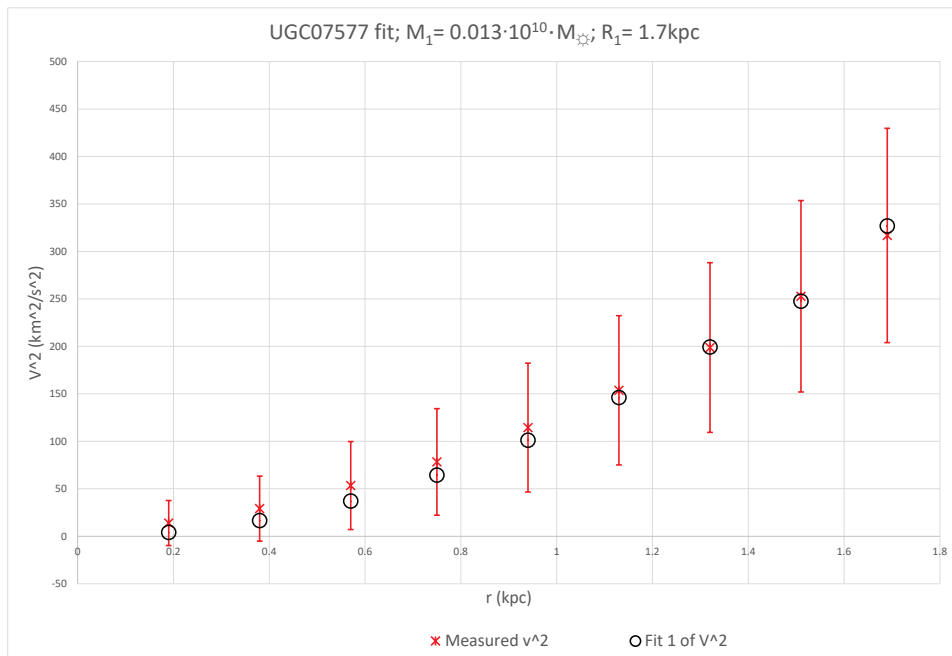


FIG. 46. UGC07577

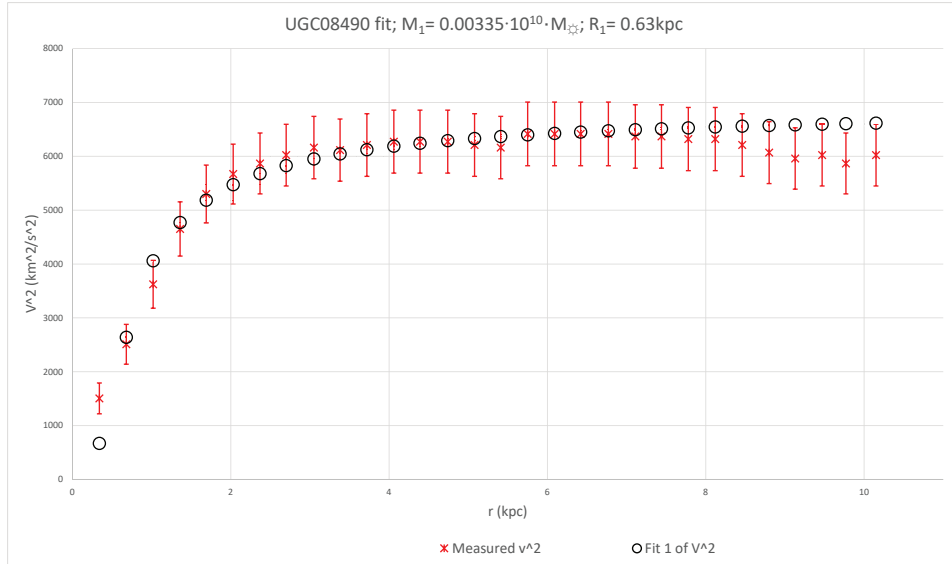


FIG. 47. UGC08490

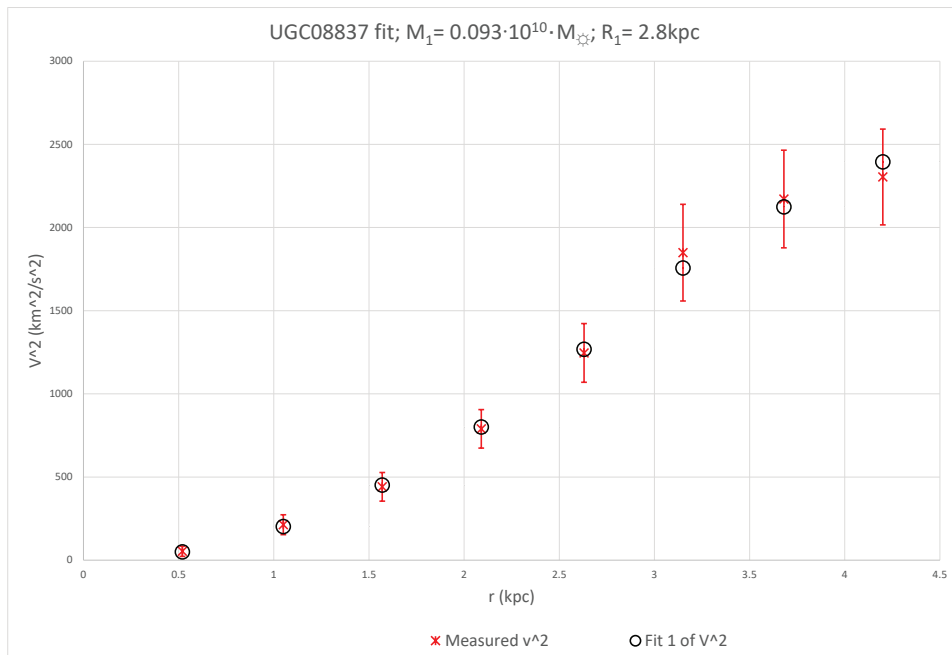


FIG. 48. UGC08837

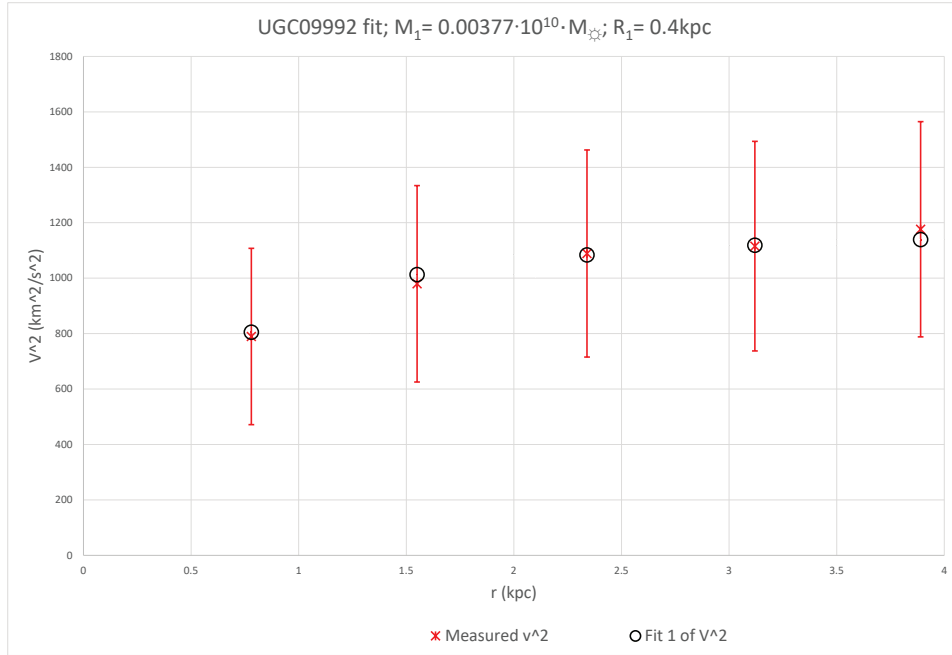


FIG. 49. UGC09992

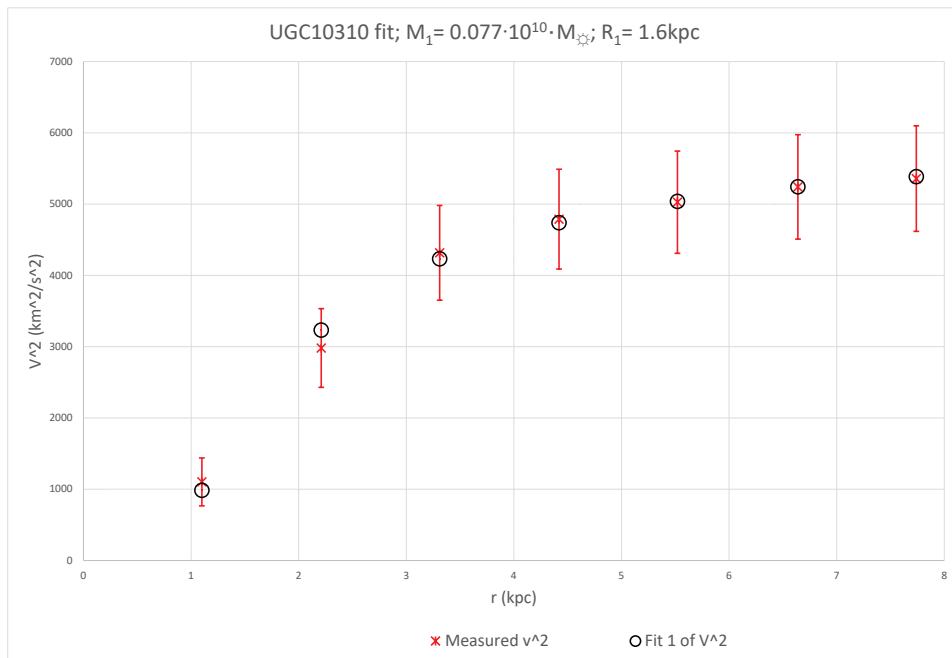


FIG. 50. UGC10310

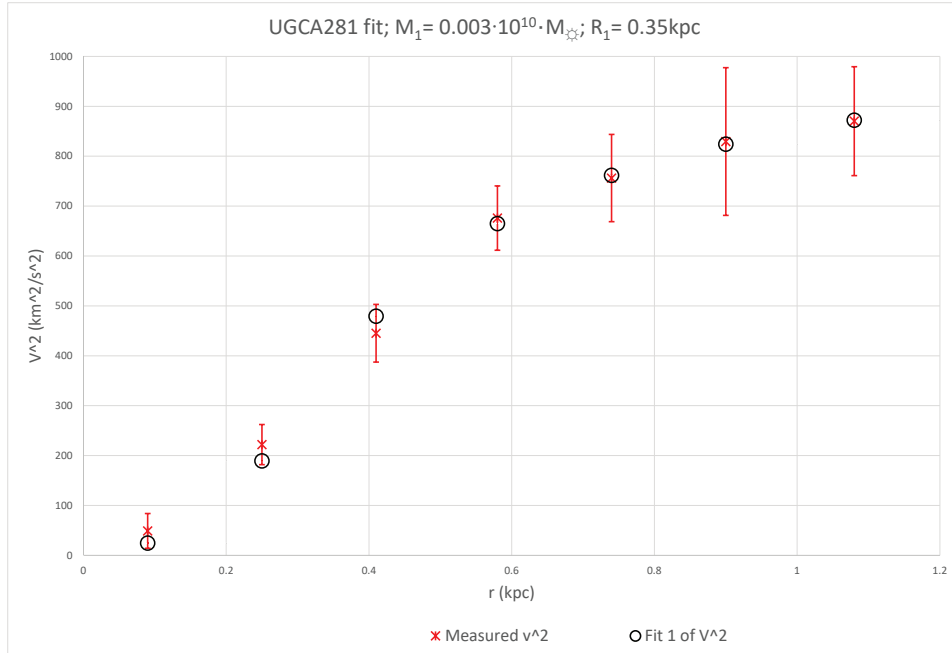


FIG. 51. UGCA281

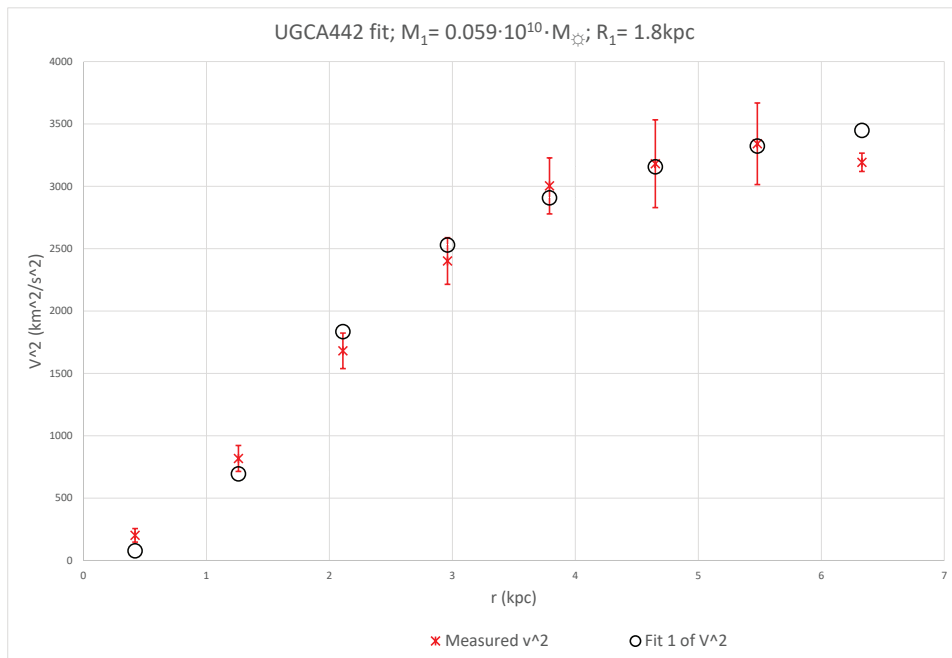


FIG. 52. UGCA442

## Appendix B: The almost single fit selection.

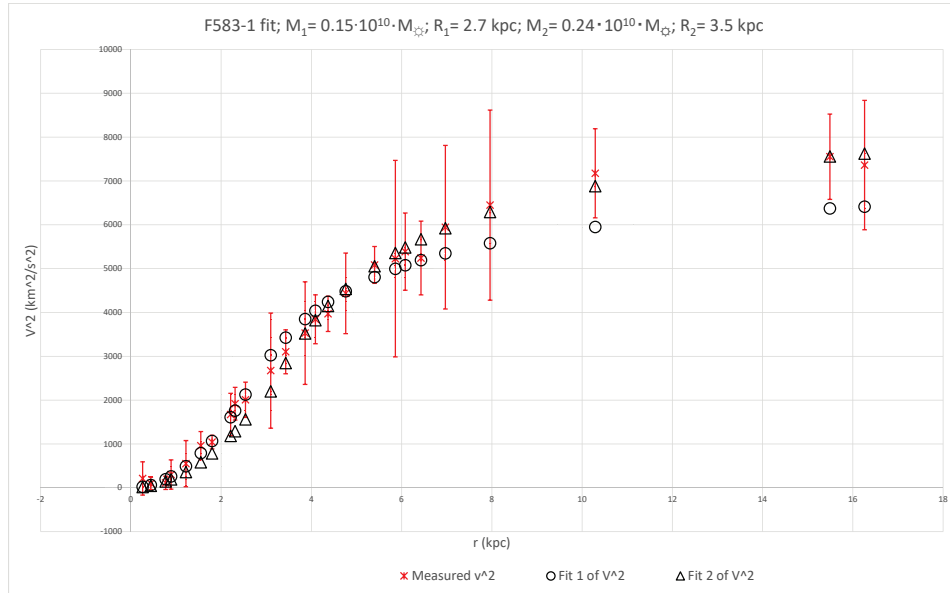


FIG. 53. F583-1

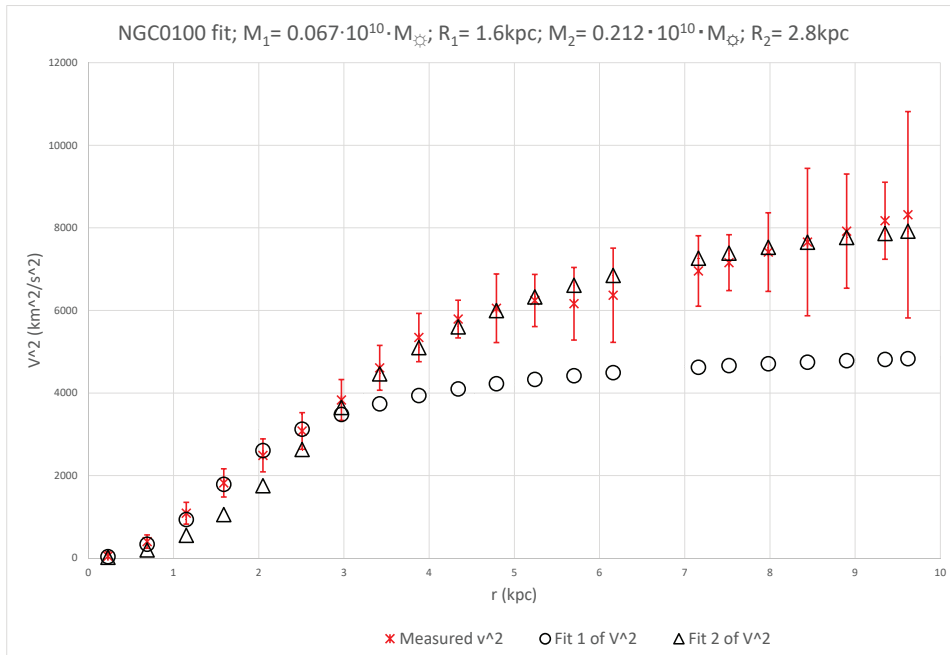


FIG. 54. NGC0100

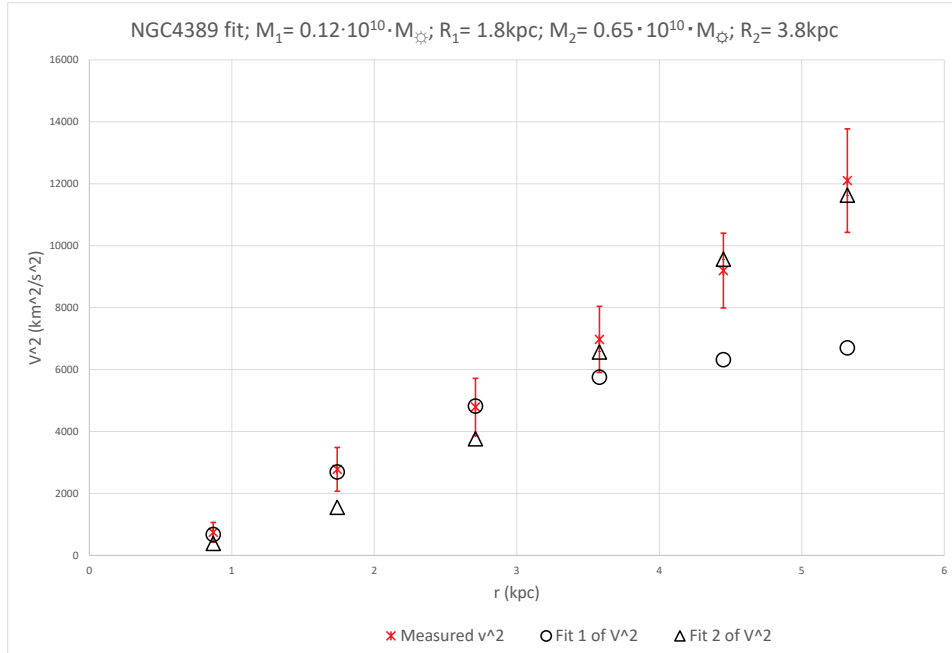


FIG. 55. NGC4389

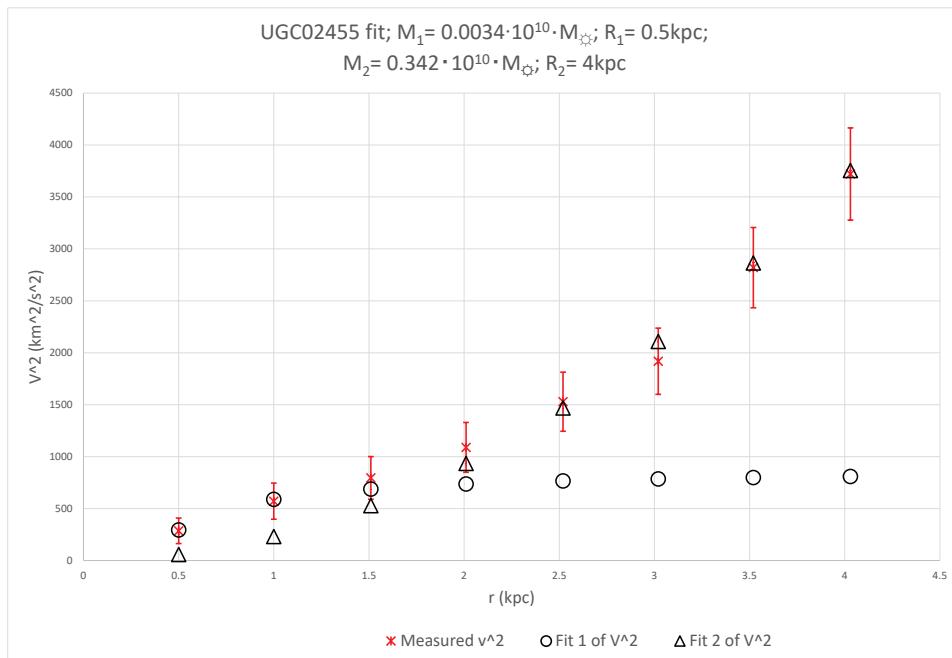


FIG. 56. UGC02455

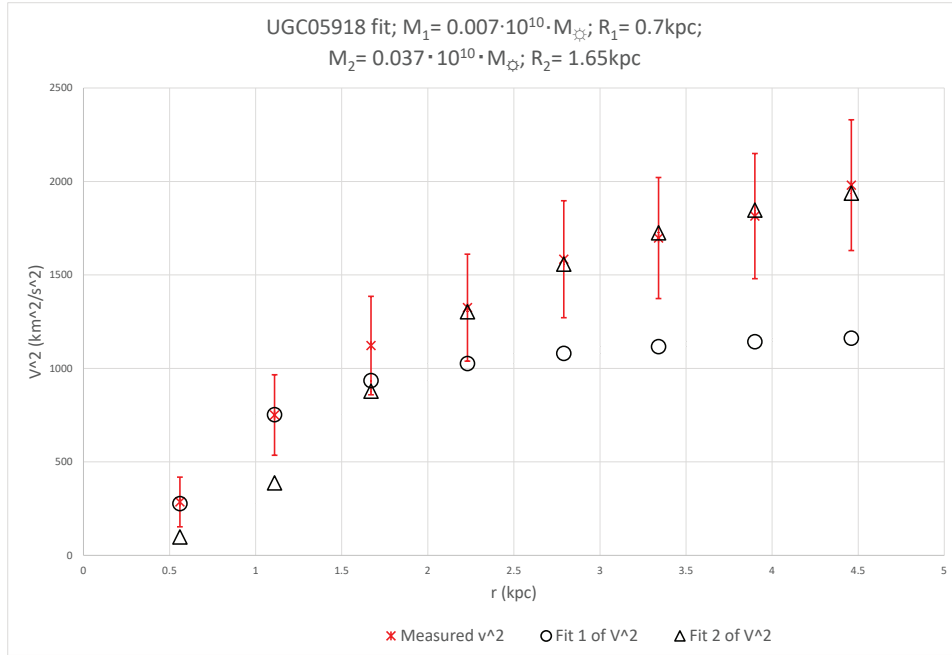


FIG. 57. UGC05918

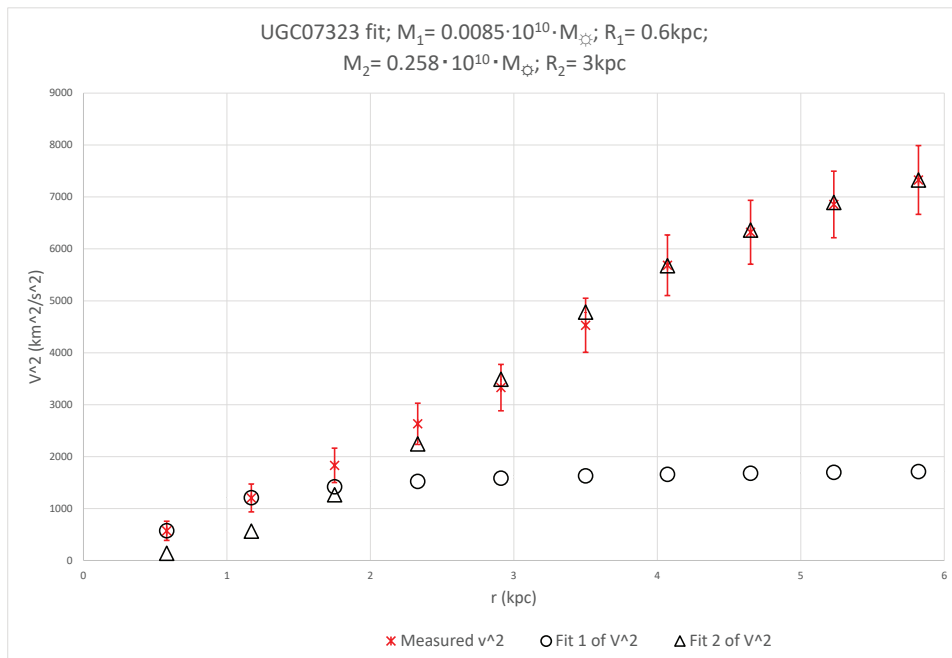


FIG. 58. UGC07323

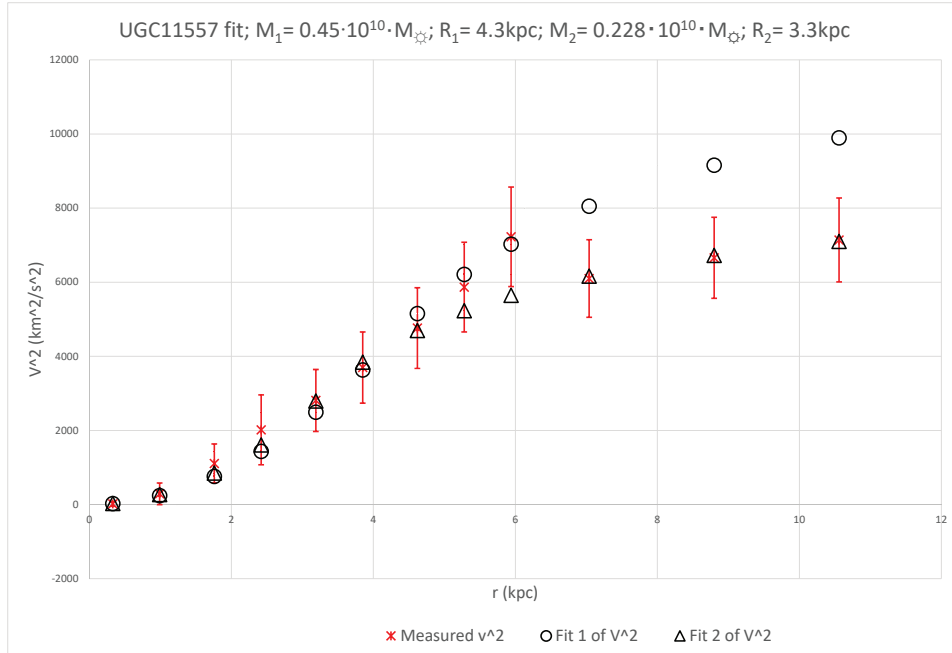


FIG. 59. UGC11557

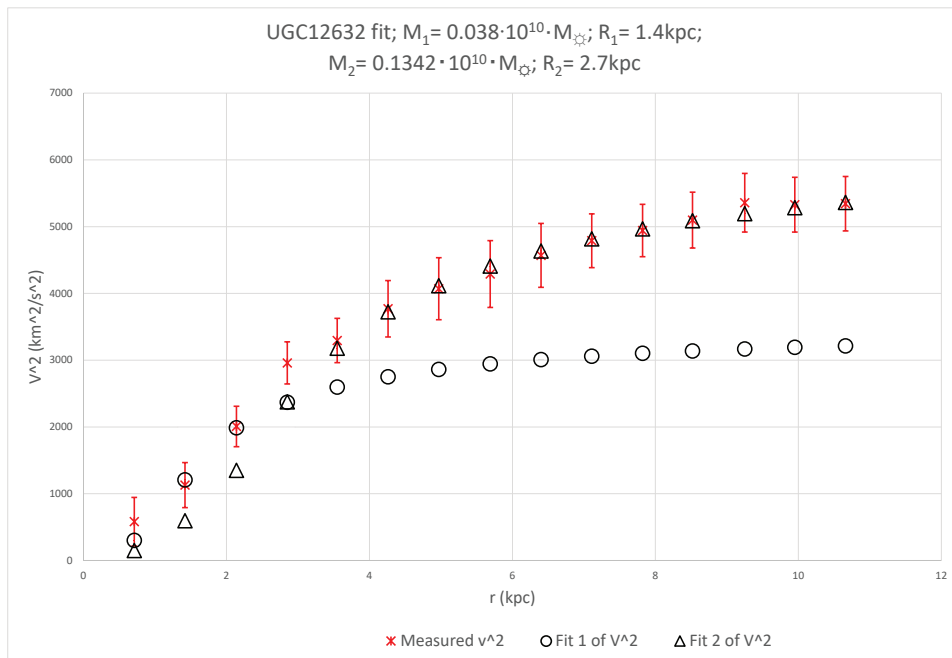


FIG. 60. UGC12632

## Appendix C: Abrupt transition crossover dual fit galaxies

### 1. Upwards abrupt crossover transition

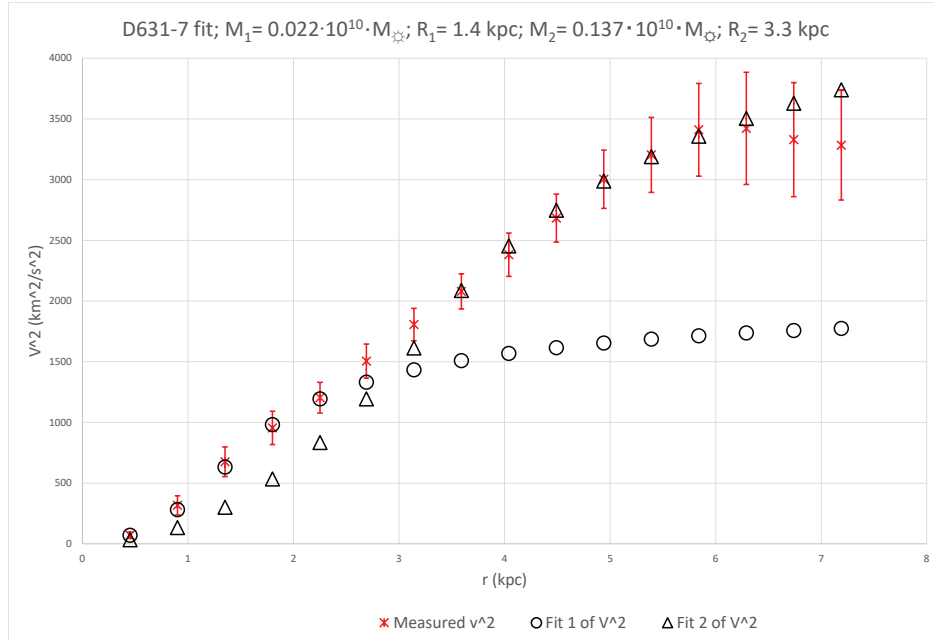


FIG. 61. D631-7

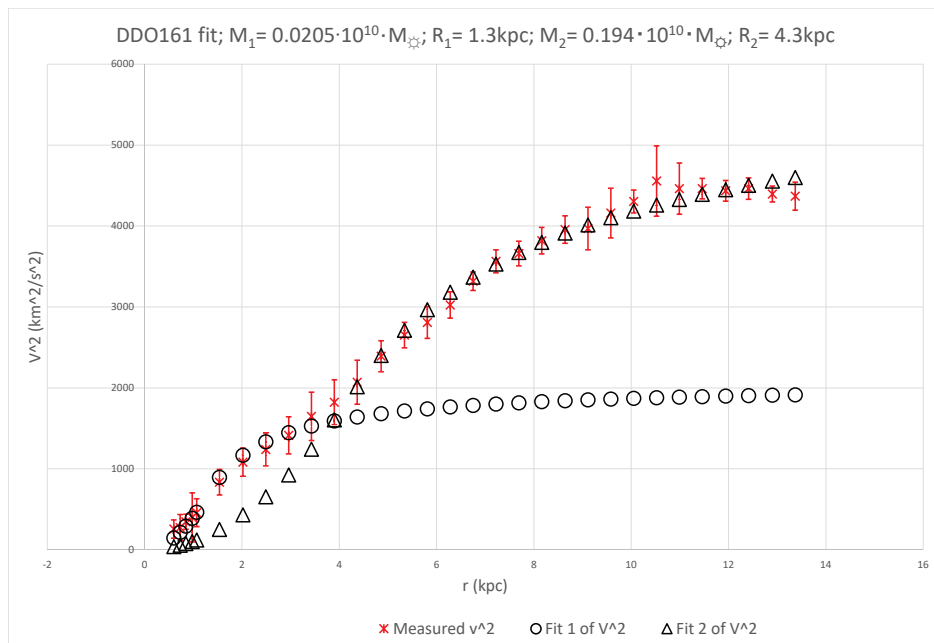


FIG. 62. DDO161

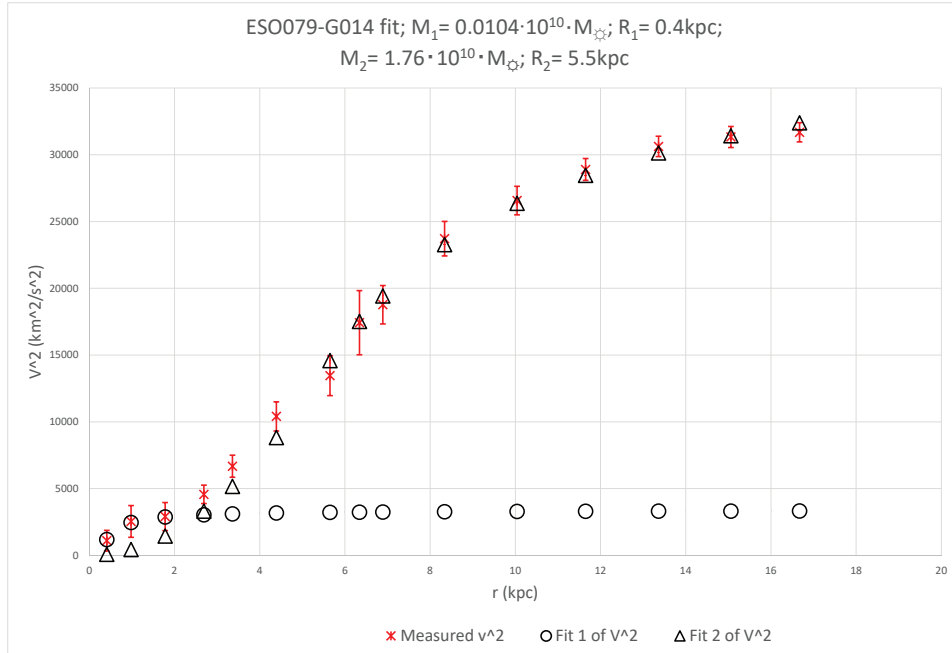


FIG. 63. ESO079-G014

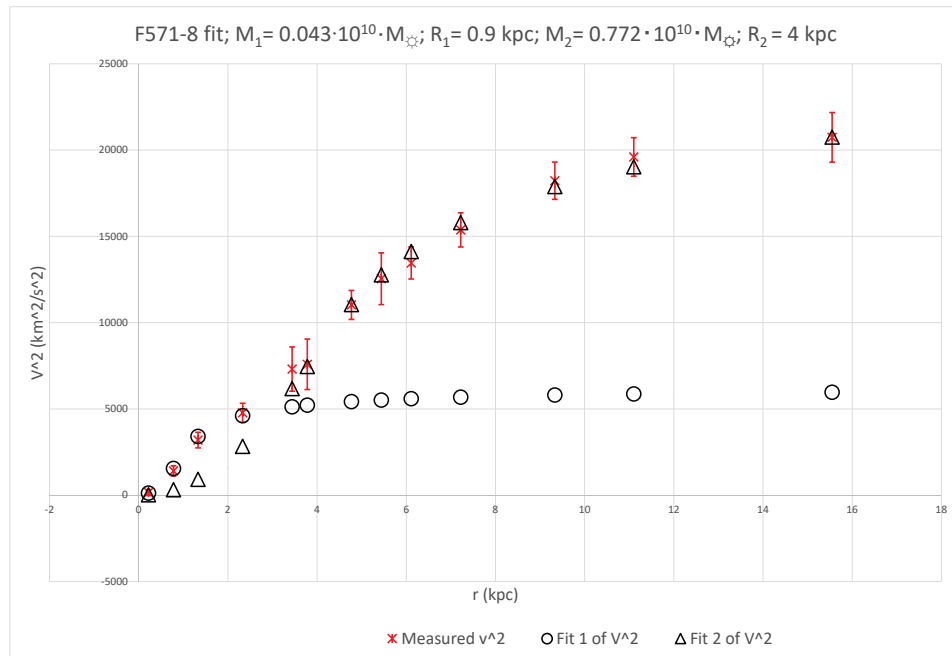


FIG. 64. F571-8

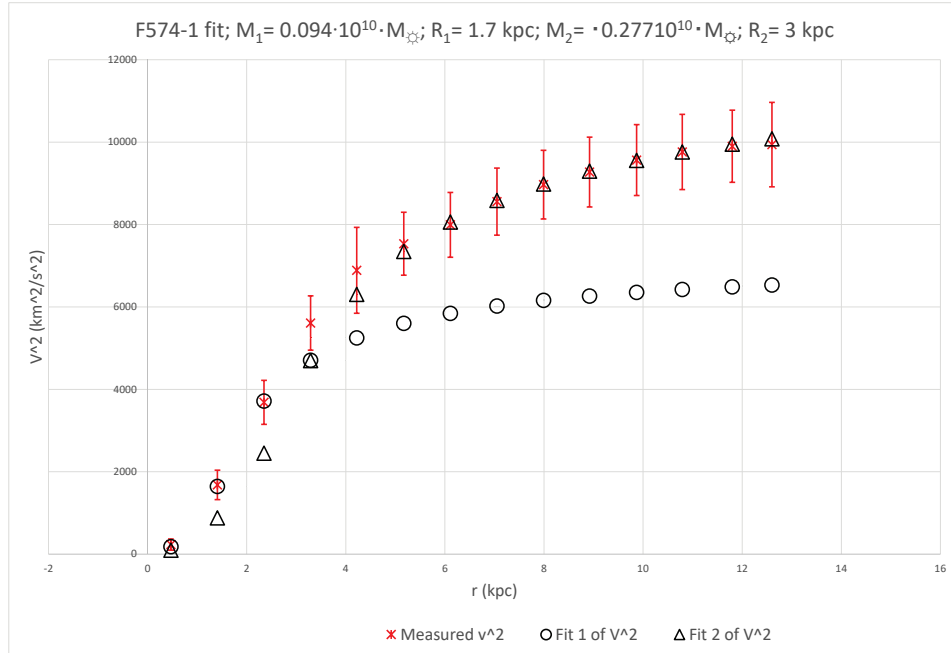


FIG. 65. F574-1

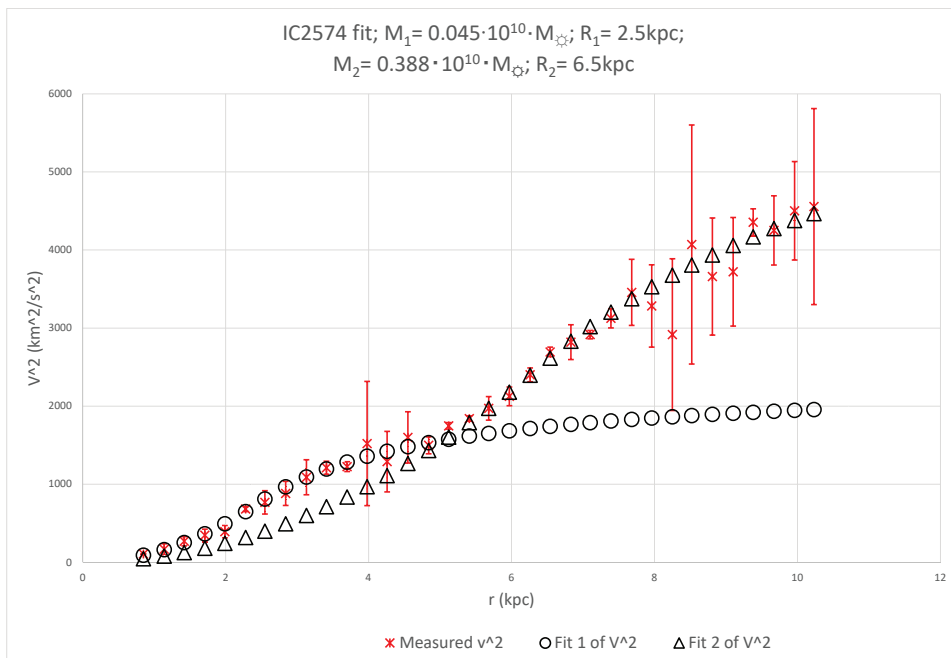


FIG. 66. IC2574

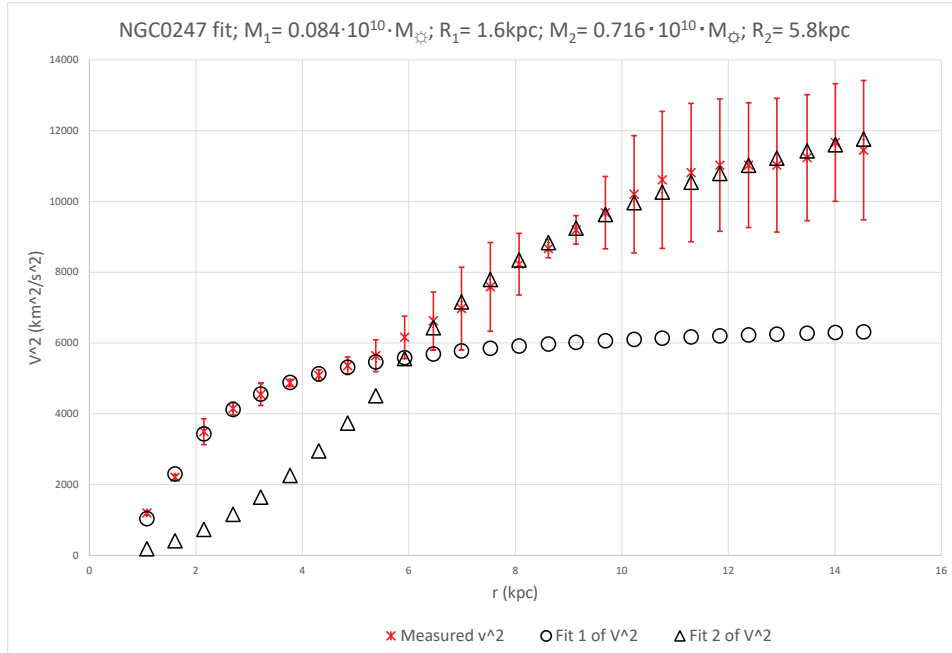


FIG. 67. NGC0247

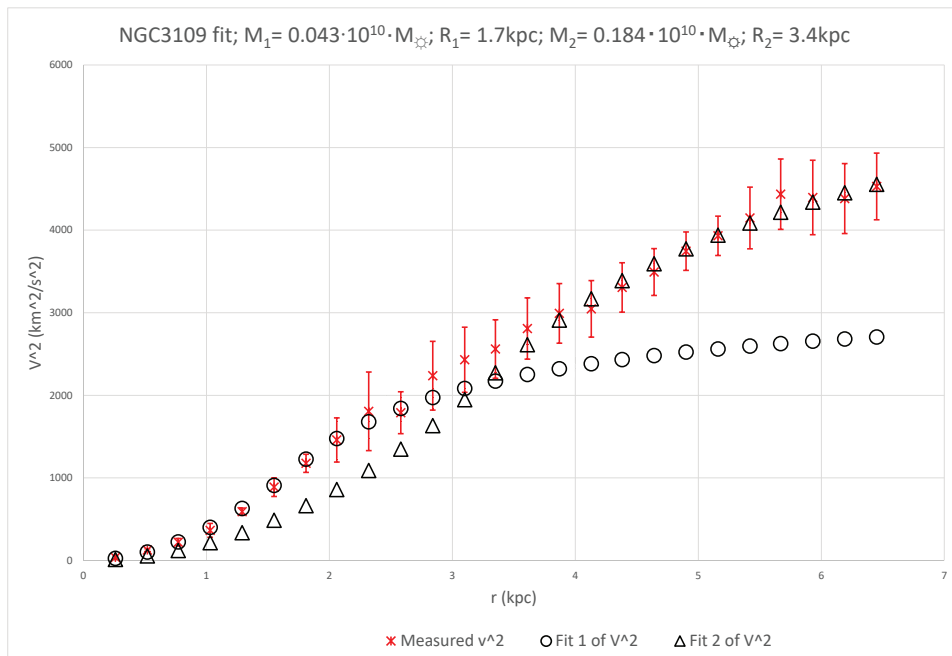


FIG. 68. NGC3109

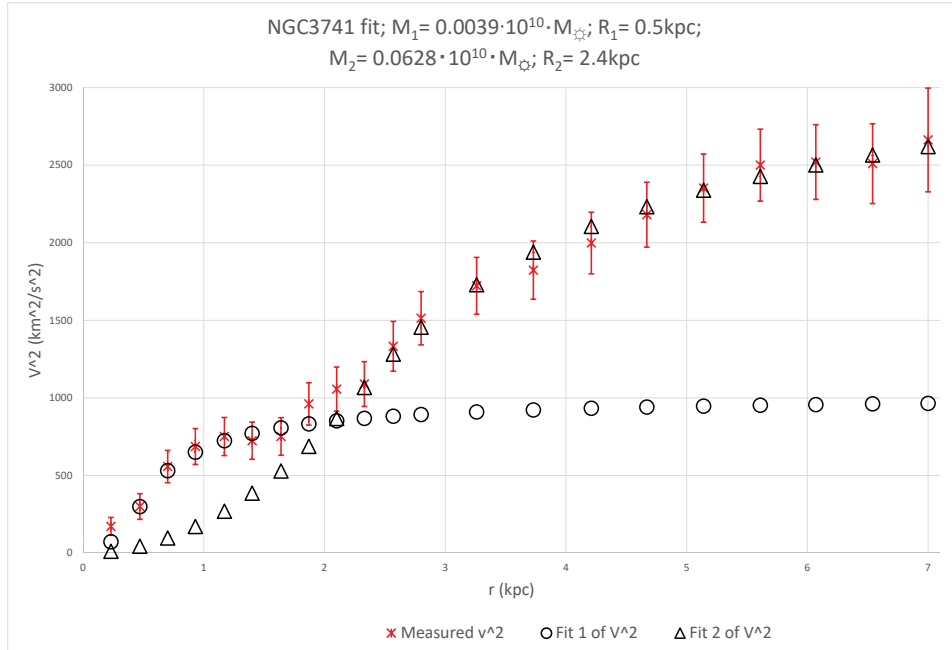


FIG. 69. NGC3741

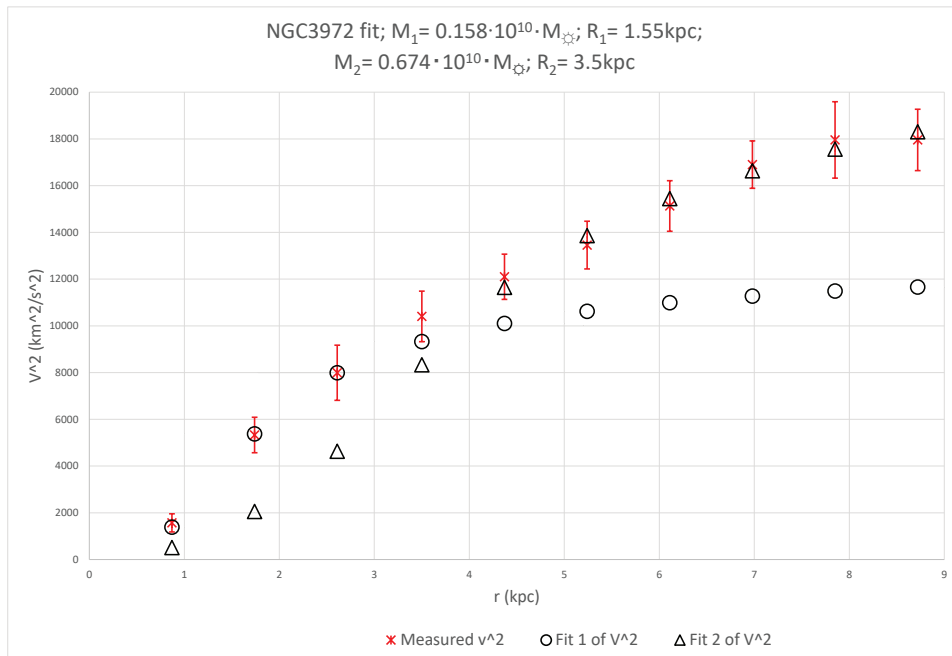


FIG. 70. NGC3972

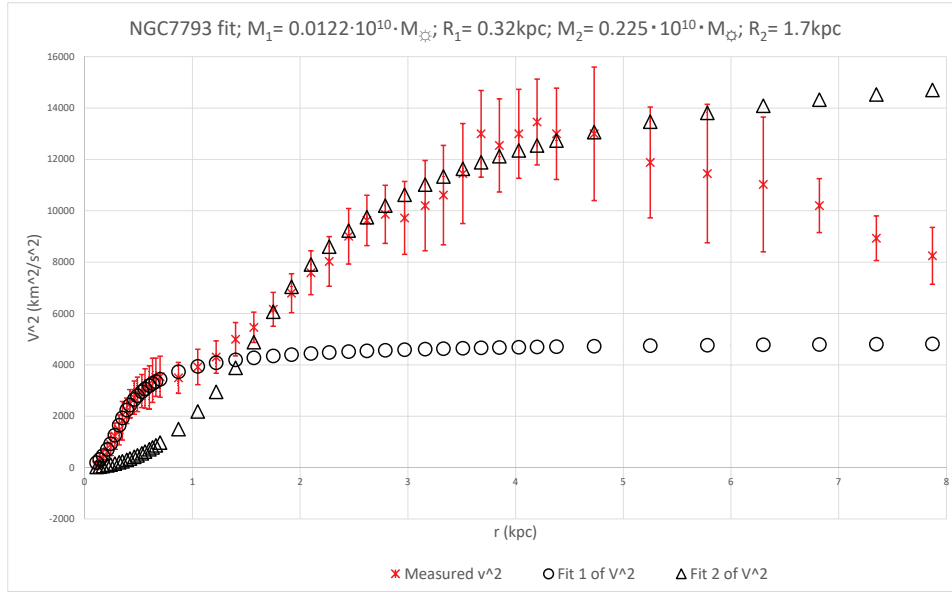


FIG. 71. NGC7793

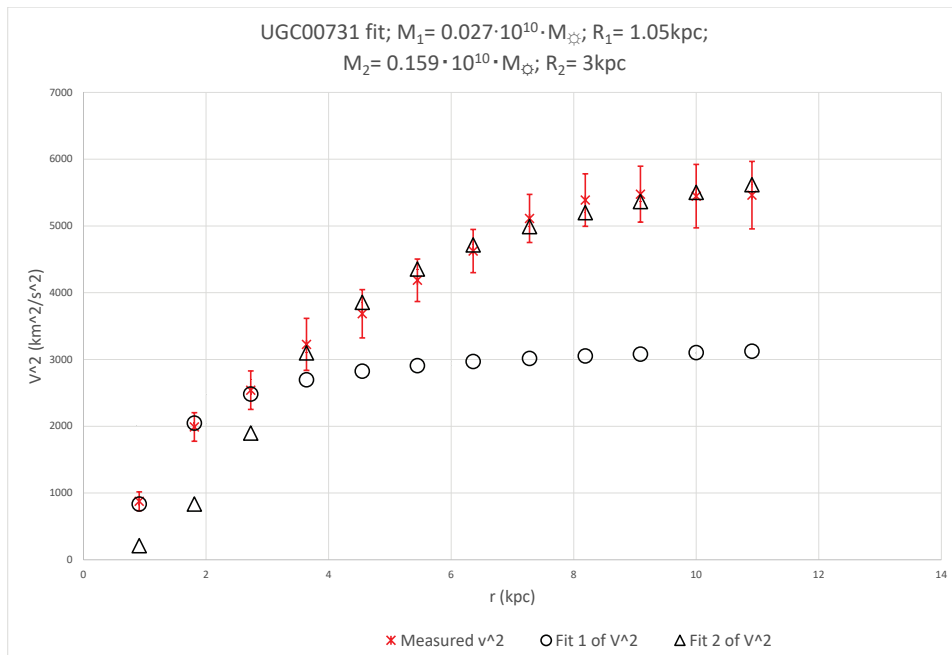


FIG. 72. UGC00731

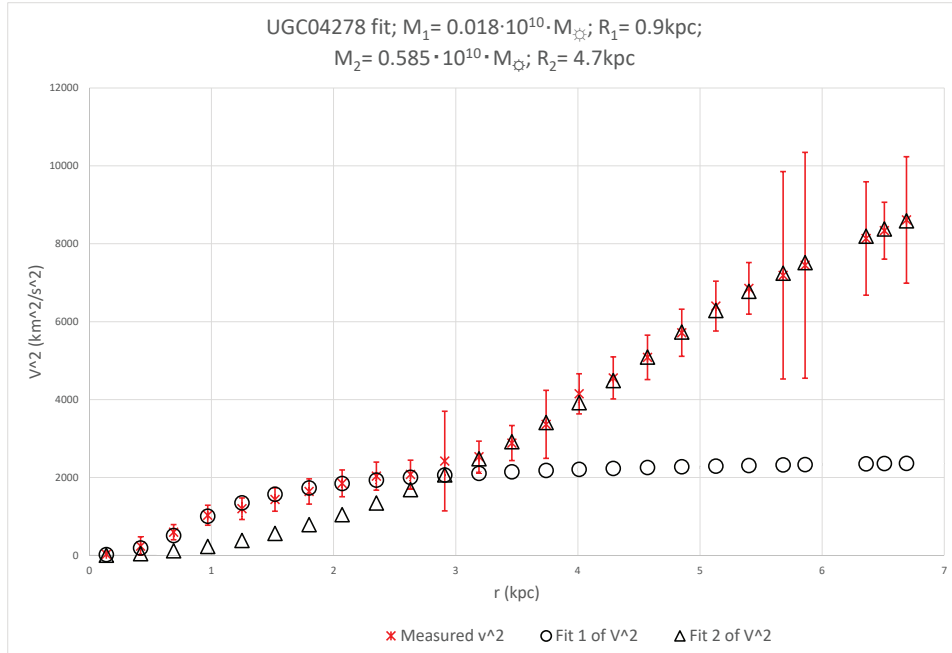


FIG. 73. UGC04278

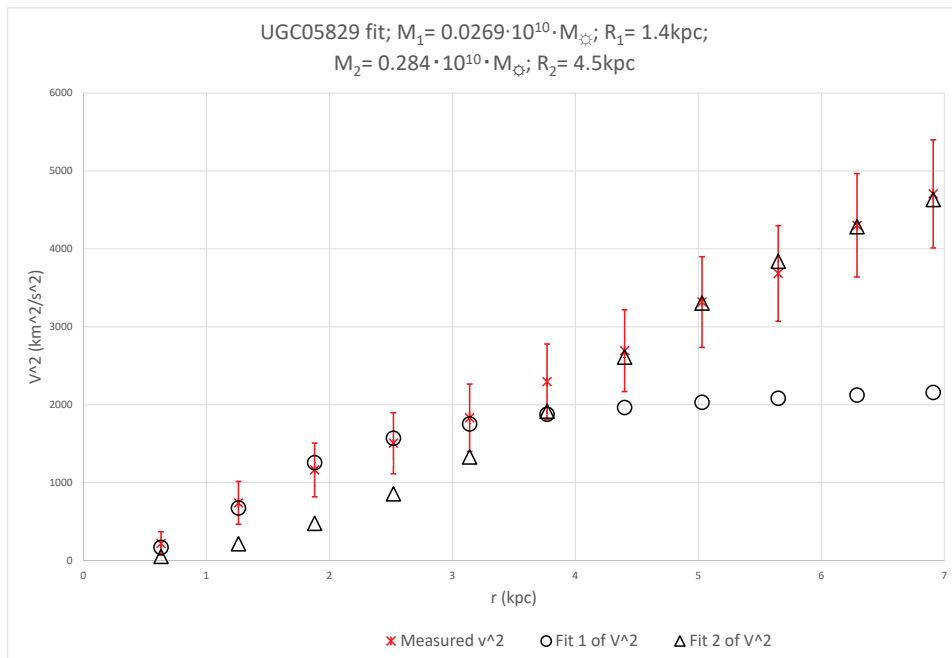


FIG. 74. UGC05829

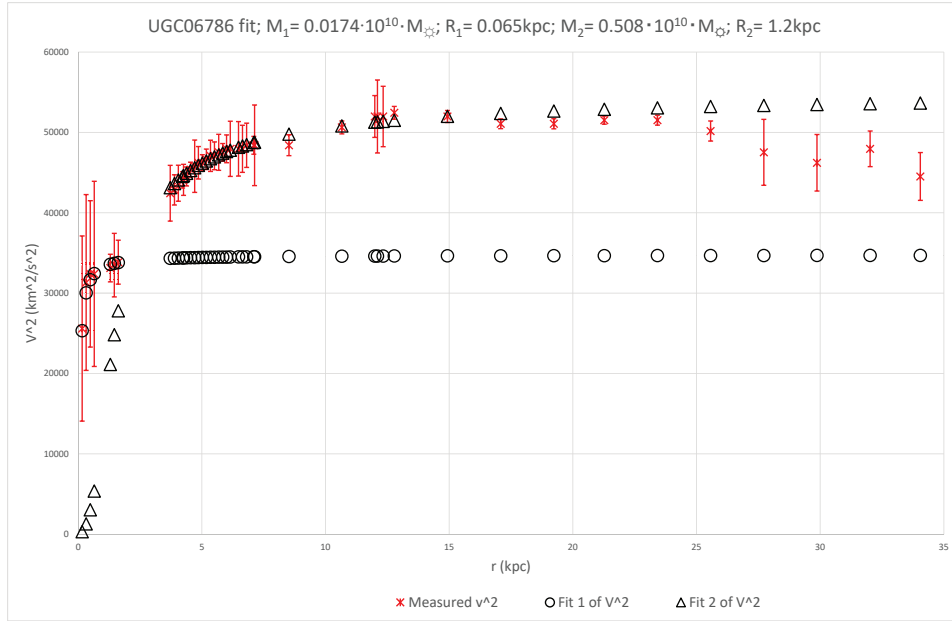


FIG. 75. UGC06786

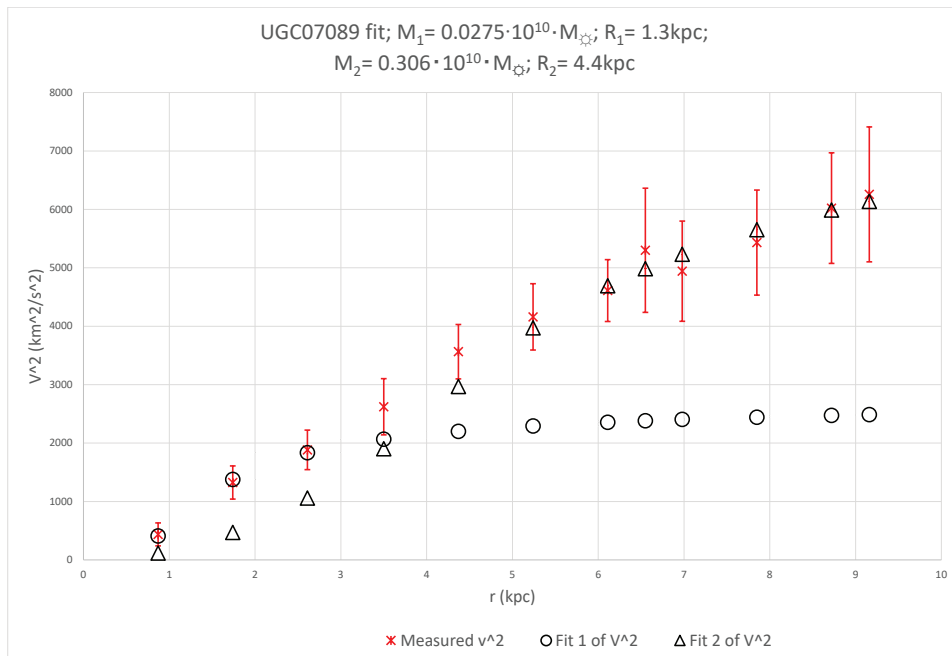


FIG. 76. UGC07089

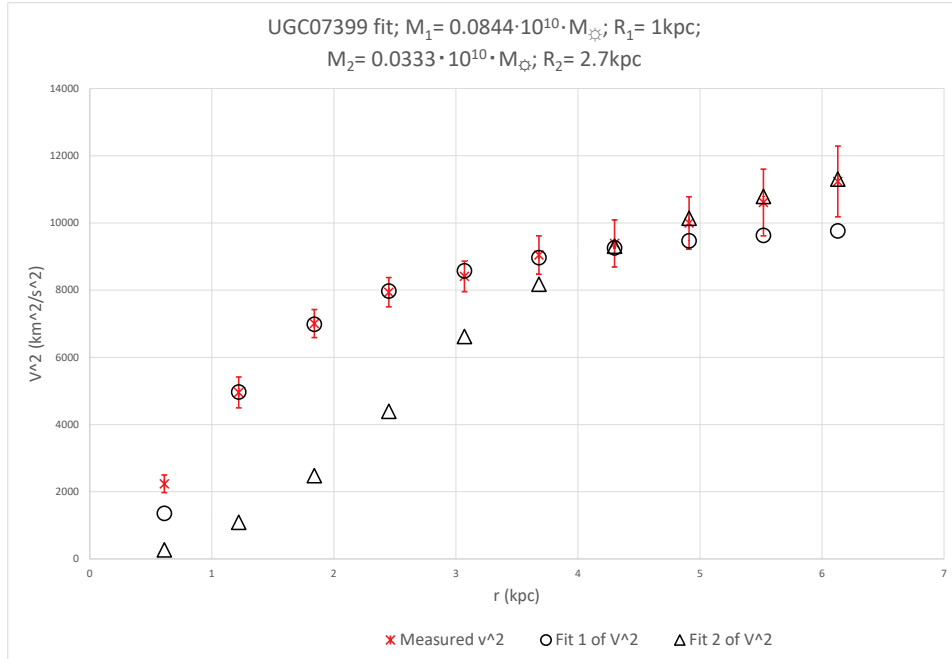


FIG. 77. UGC07399

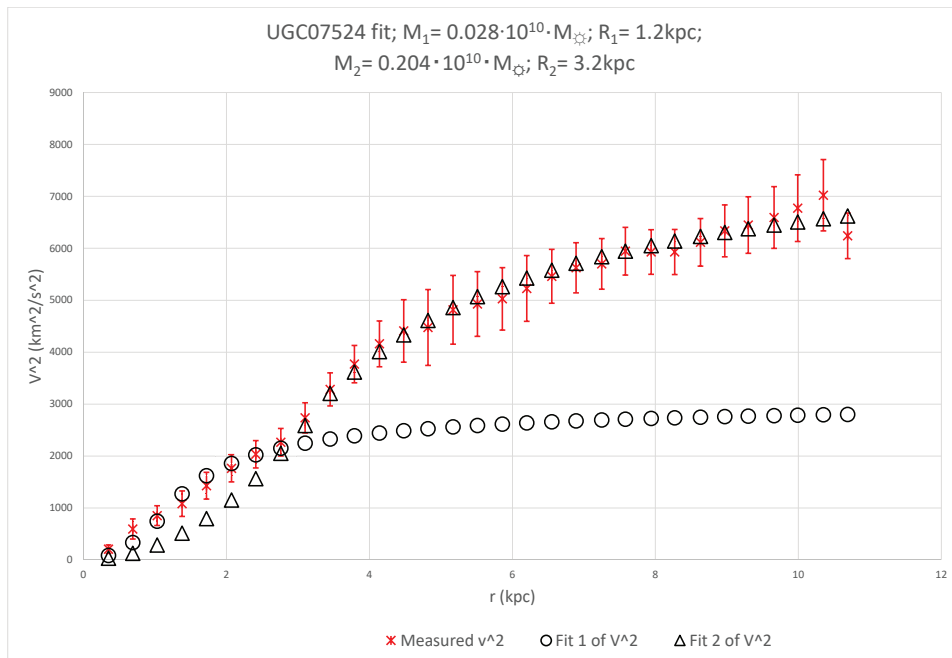


FIG. 78. UGC07524

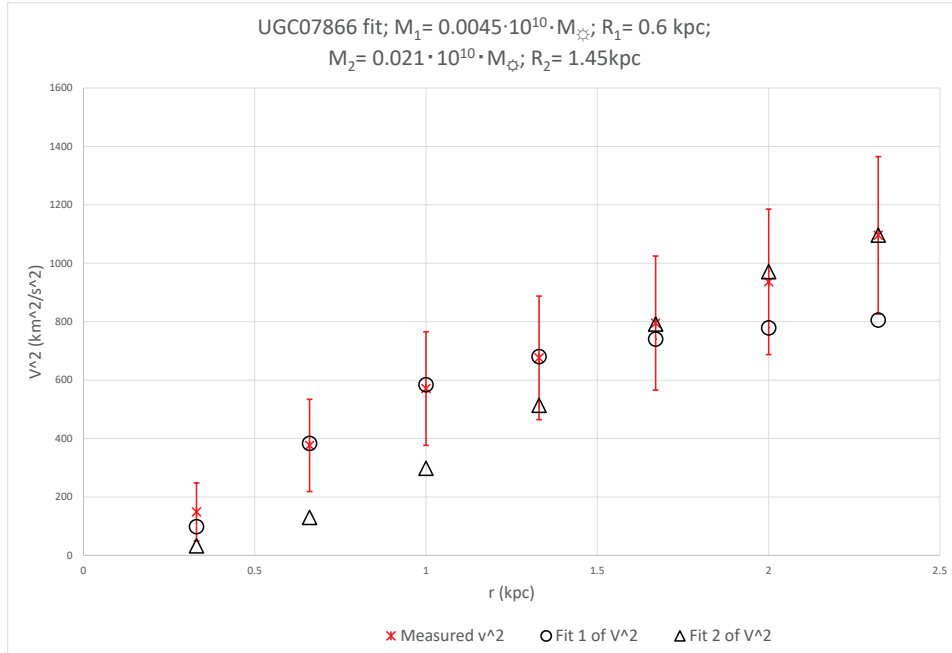


FIG. 79. UGC07866

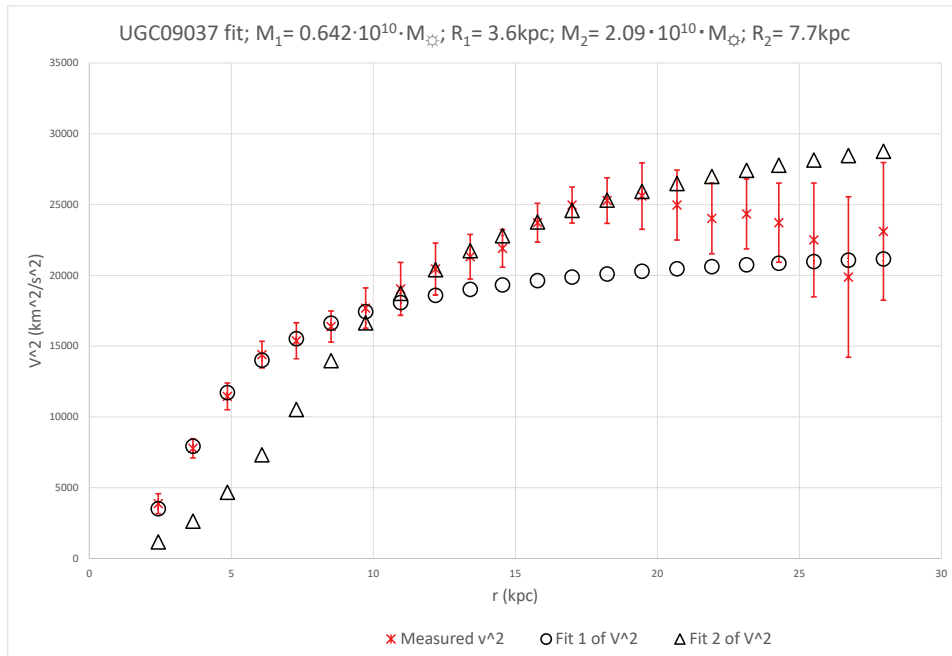


FIG. 80. UGC09037

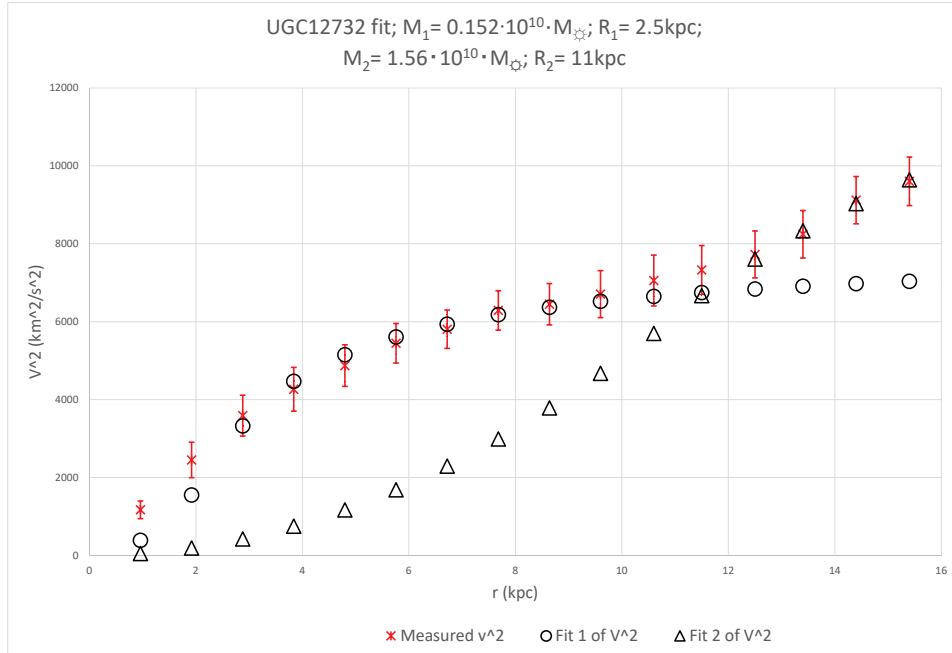


FIG. 81. UGC12732

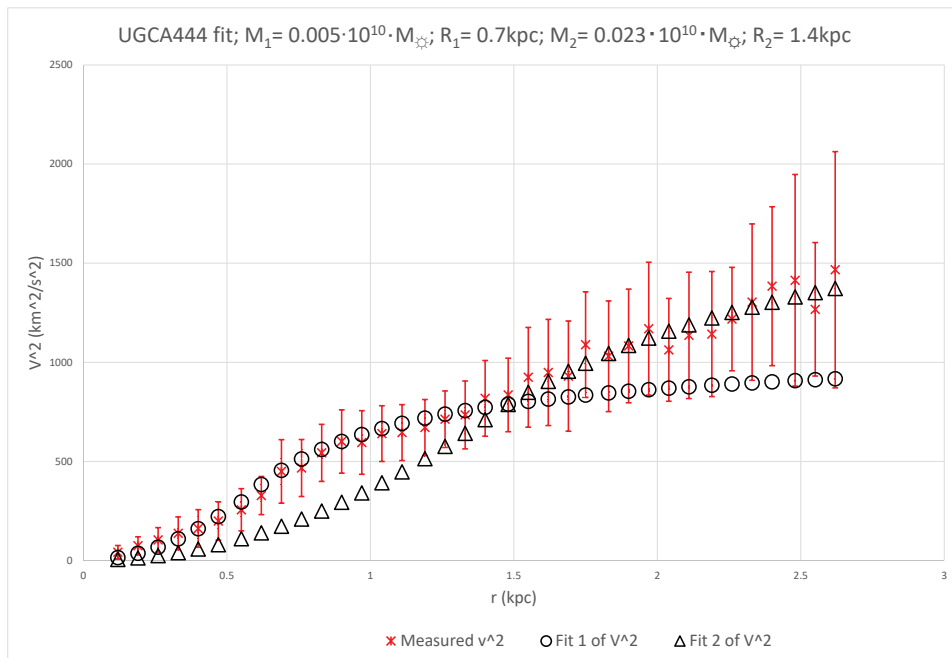


FIG. 82. UGCA444

## 2. Right corner abrupt crossover transition

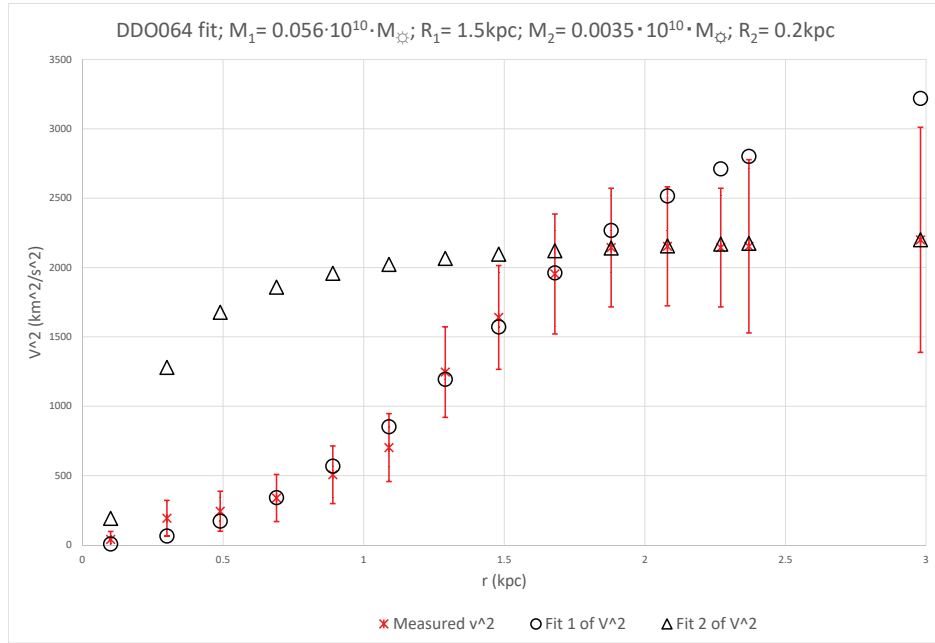


FIG. 83. DDO064

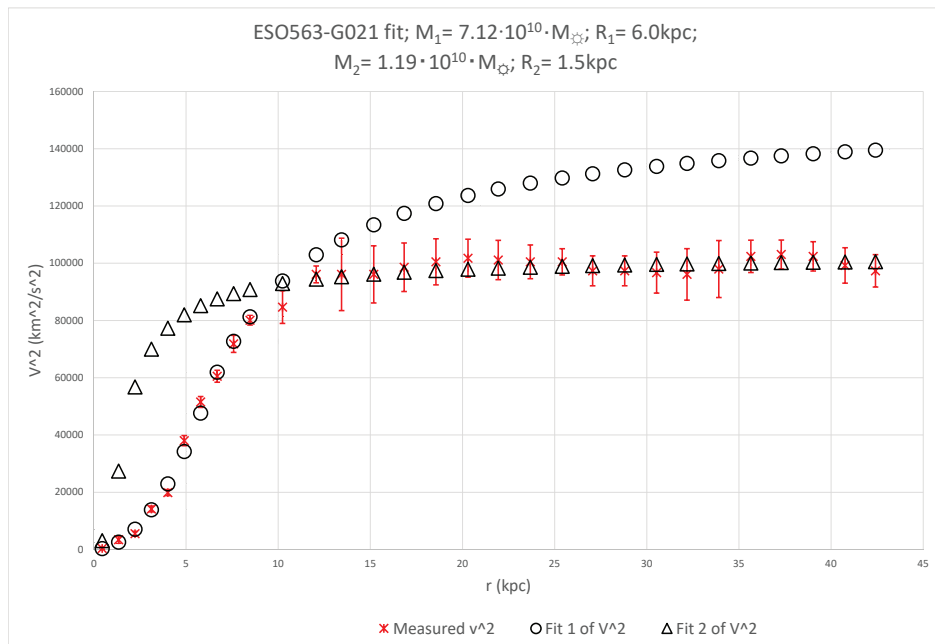


FIG. 84. ESO563-G021

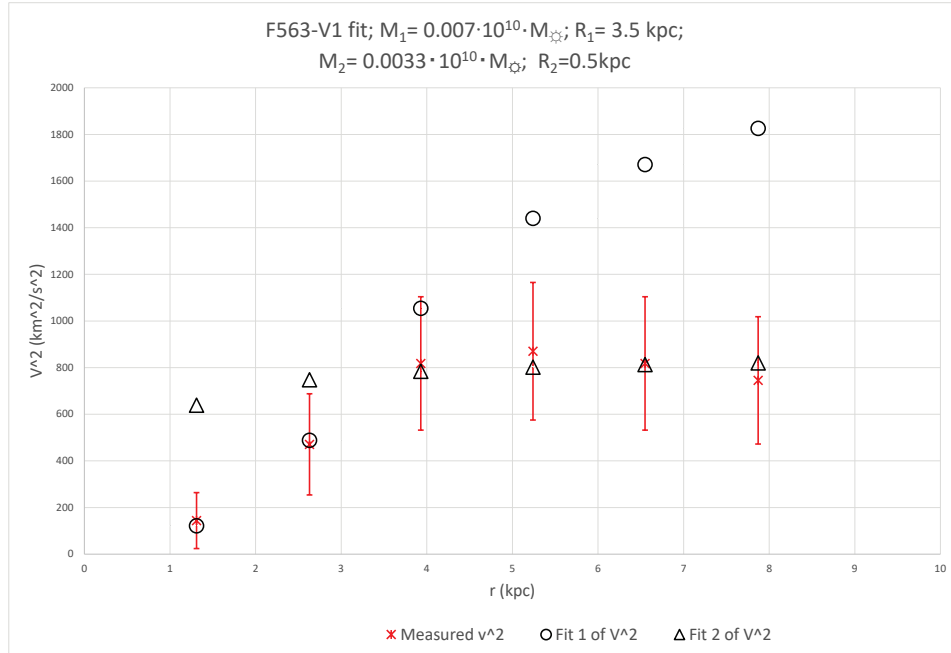


FIG. 85. F563-V1

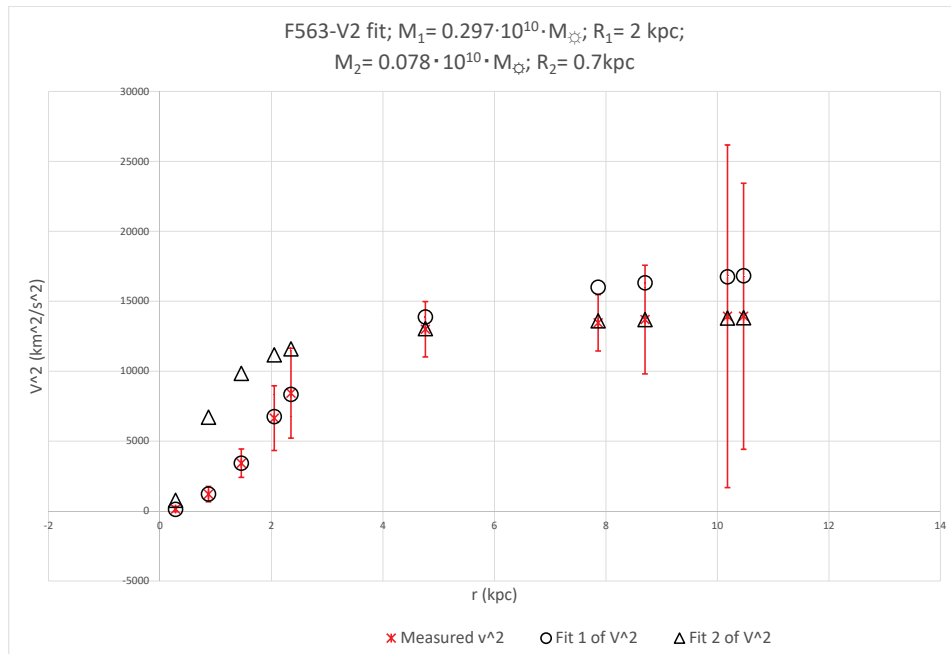


FIG. 86. F563-V2

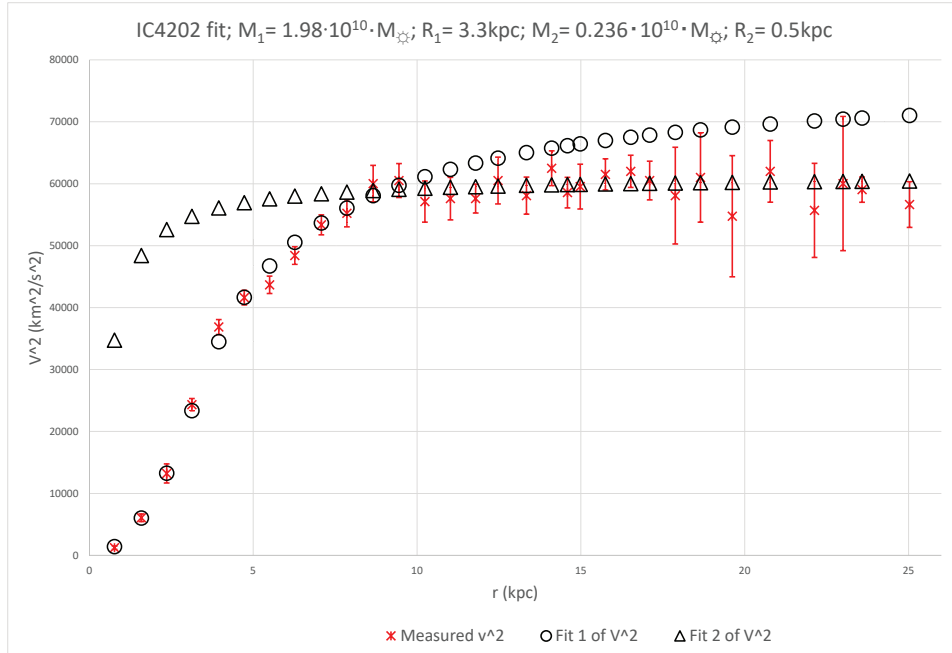


FIG. 87. IC4202

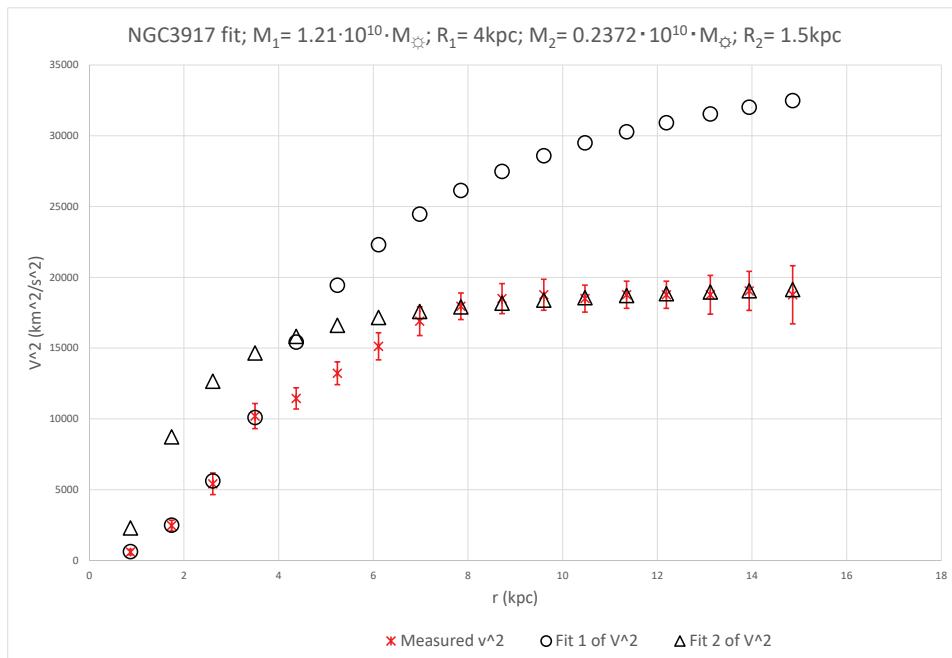


FIG. 88. NGC3917

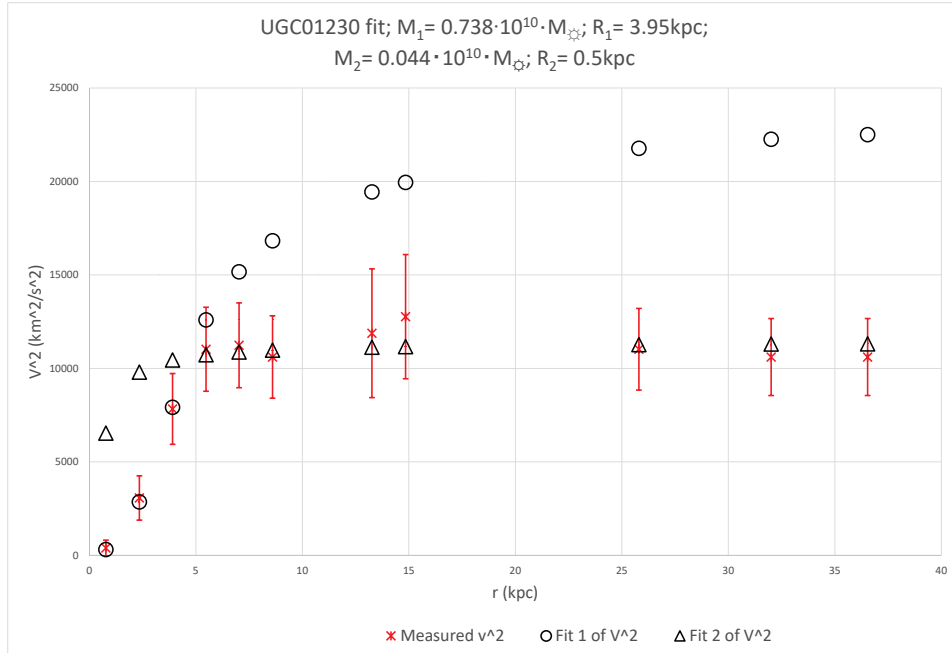


FIG. 89. UGC01230

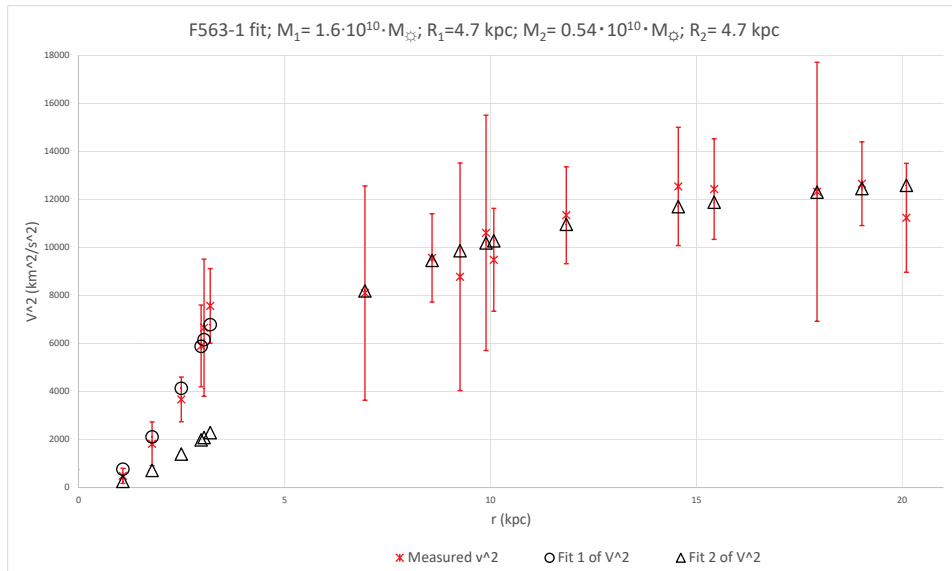


FIG. 90. F563-1

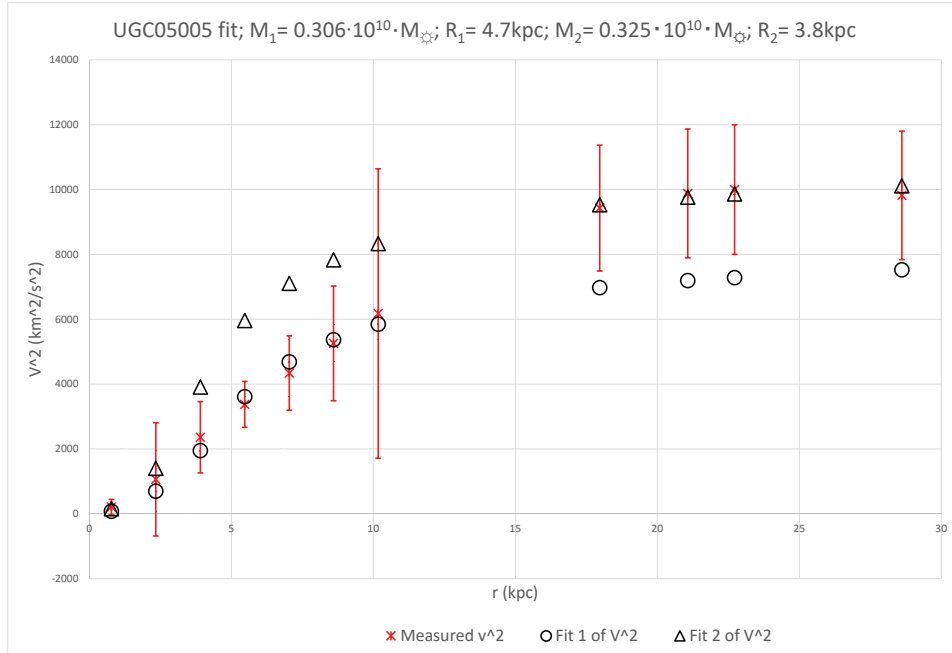


FIG. 91. UGC05005

## Appendix D: Non-crossover, parallel transition dual fit galaxies

### 1. Non-crossover upwards transition dual fit galaxies

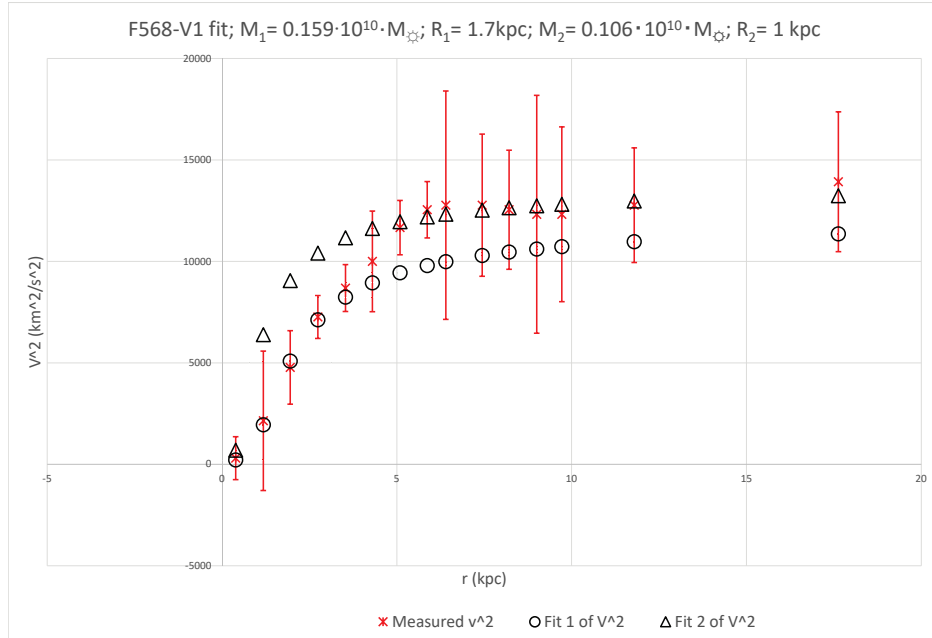


FIG. 92. F568-V1

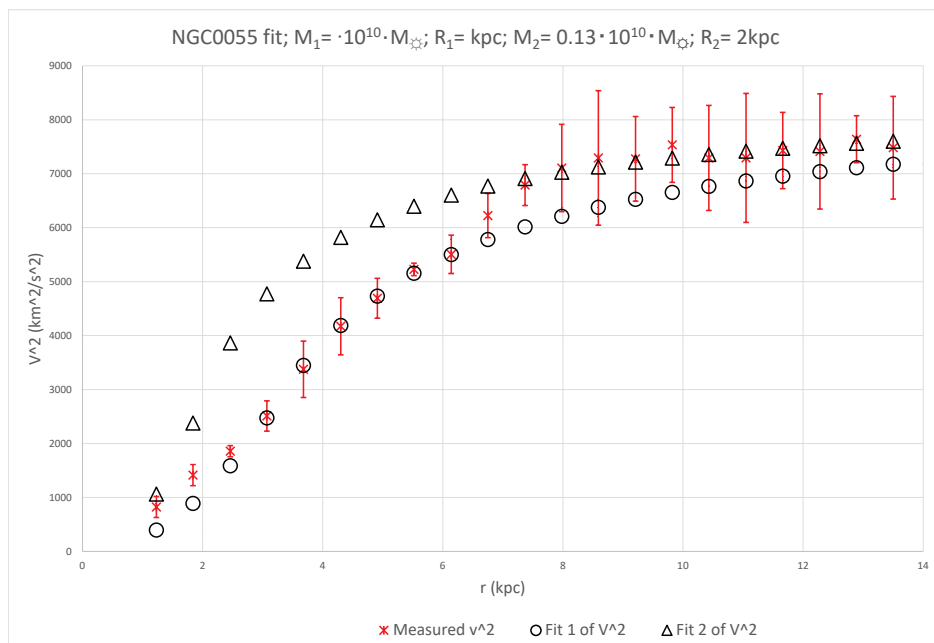


FIG. 93. NGC0055

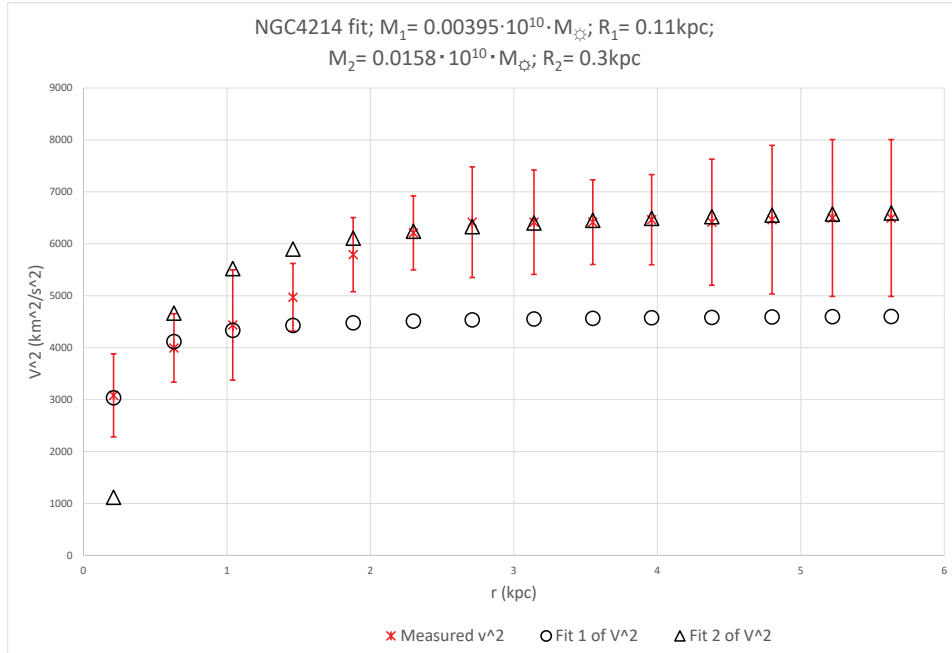


FIG. 94. NGC4214

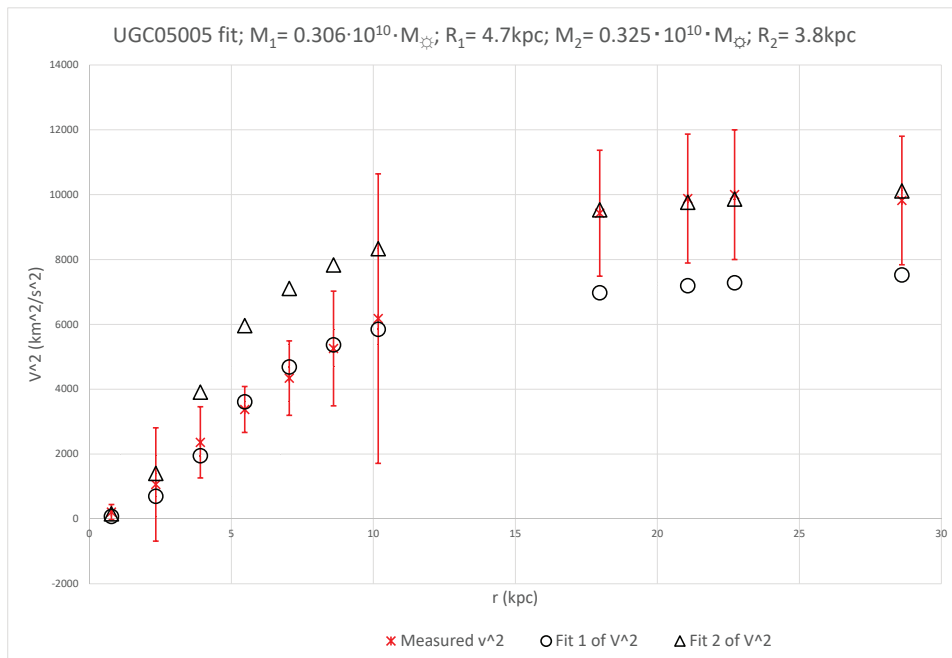


FIG. 95. UGC05005

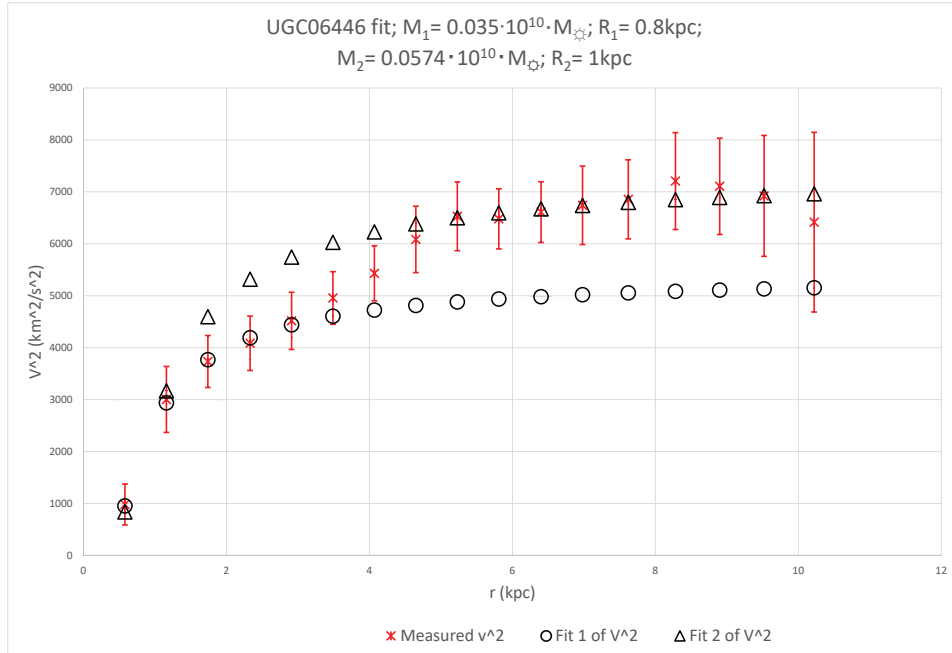


FIG. 96. UGC06446

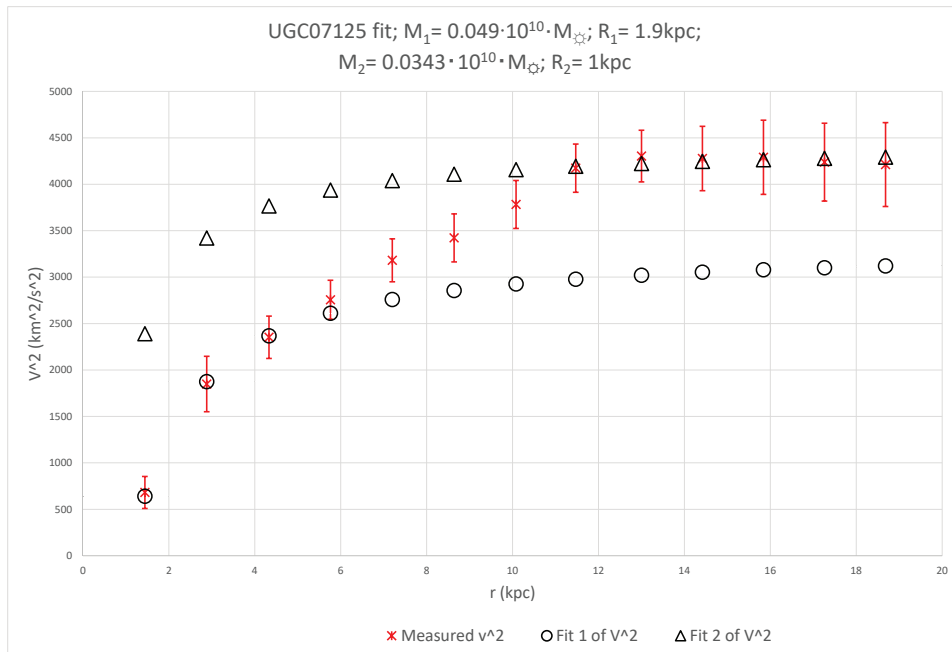


FIG. 97. UGC07125

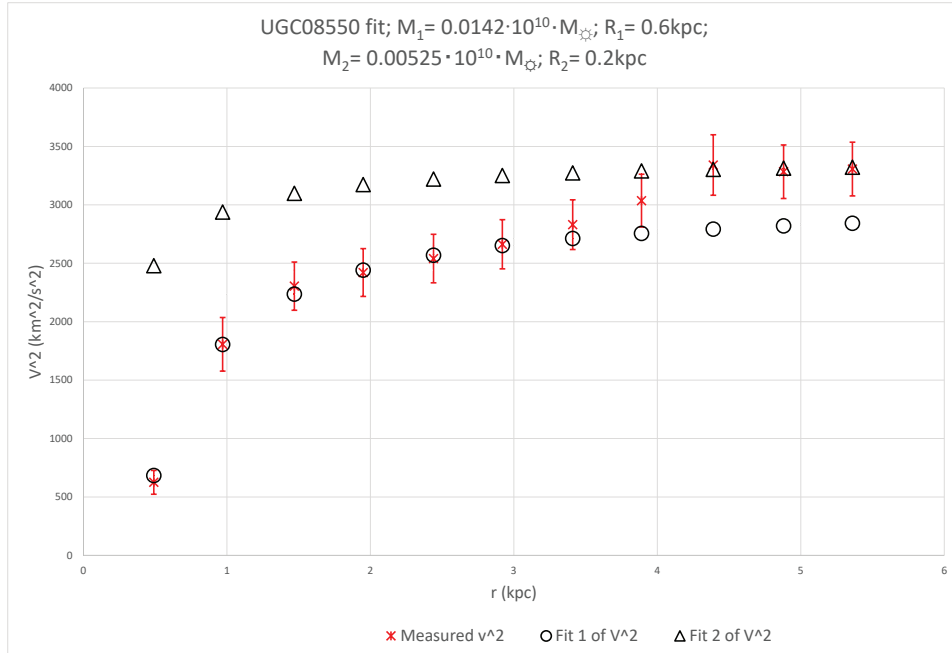


FIG. 98. UGC08550

## 2. Non-crossover downwards transition dual fit galaxies

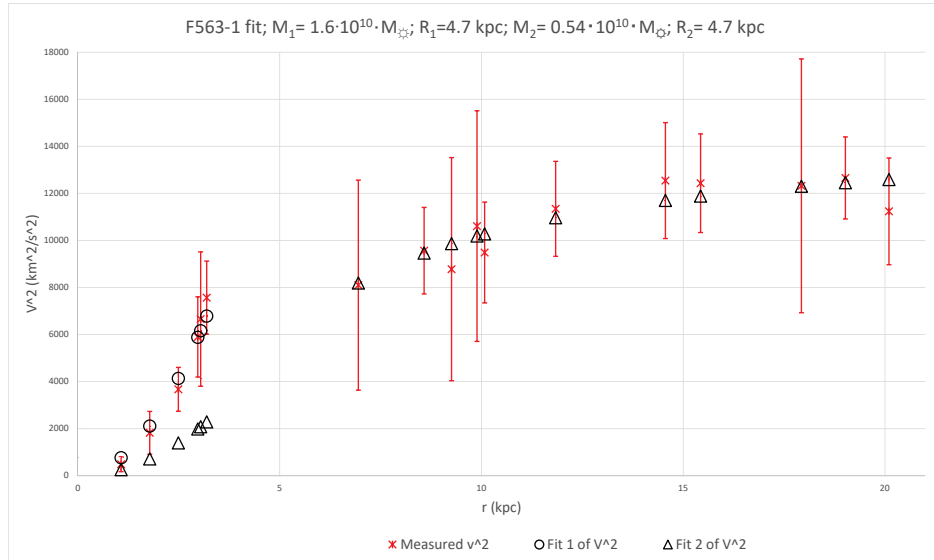


FIG. 99. F563-1

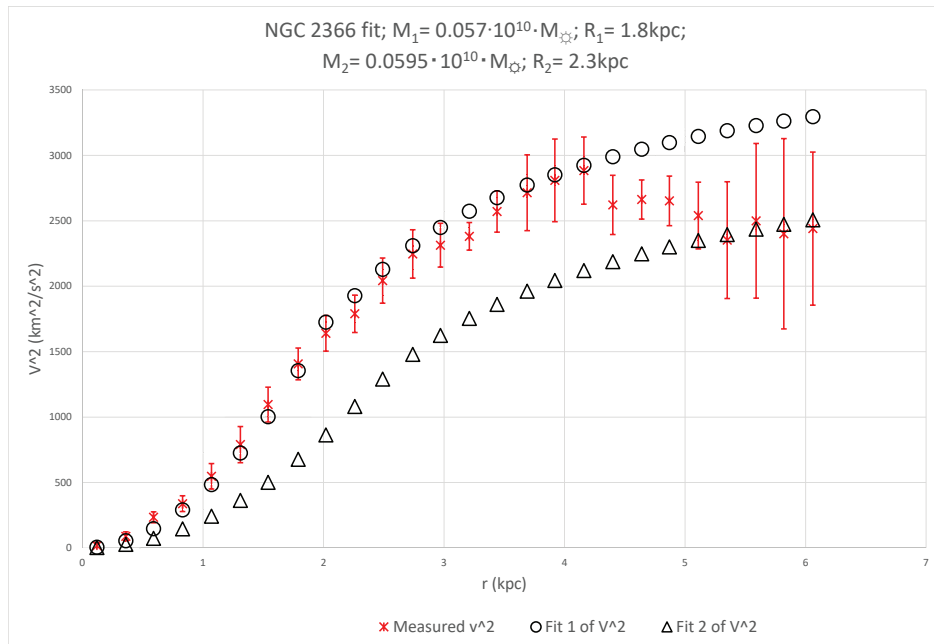


FIG. 100. NGC2366

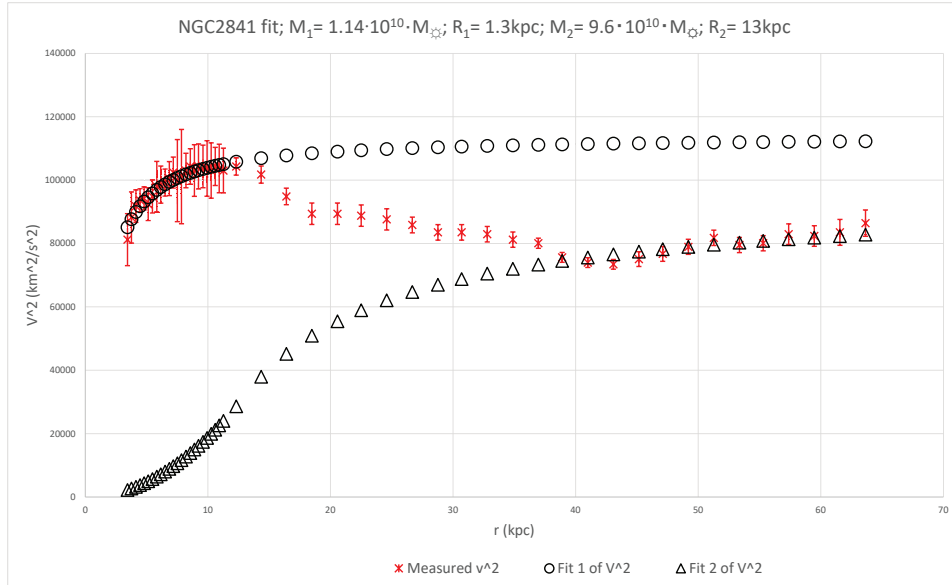


FIG. 101. NGC2841

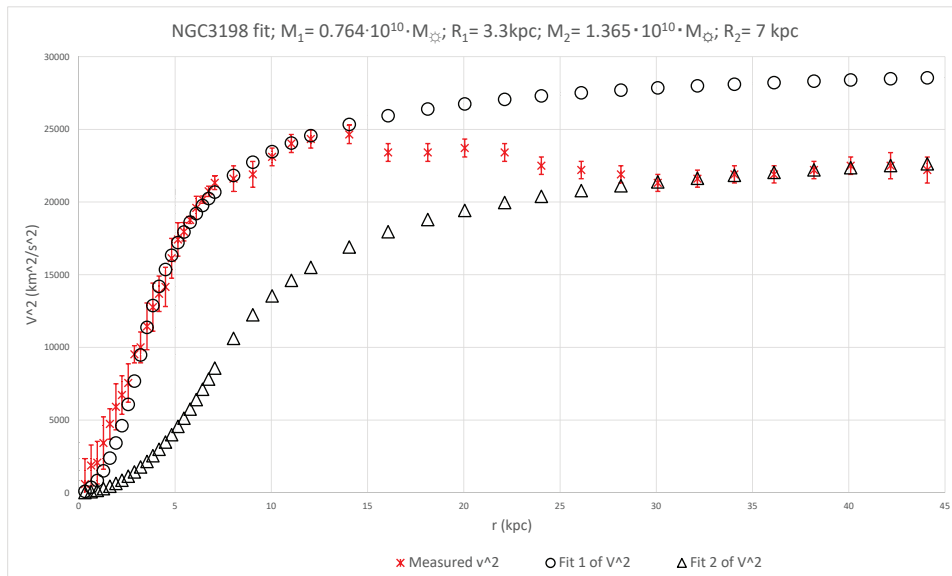


FIG. 102. NGC3198

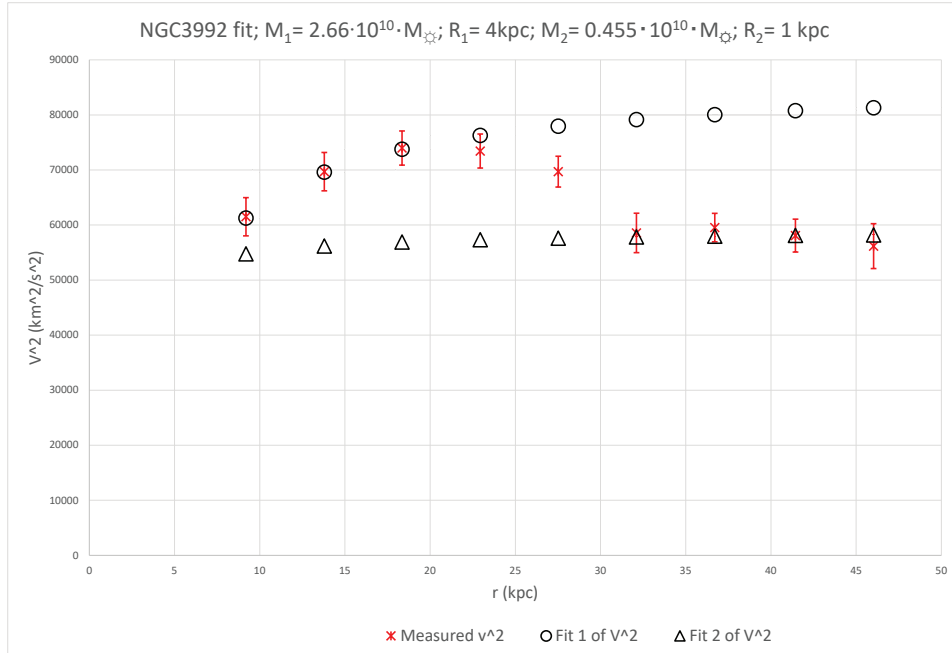


FIG. 103. NGC3992

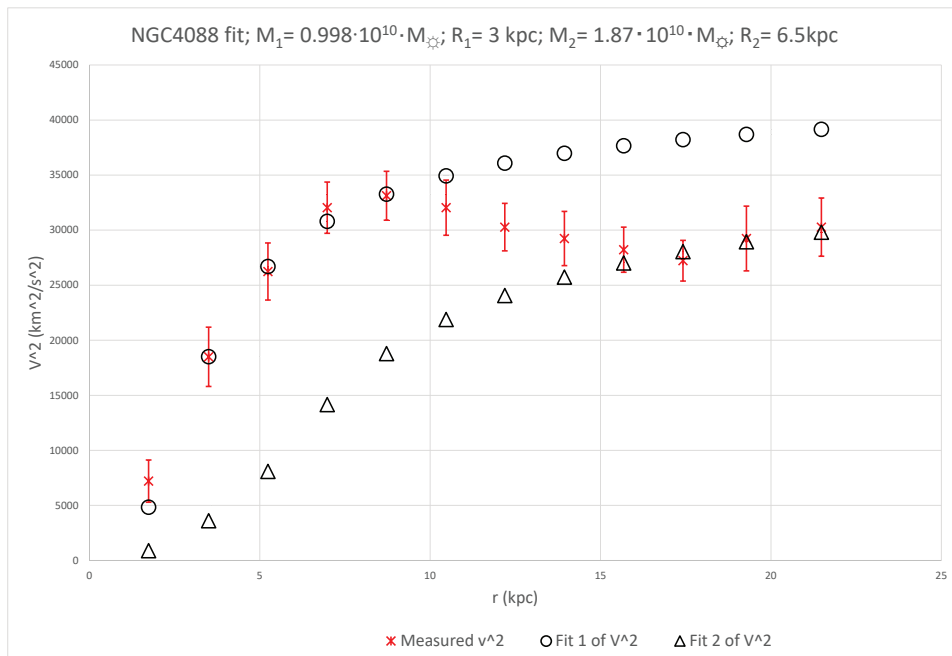


FIG. 104. NGC4088

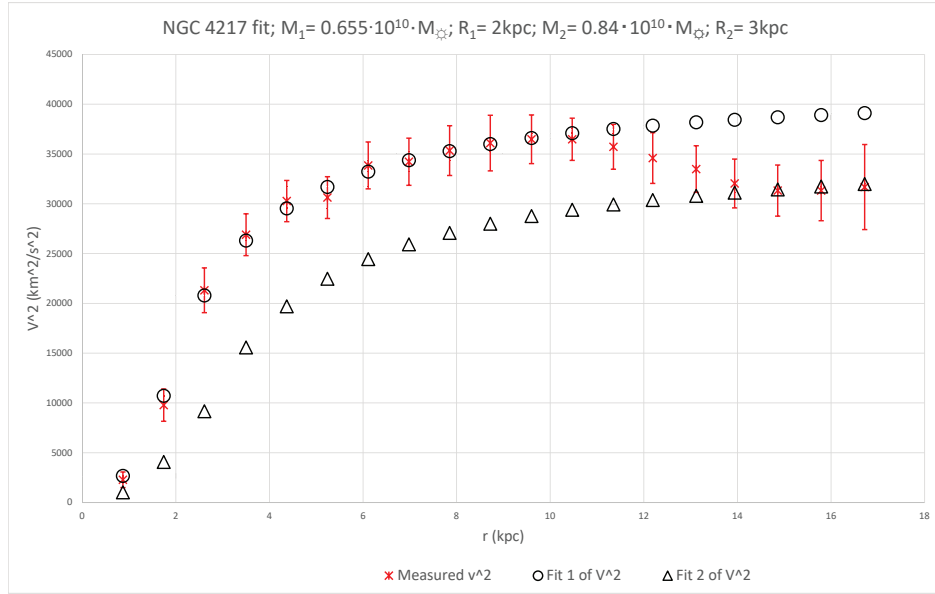


FIG. 105. NGC4217

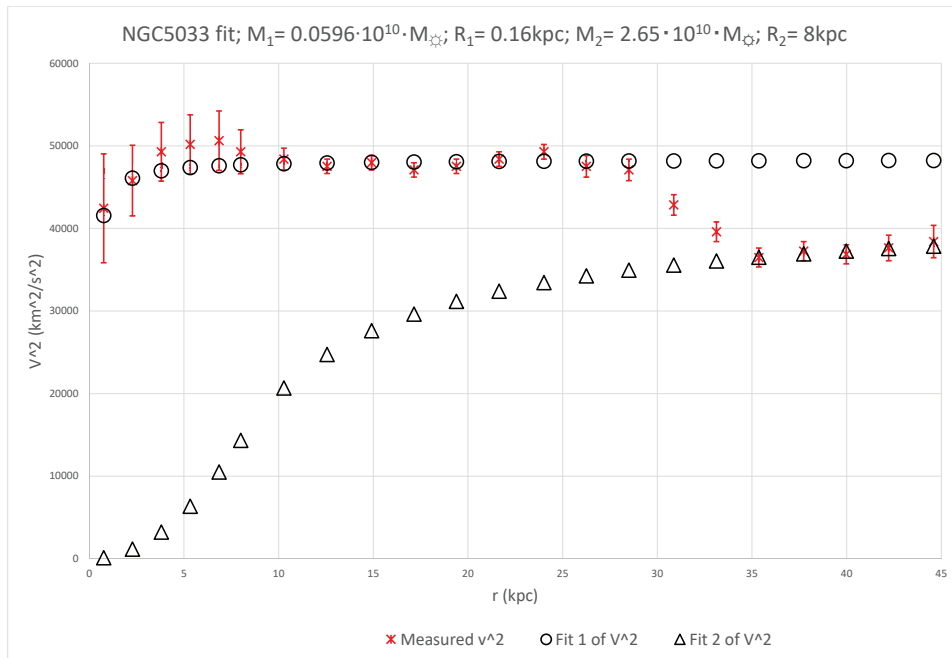


FIG. 106. NGC5033

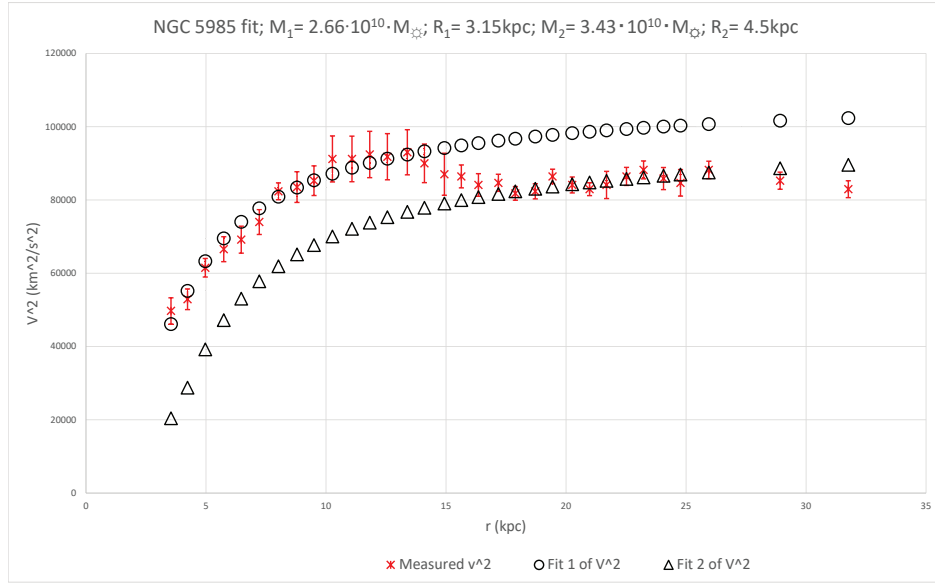


FIG. 107. NGC5985

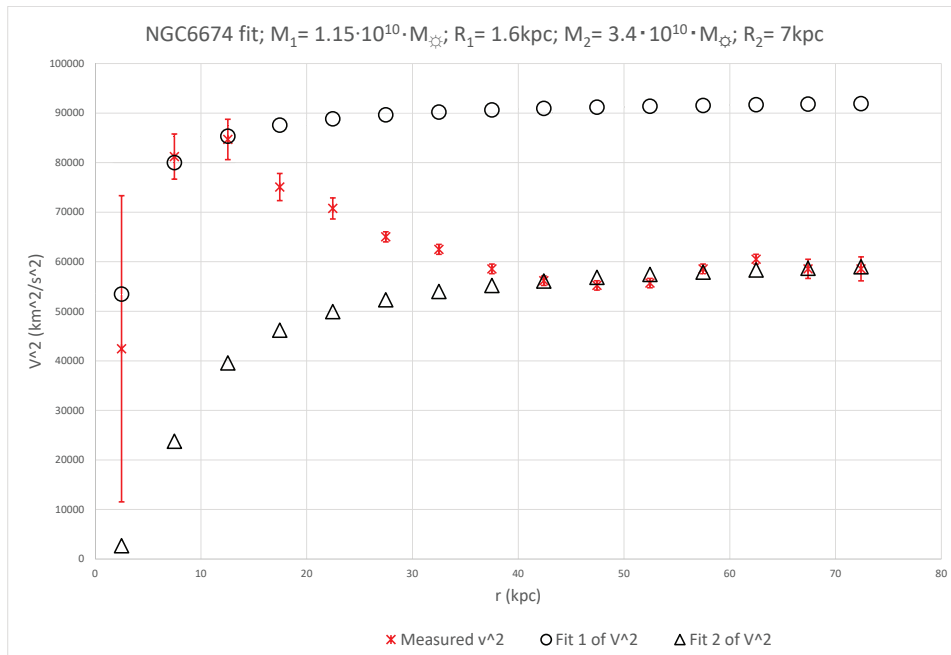


FIG. 108. NGC6674

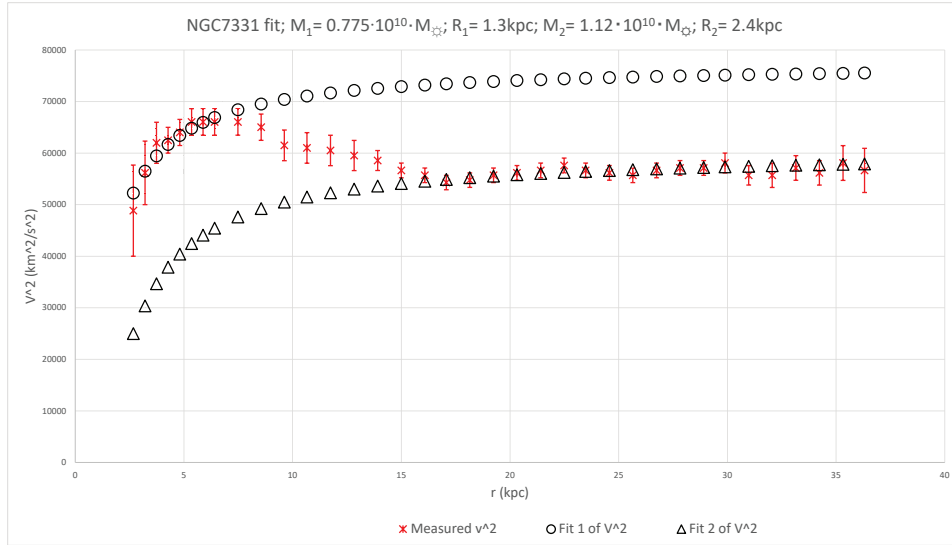


FIG. 109. NGC7331

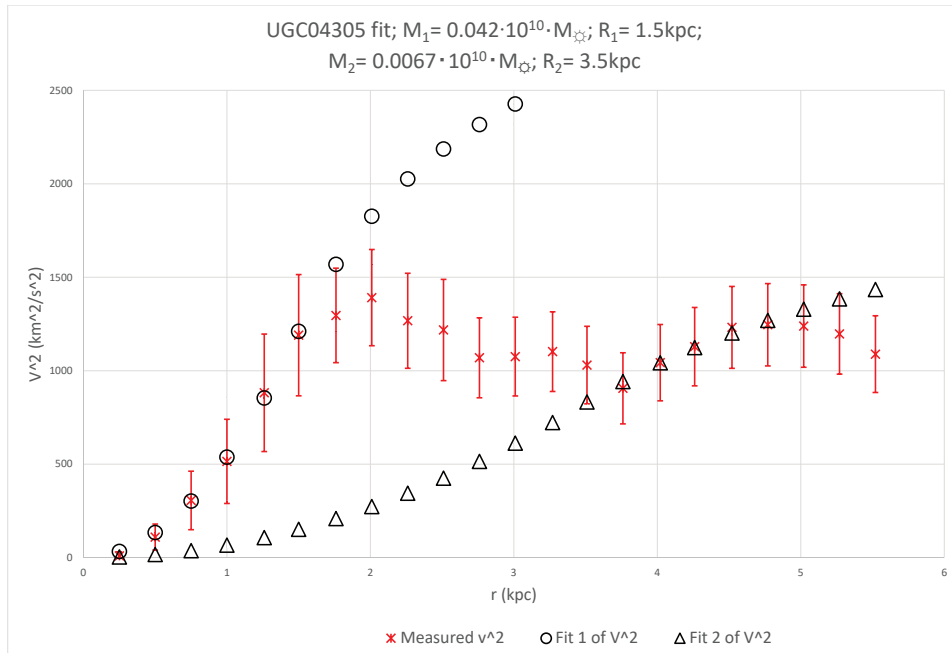


FIG. 110. UGC04305

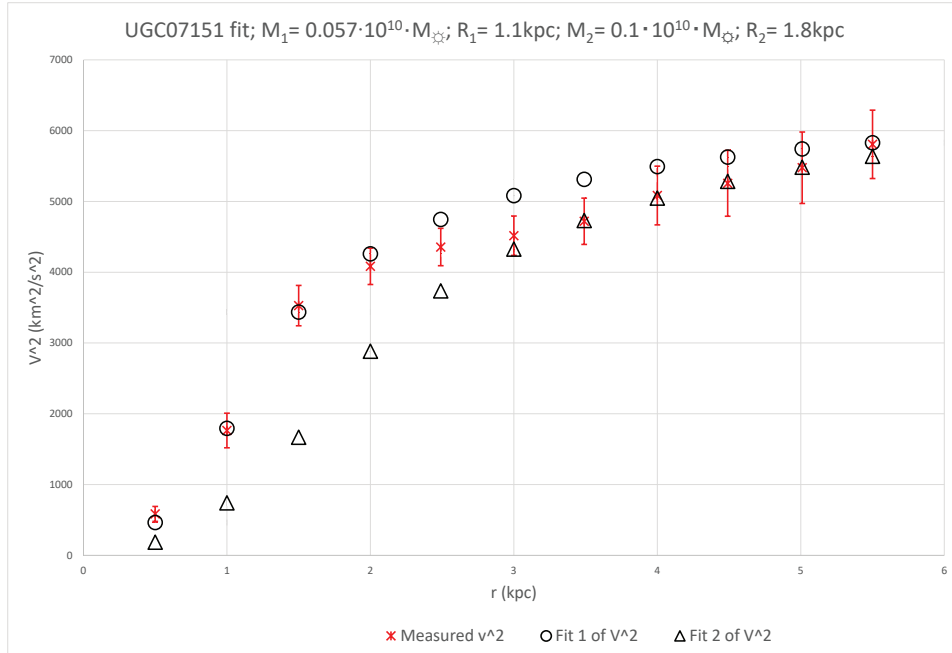


FIG. 111. UGC07151

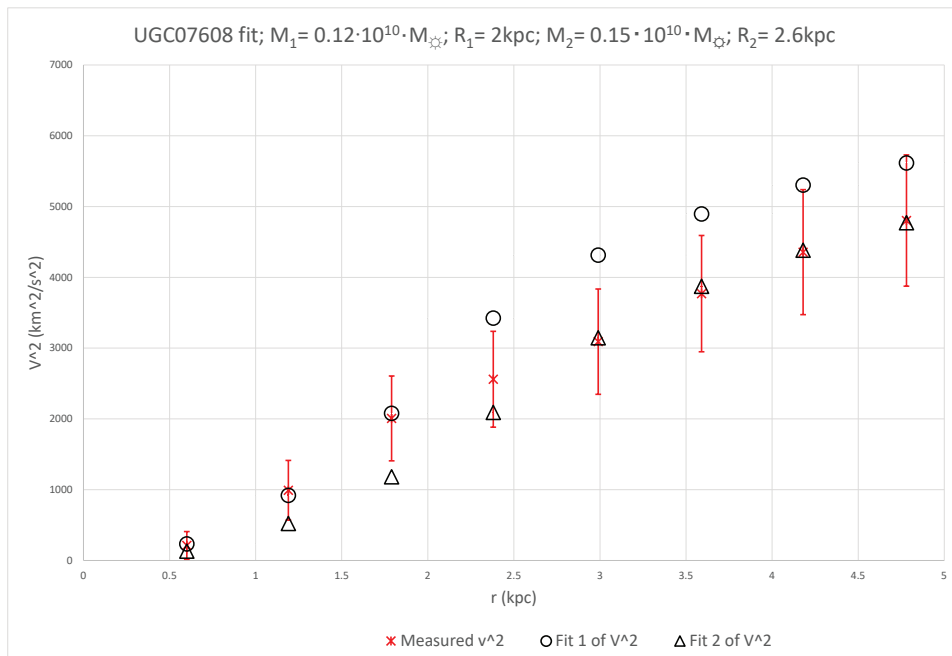


FIG. 112. UGC07608

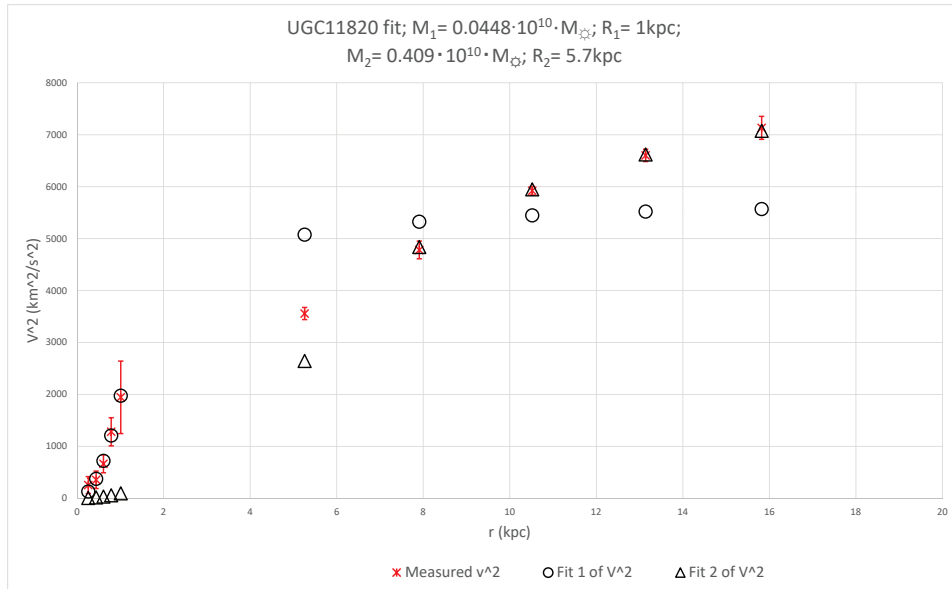


FIG. 113. UGC11820

## Appendix E: Triple fit galaxies and beyond

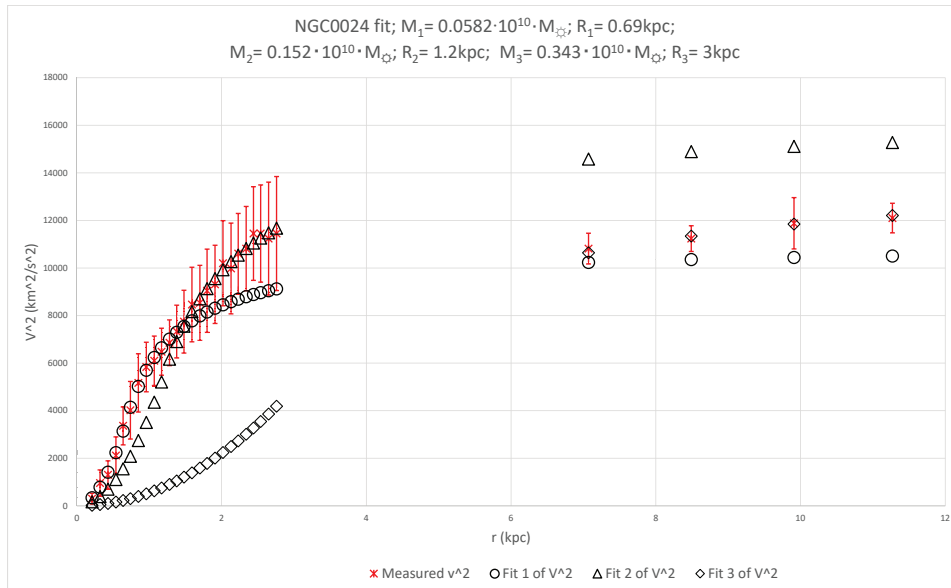


FIG. 114. NGC0024

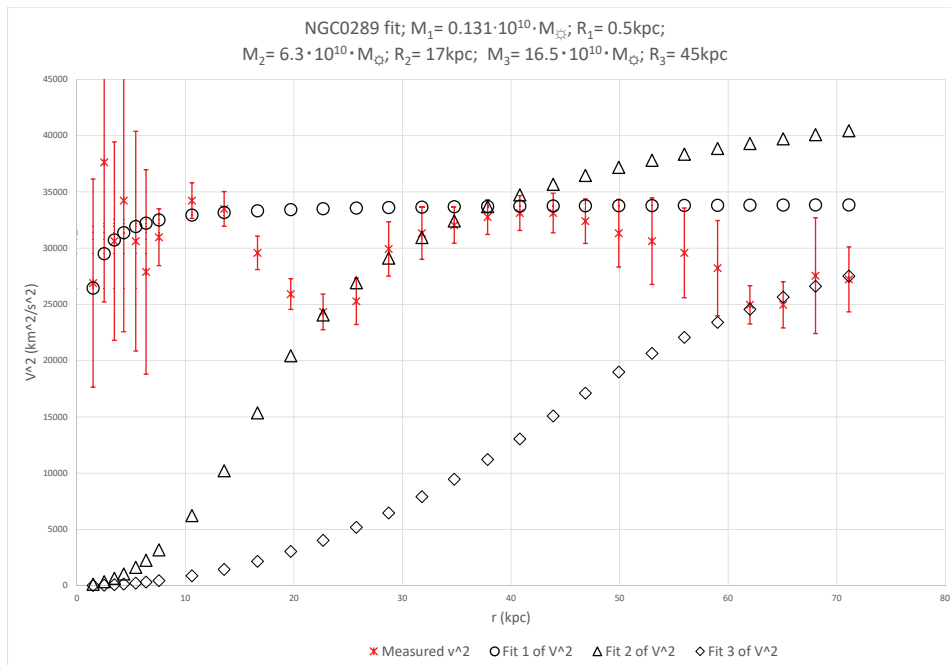


FIG. 115. NGC0289

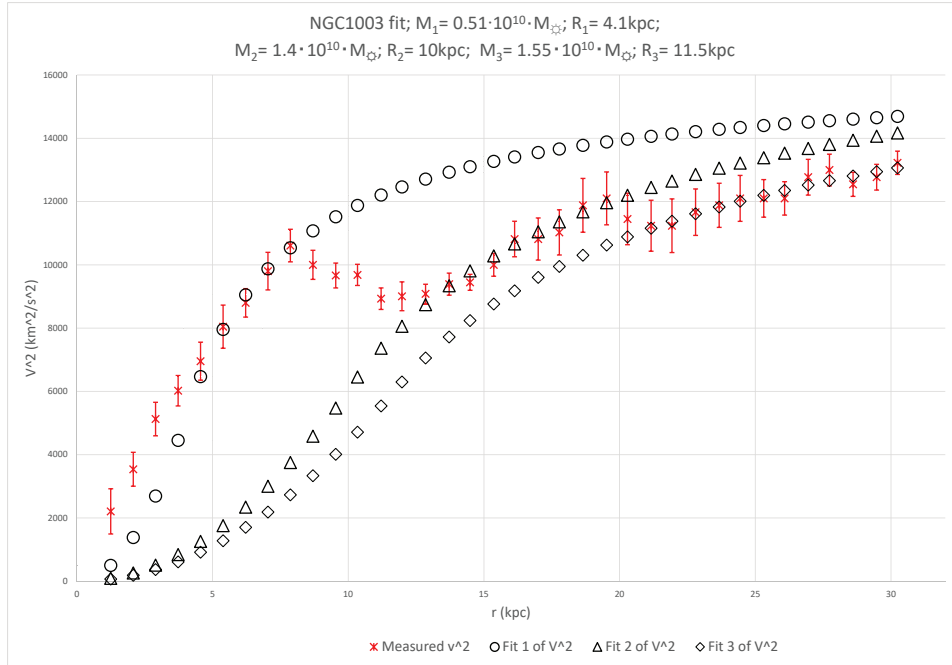


FIG. 116. NGC1003

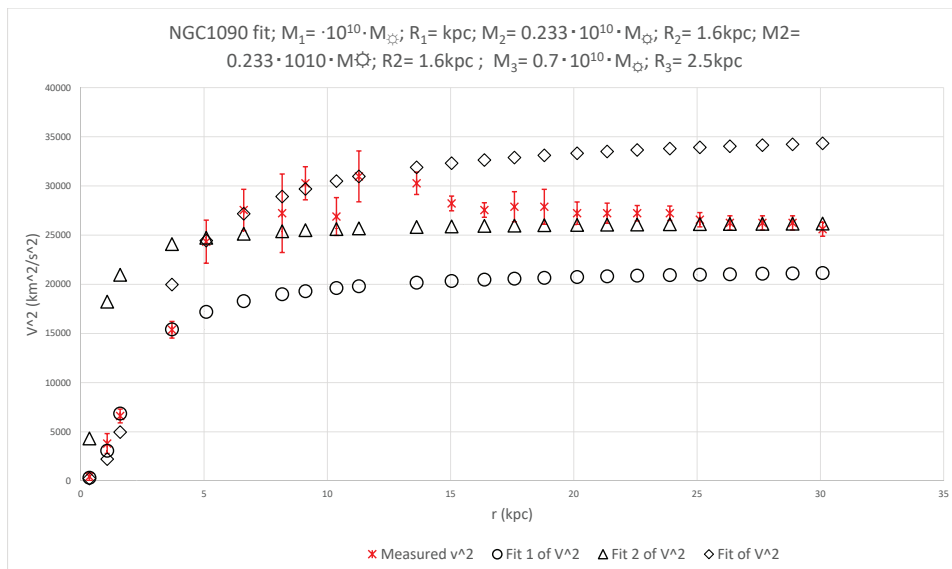


FIG. 117. NGC1090

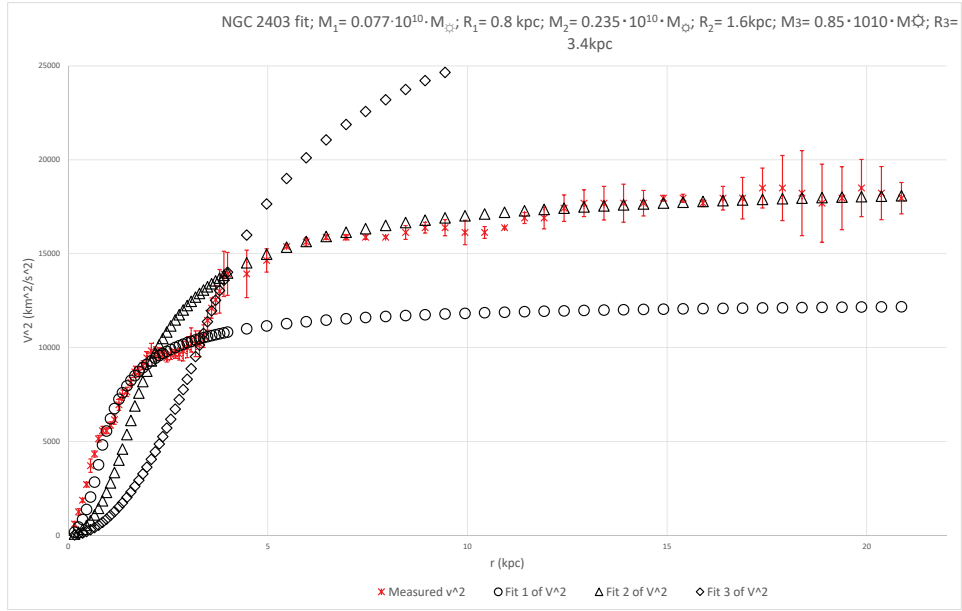


FIG. 118. NGC2403

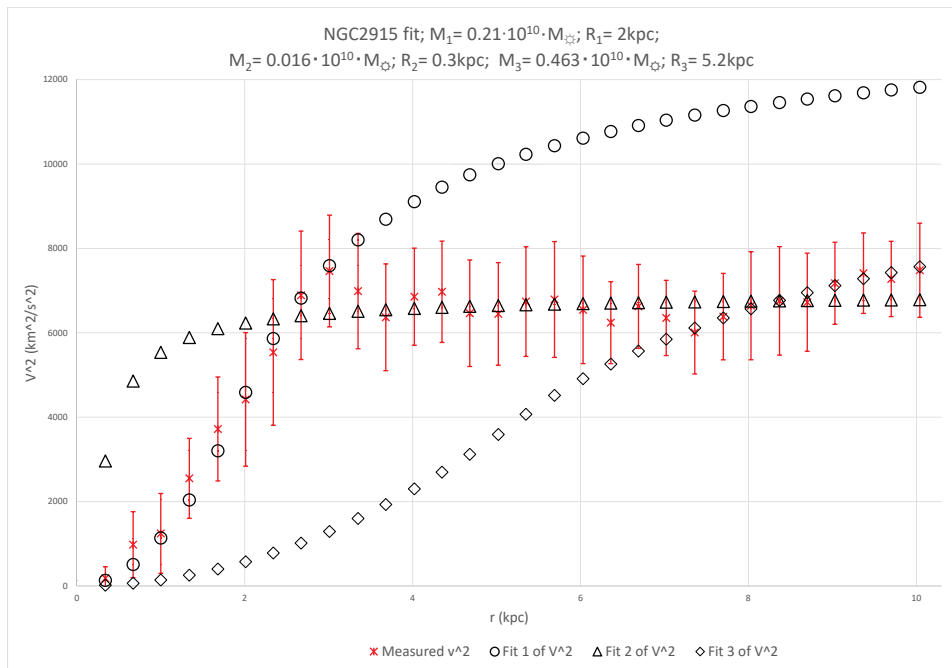


FIG. 119. NGC2915

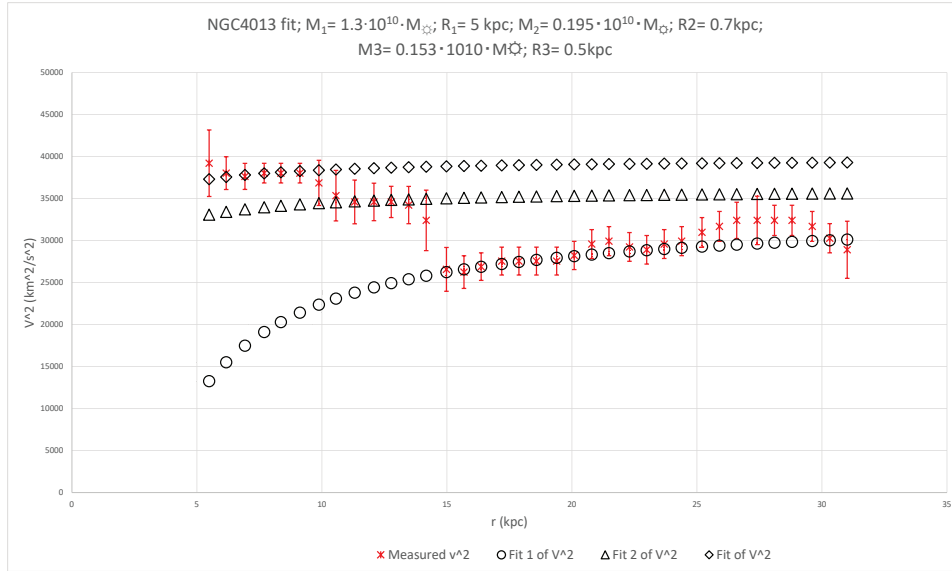


FIG. 120. NGC4013

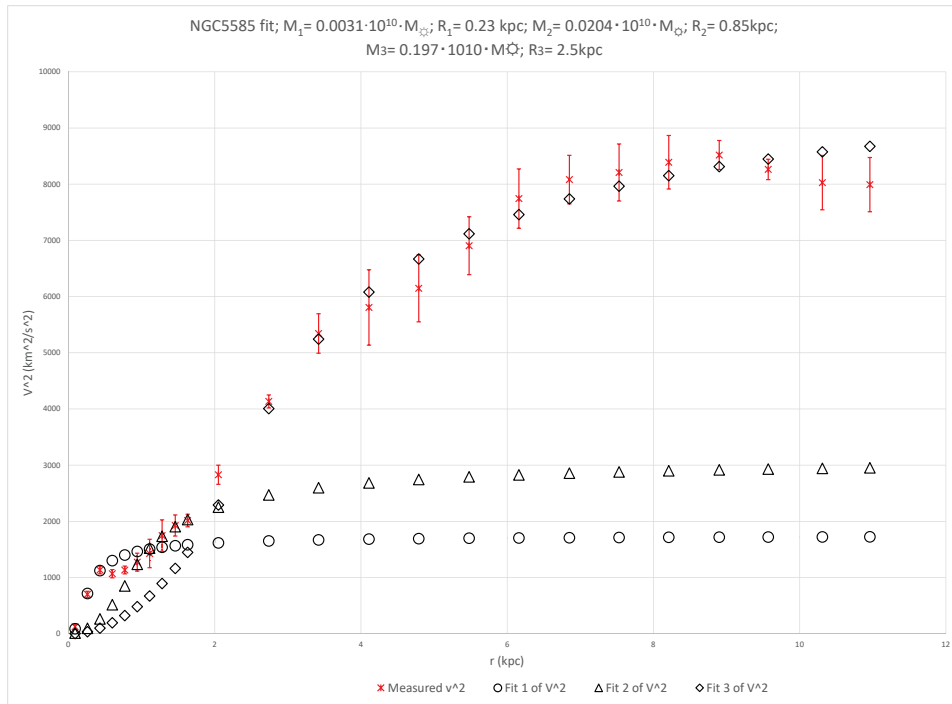


FIG. 121. NGC5585

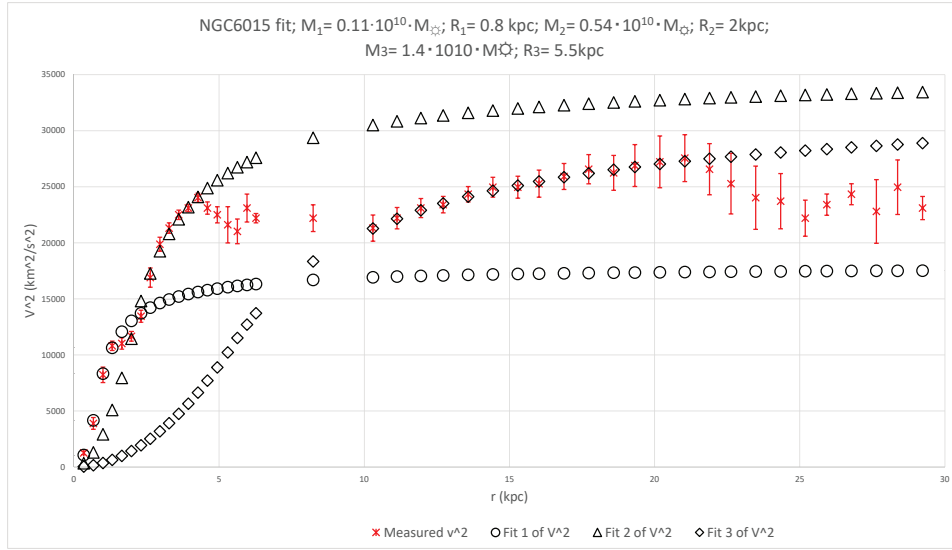


FIG. 122. NGC6015

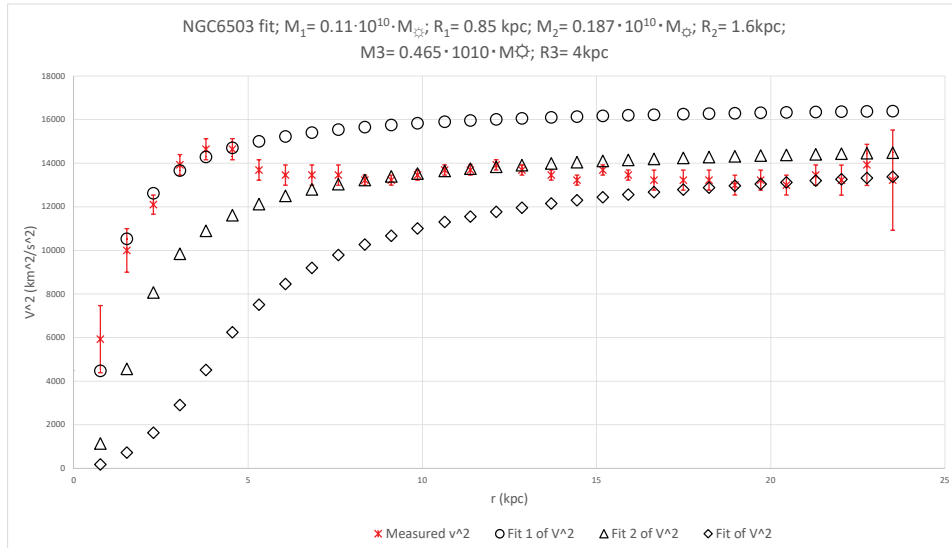


FIG. 123. NGC6503

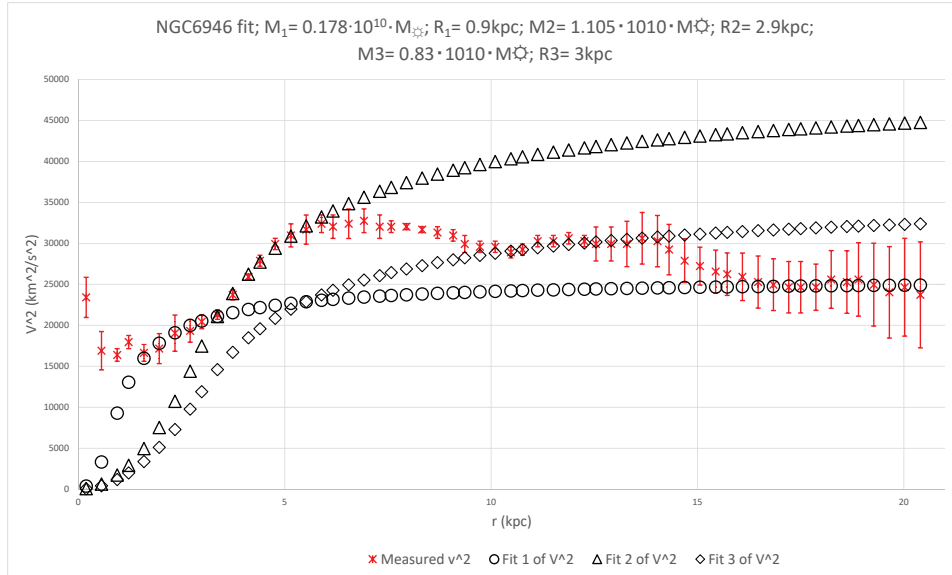


FIG. 124. NGC6946

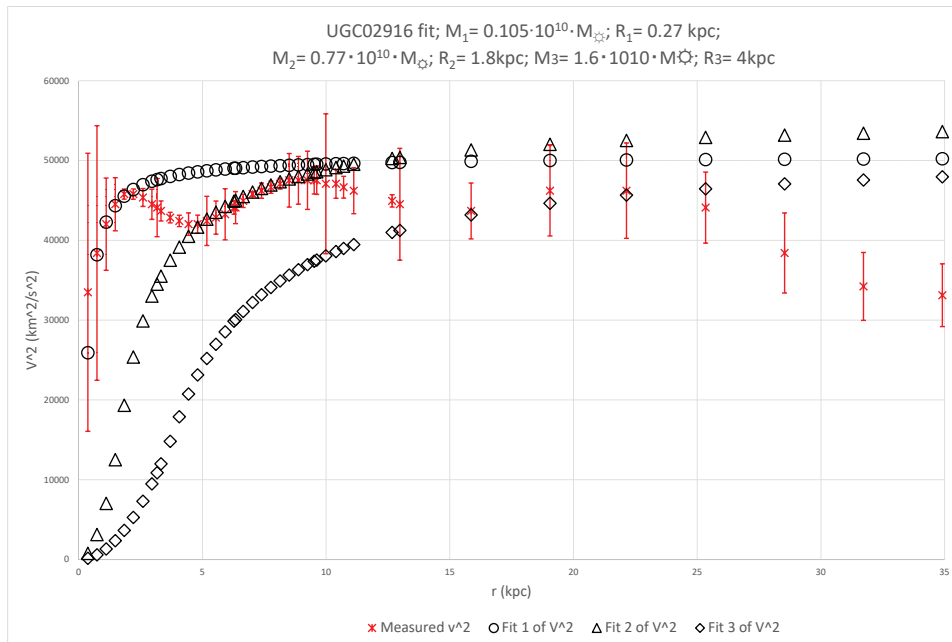


FIG. 125. UGC02916

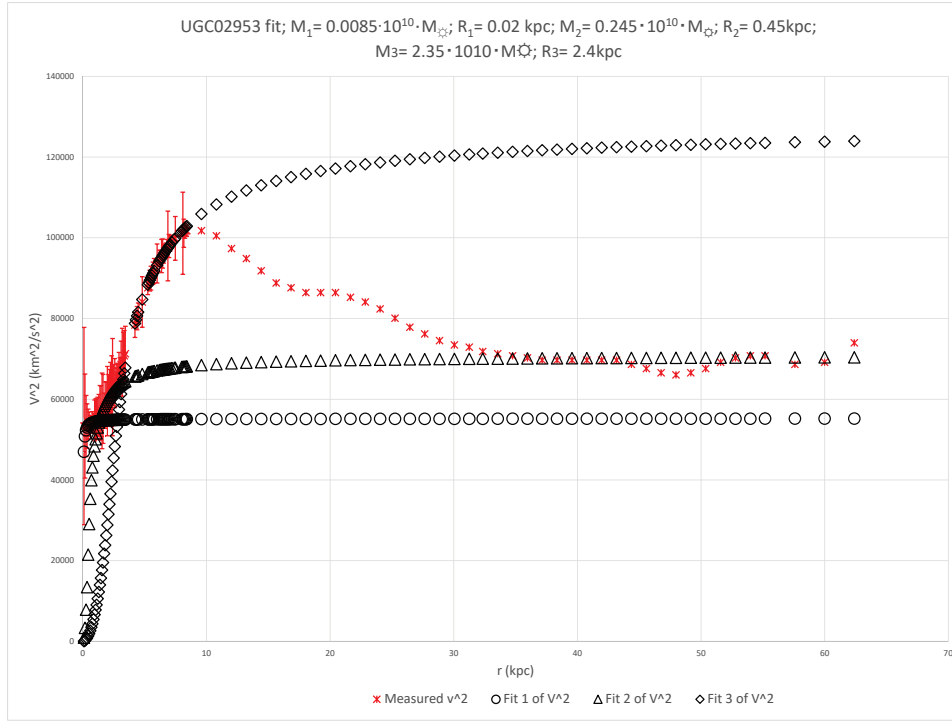


FIG. 126. UGC02953

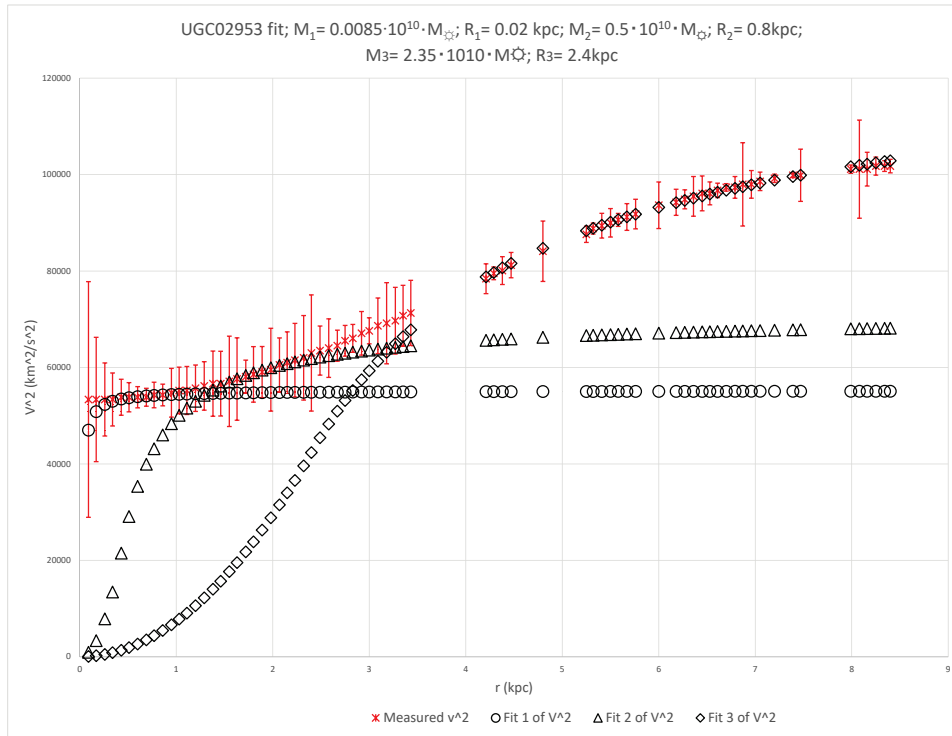


FIG. 127. Zooming in on UGC02953

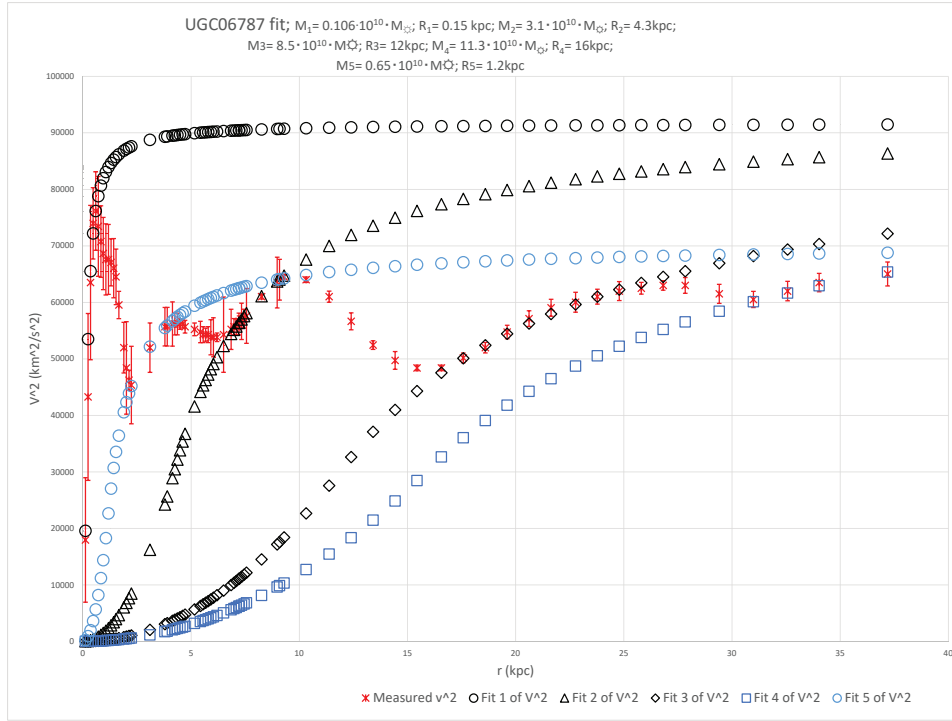


FIG. 128. UGC06787

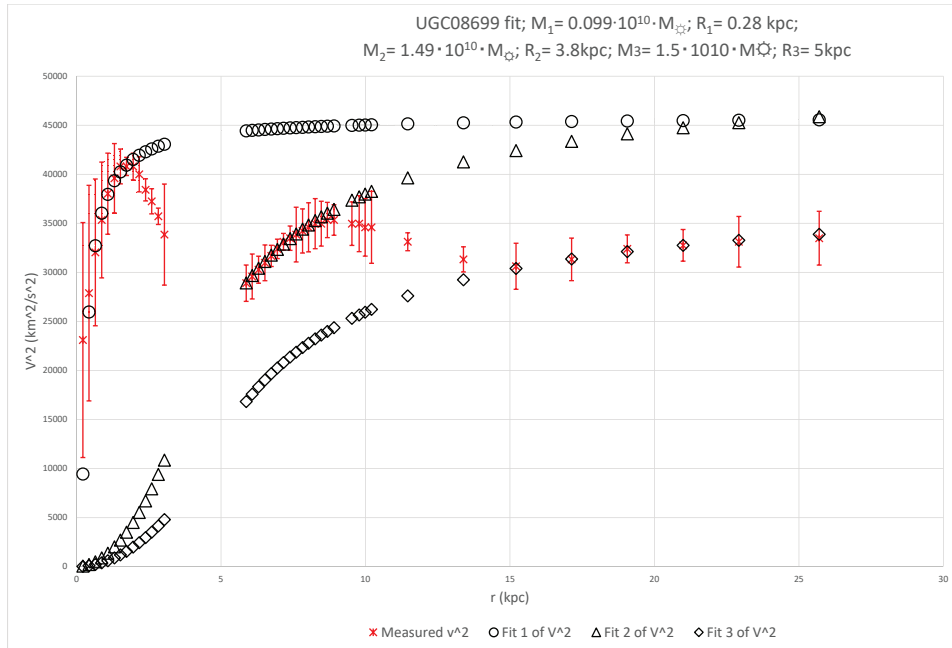


FIG. 129. UGC08699

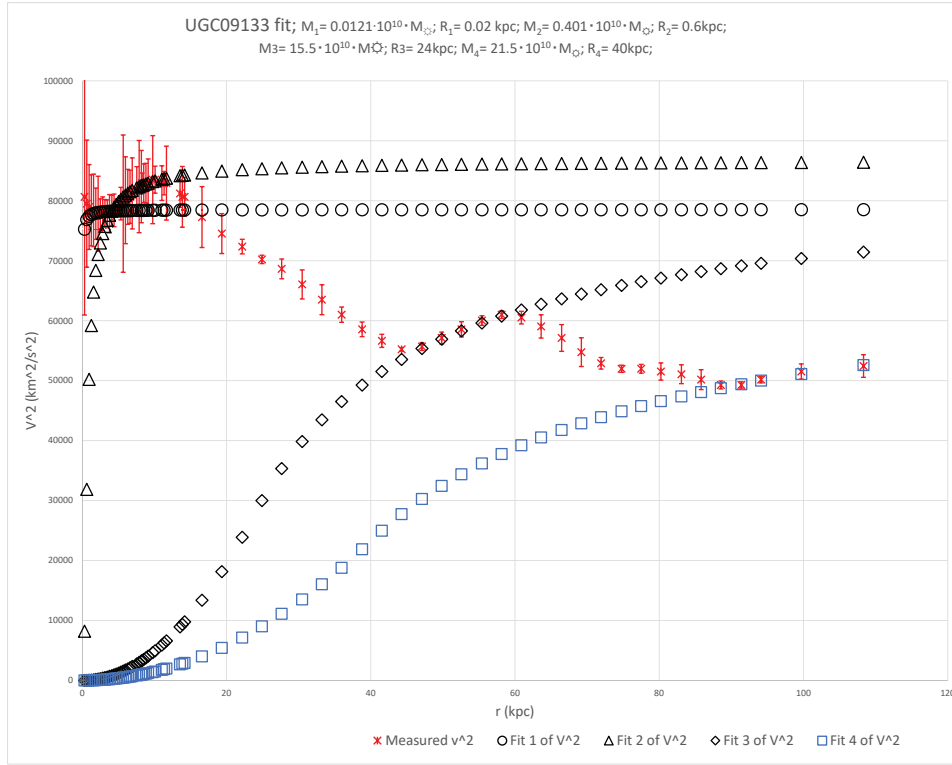


FIG. 130. UGC09133

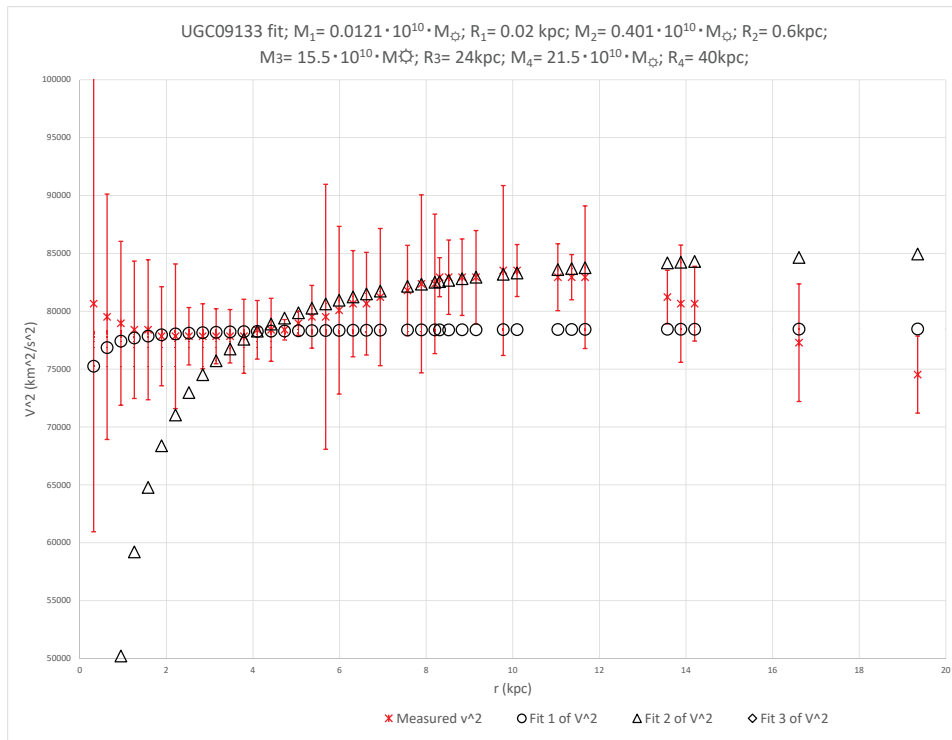


FIG. 131. Zooming in on UGC09133

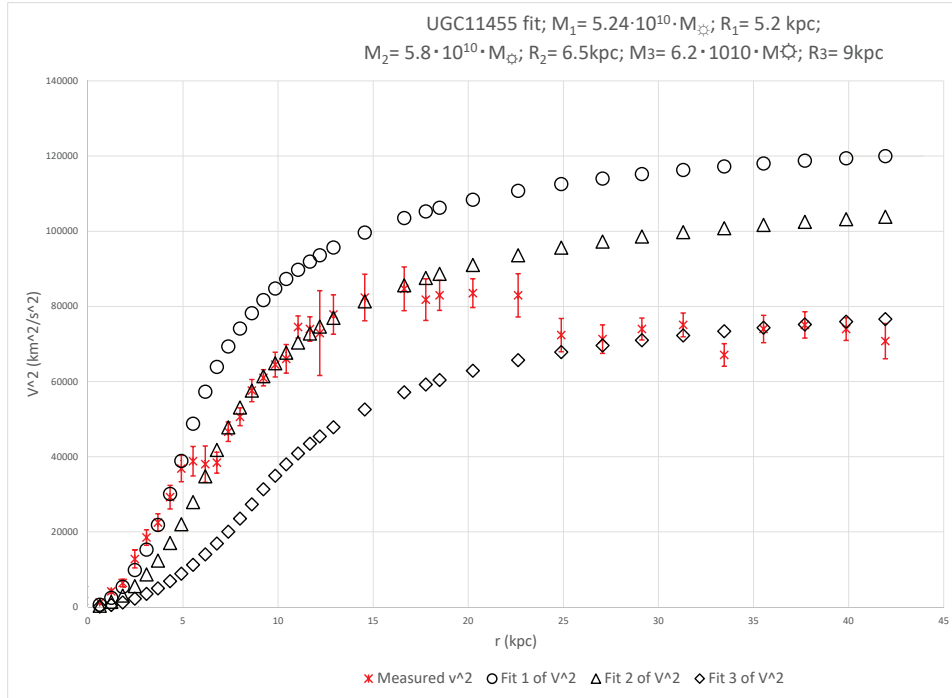


FIG. 132. UGC11455

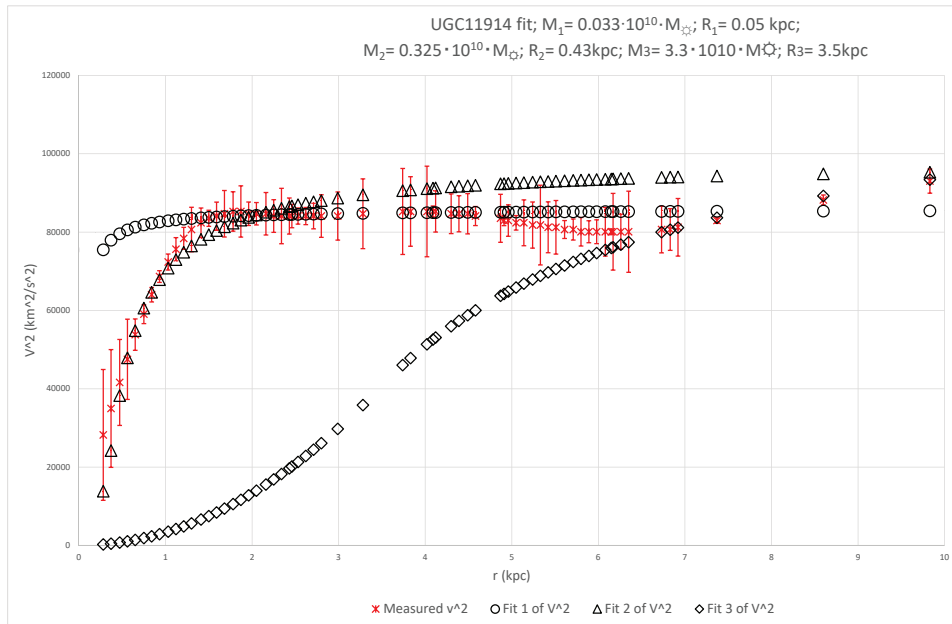


FIG. 133. UGC11914

## Appendix F: Rest 'dual' fit galaxies

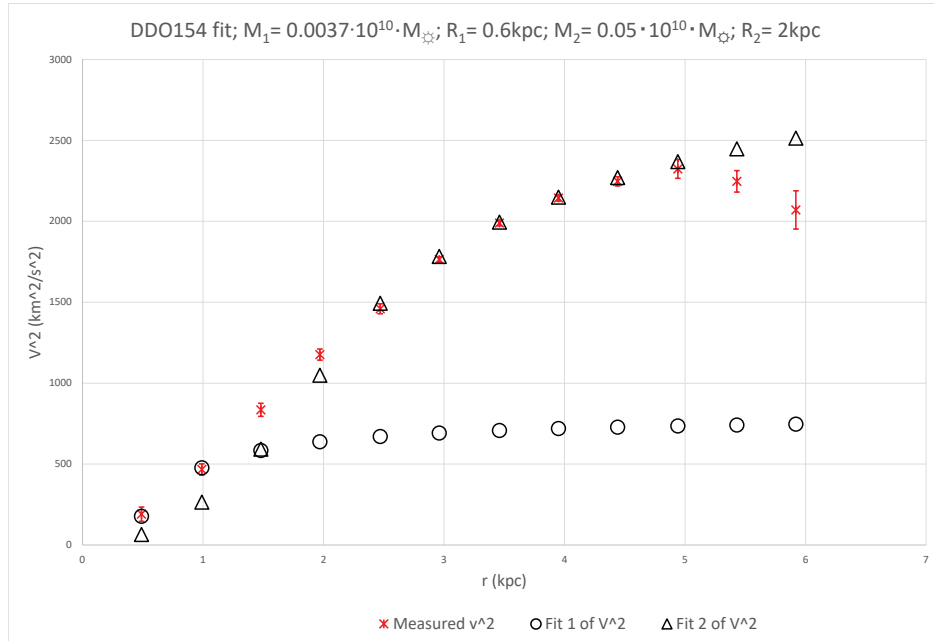


FIG. 134. DDO154

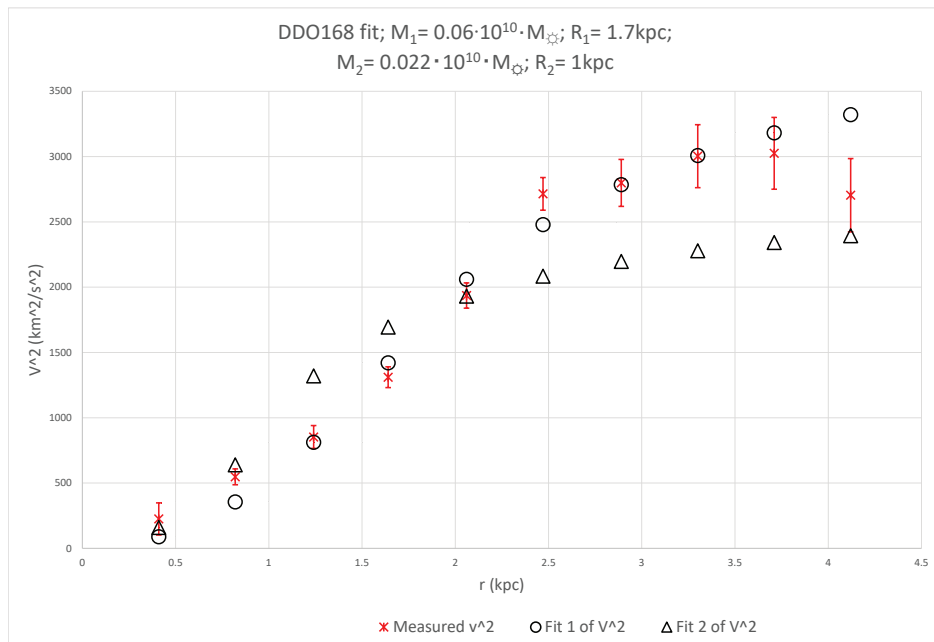


FIG. 135. DDO168

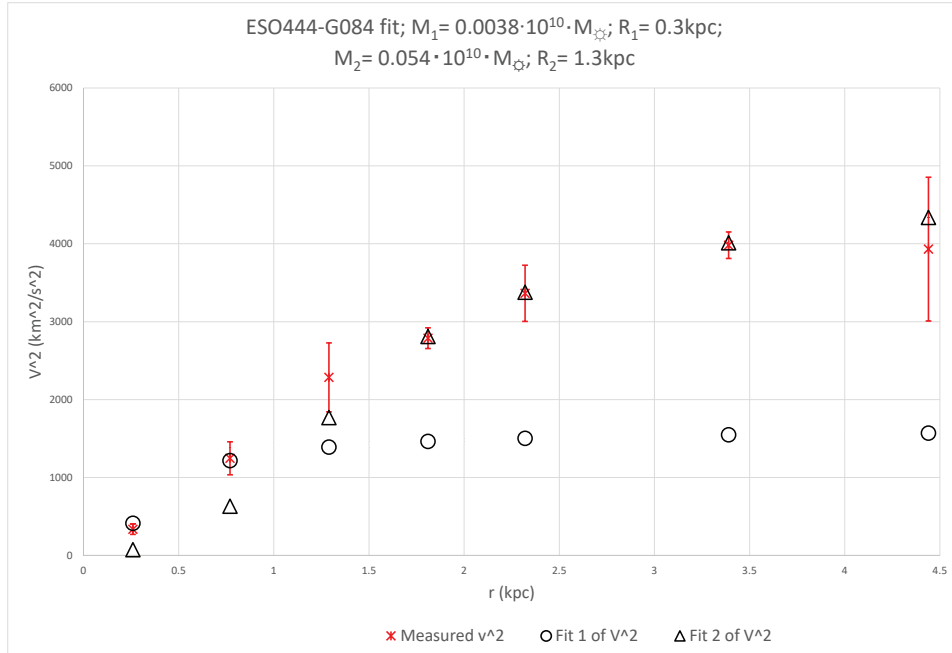


FIG. 136. ESO444-G084

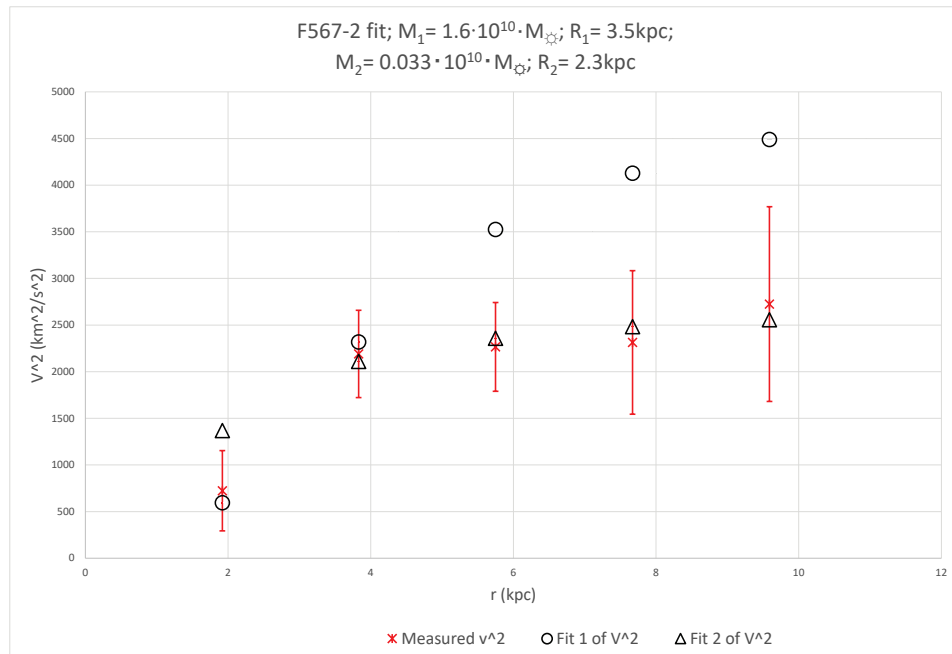


FIG. 137. F567-2

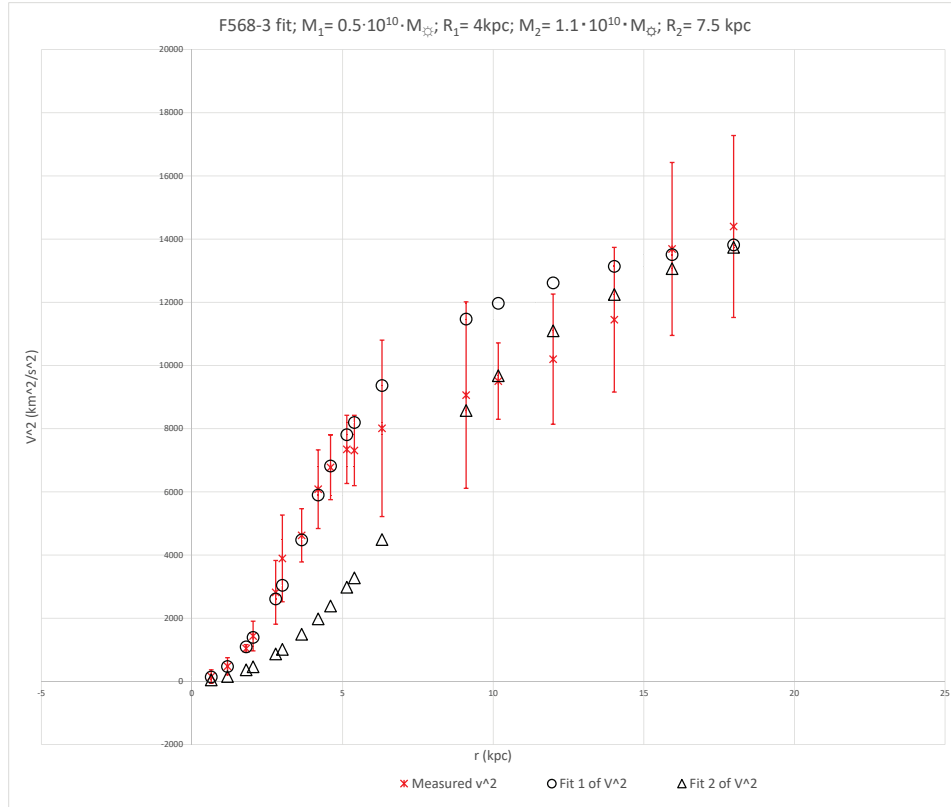


FIG. 138. F568-3

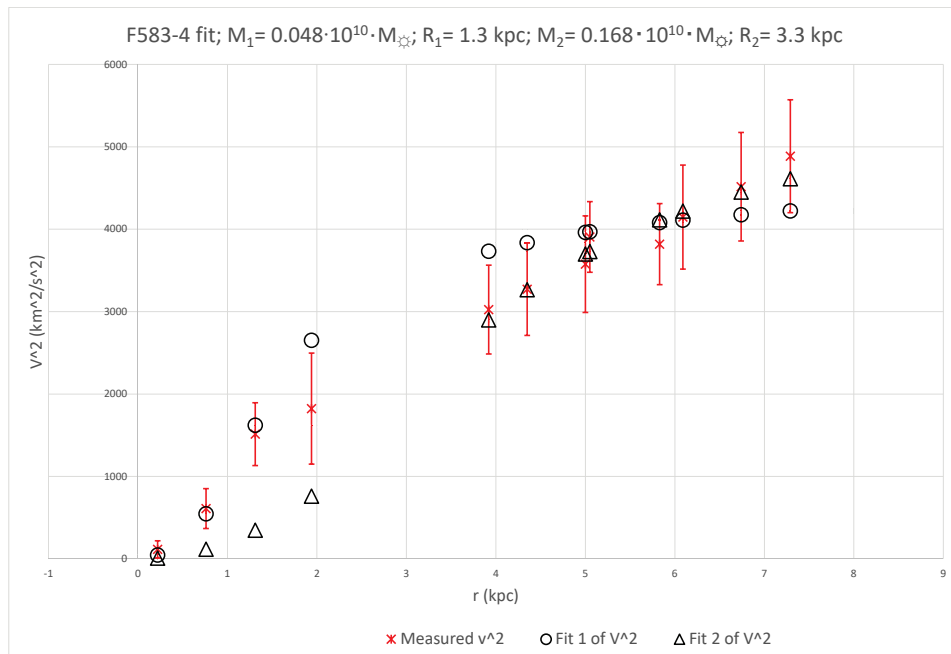


FIG. 139. F583-4

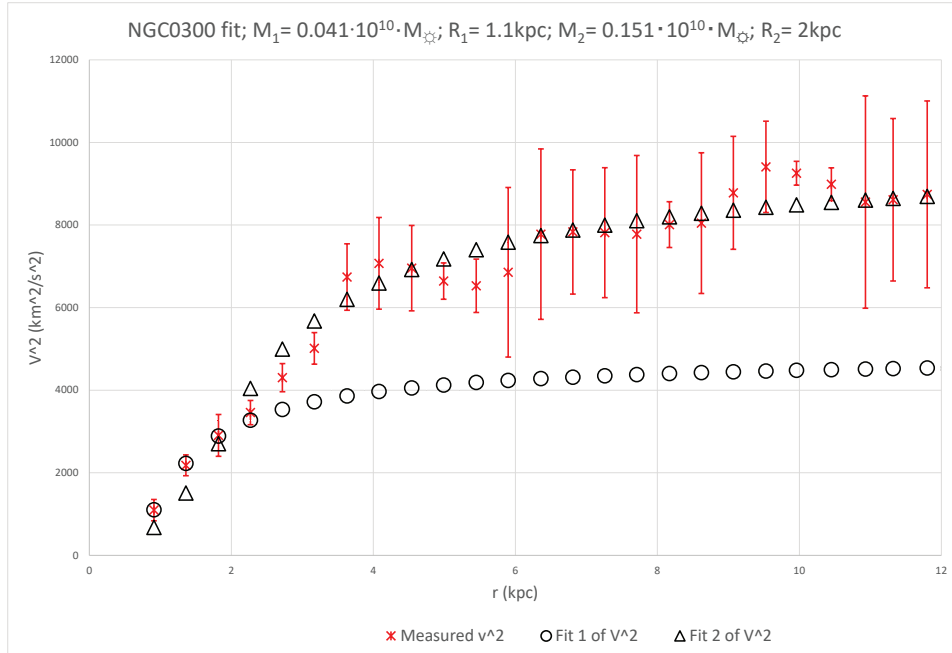


FIG. 140. NGC0300

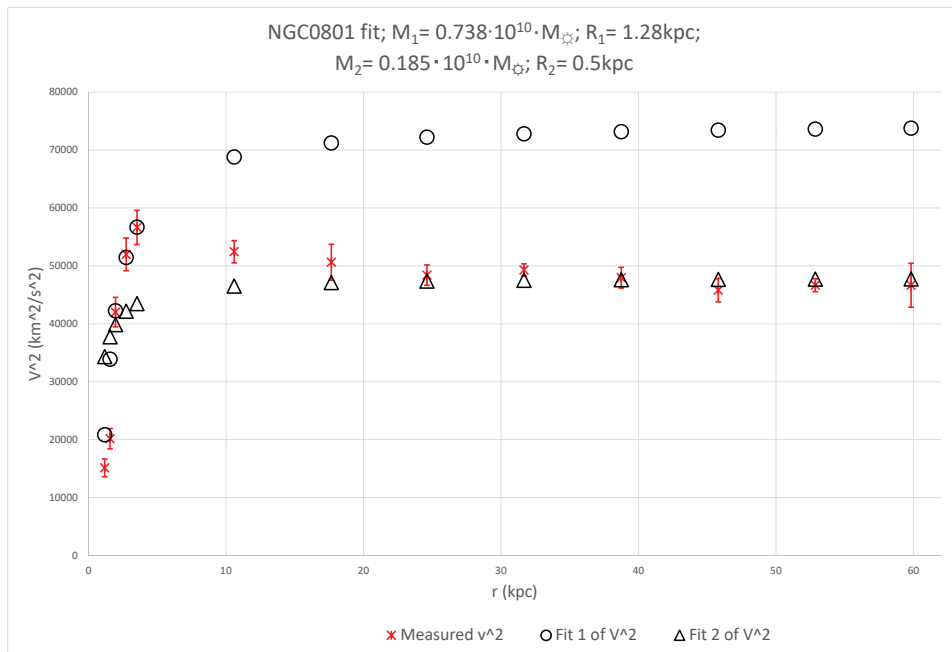


FIG. 141. NGC0801

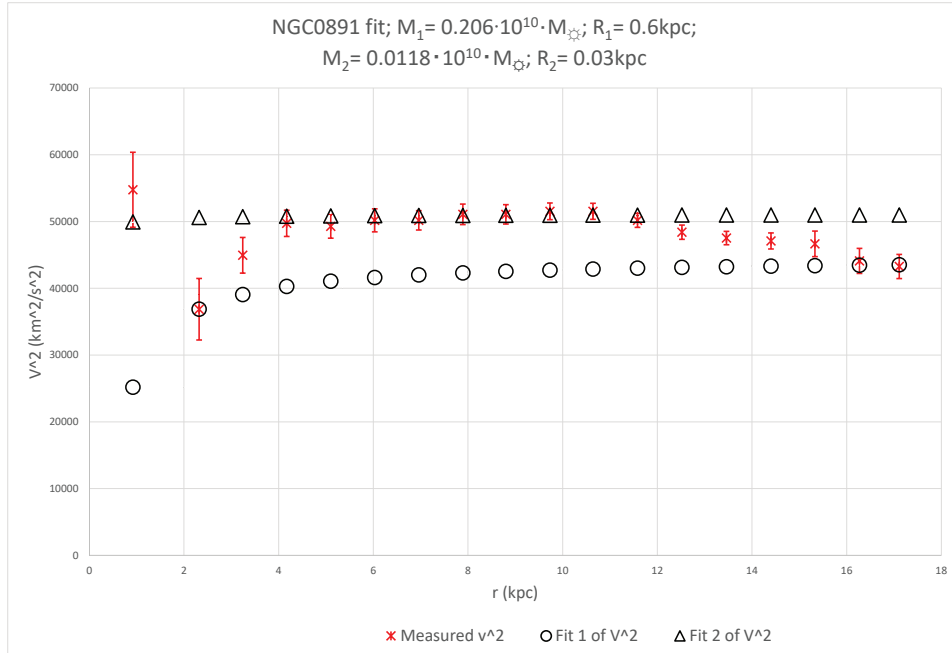


FIG. 142. NGC0891

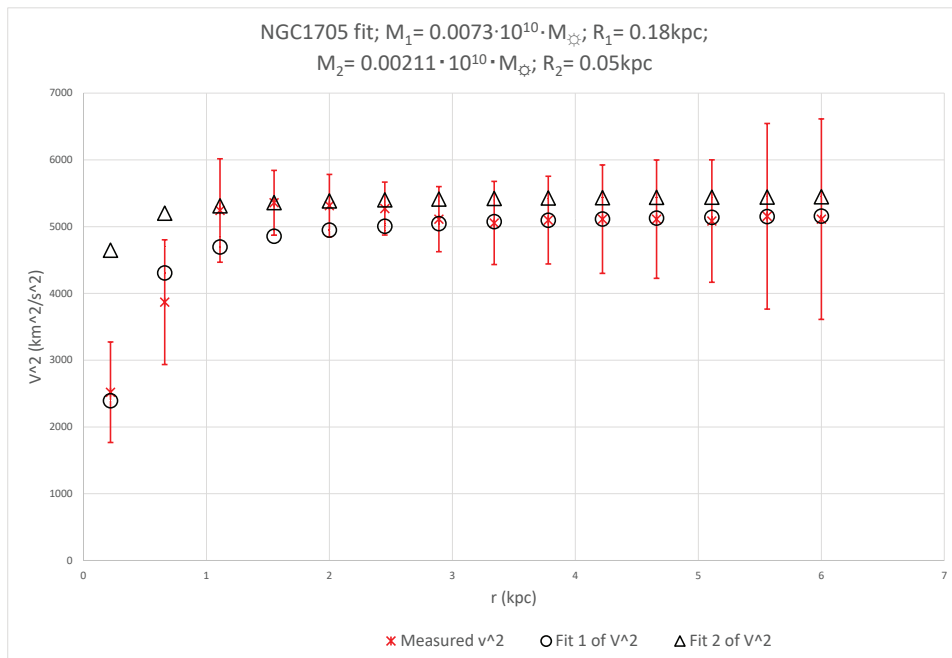


FIG. 143. NGC1705

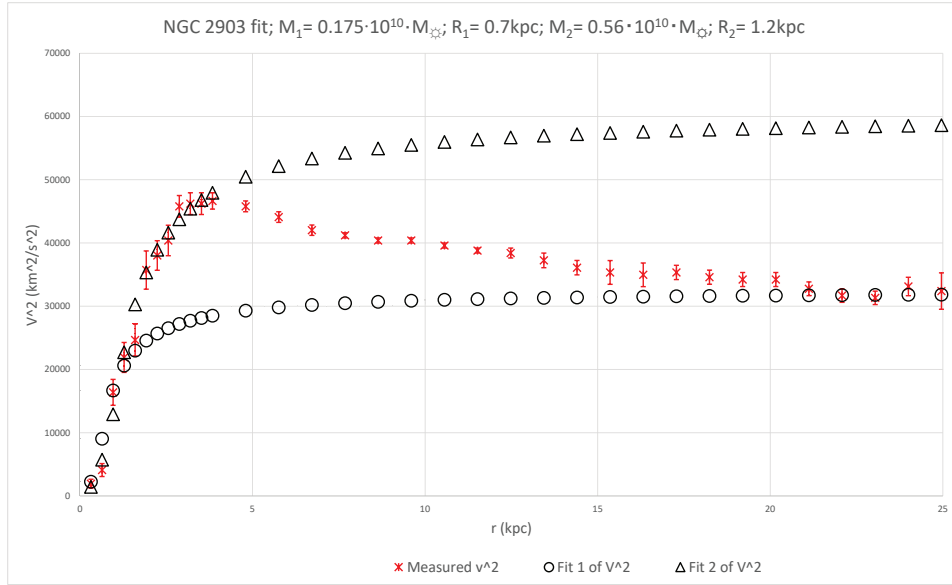


FIG. 144. NGC2903

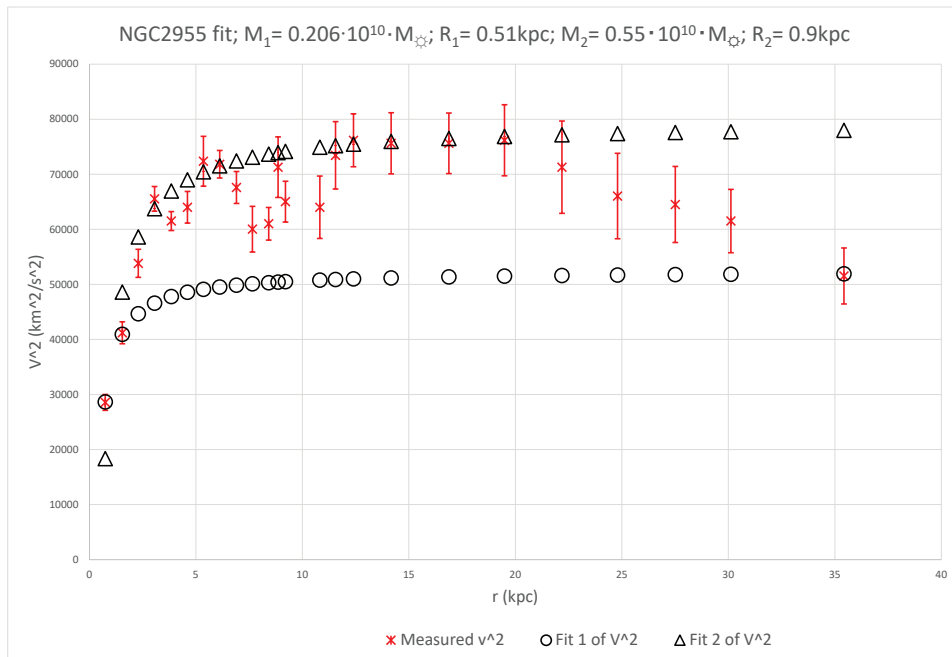


FIG. 145. NGC2955

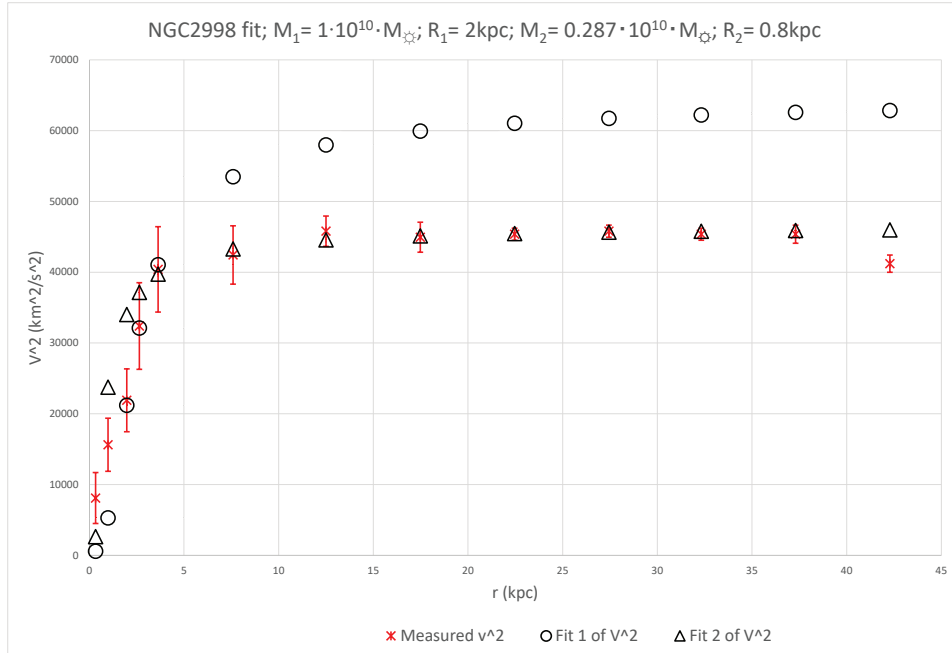


FIG. 146. NGC2998

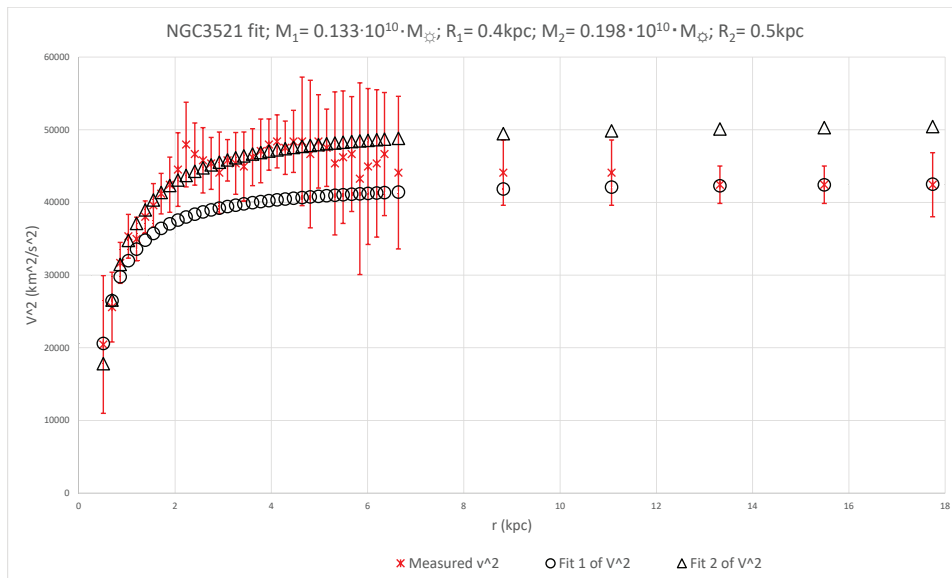


FIG. 147. NGC3521

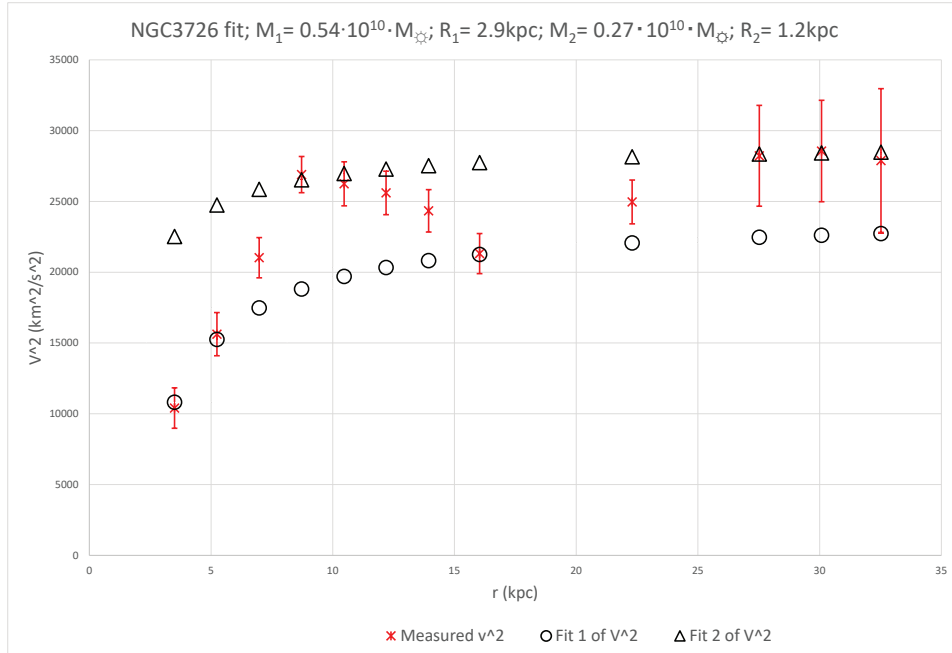


FIG. 148. NGC3726

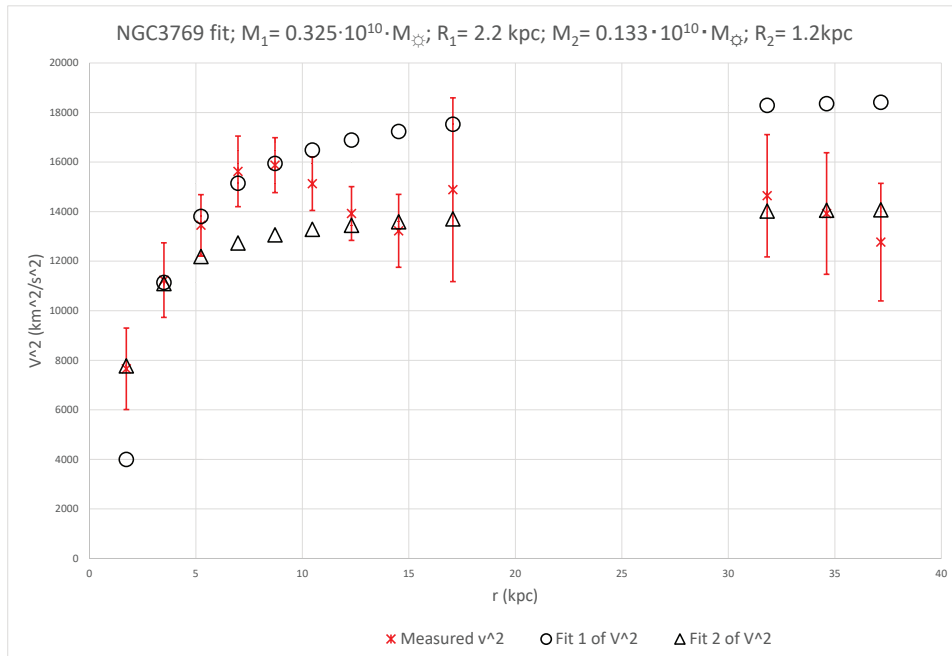


FIG. 149. NGC3769

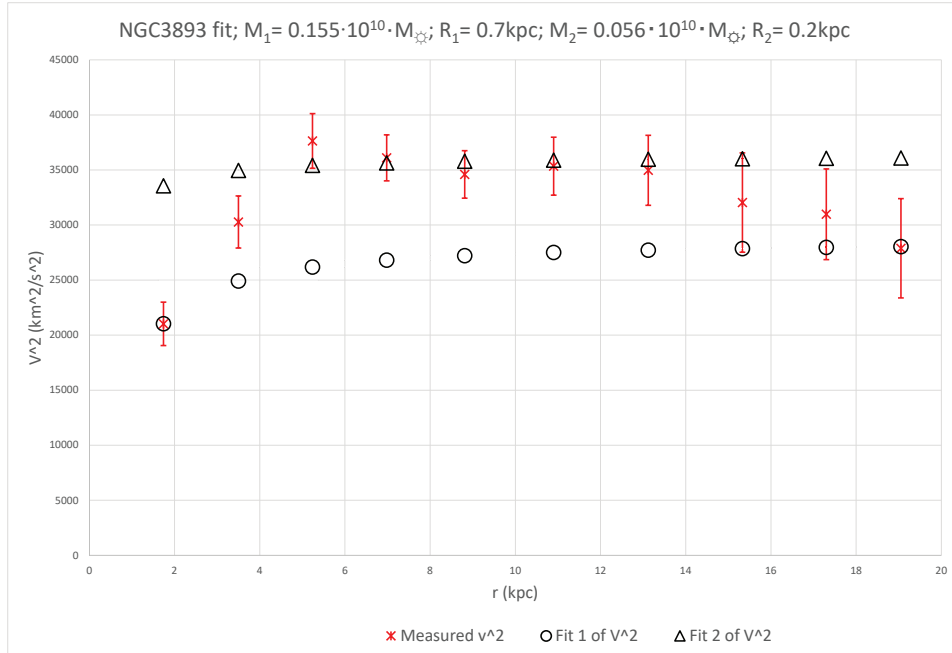


FIG. 150. NGC3893

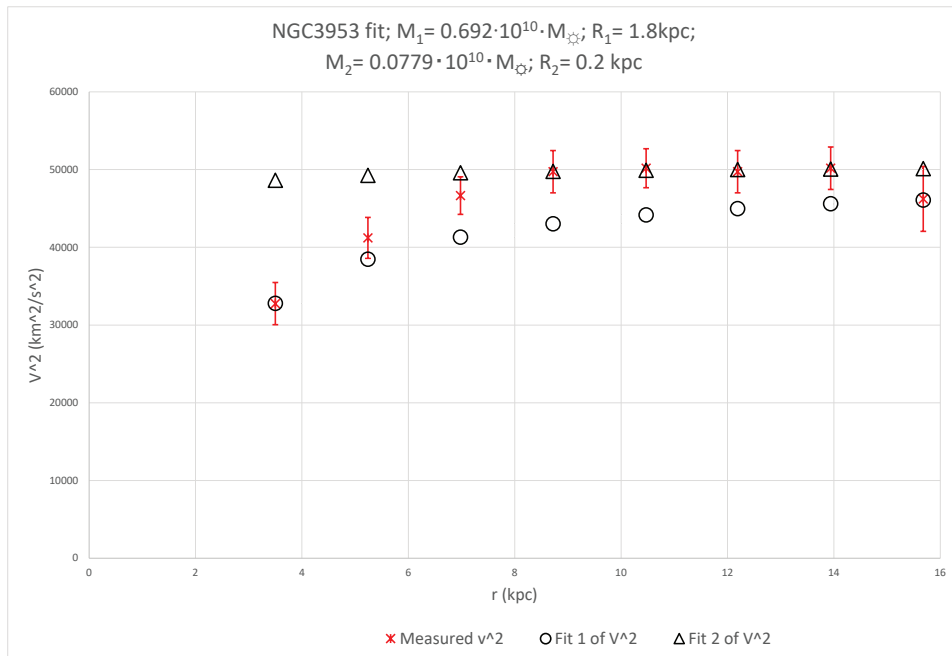


FIG. 151. NGC3953

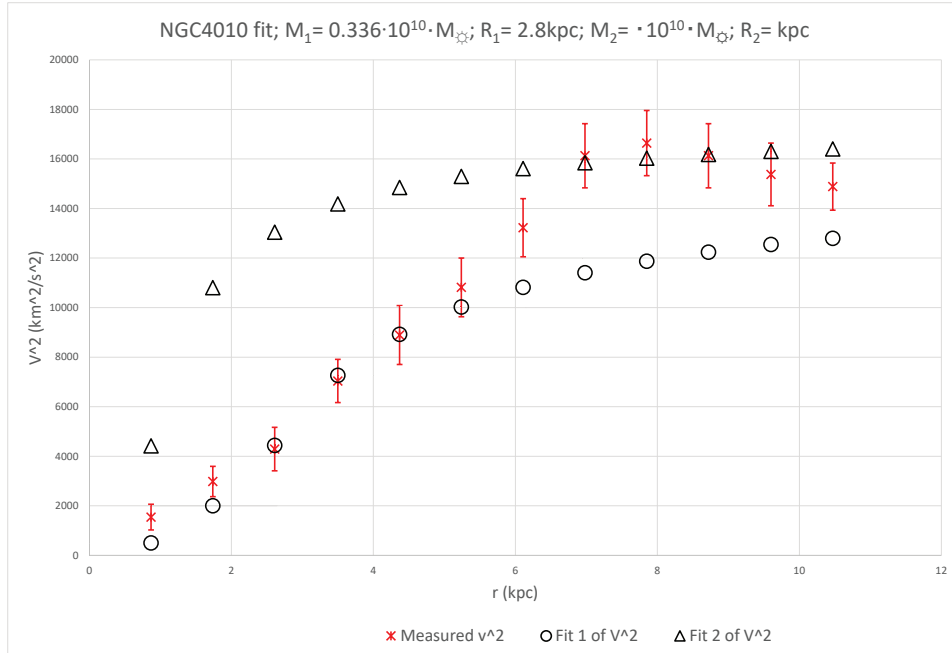


FIG. 152. NGC4010

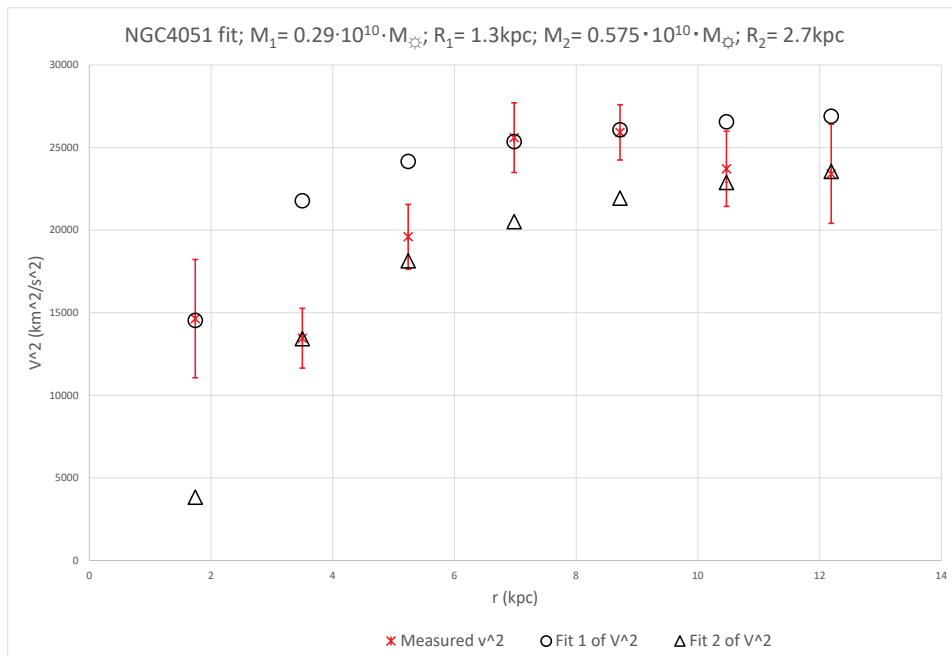


FIG. 153. NGC4051

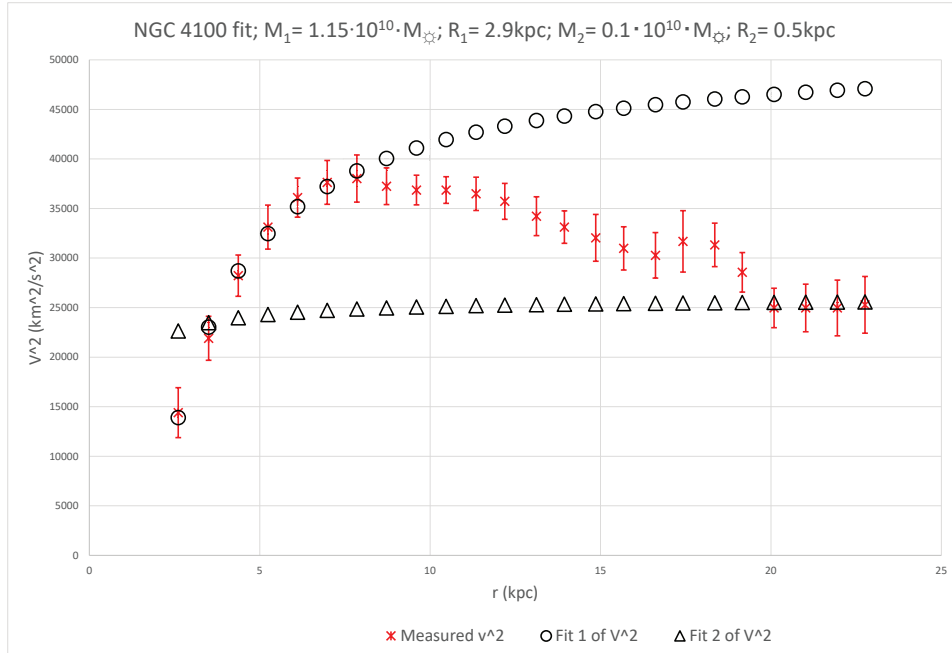


FIG. 154. NGC4100

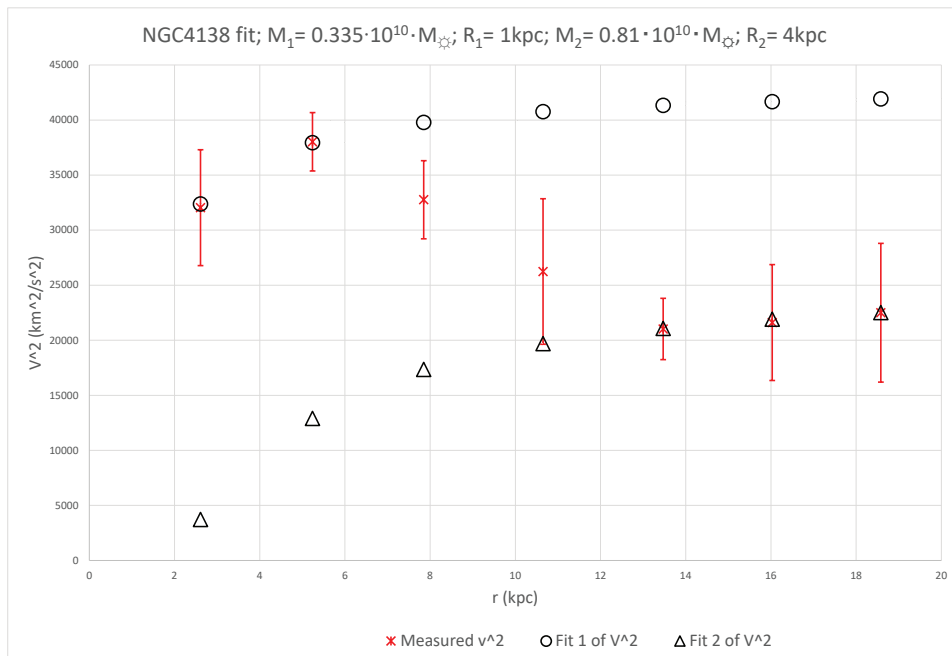


FIG. 155. NGC4138

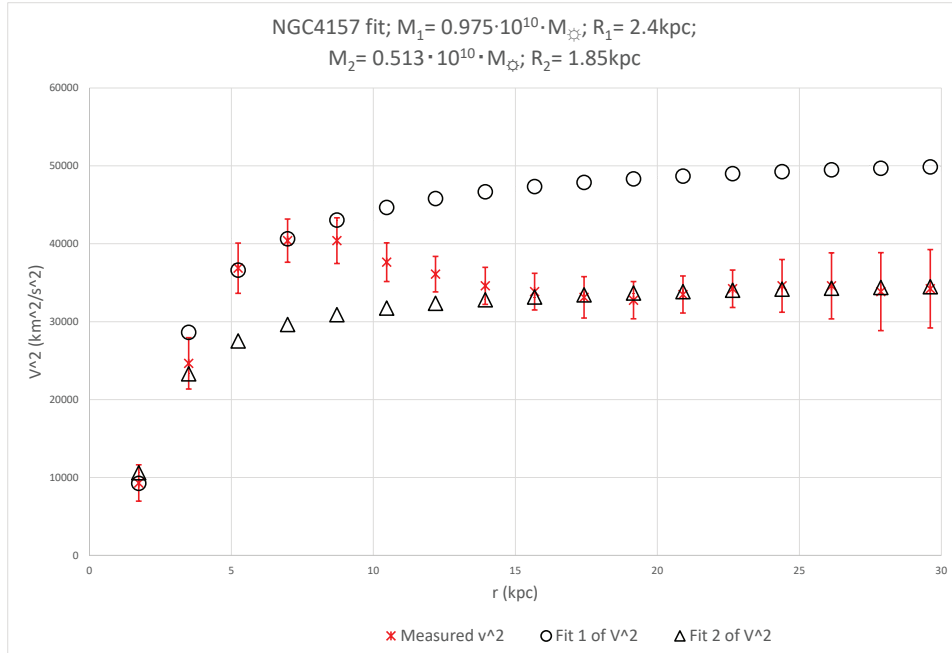


FIG. 156. NGC4157

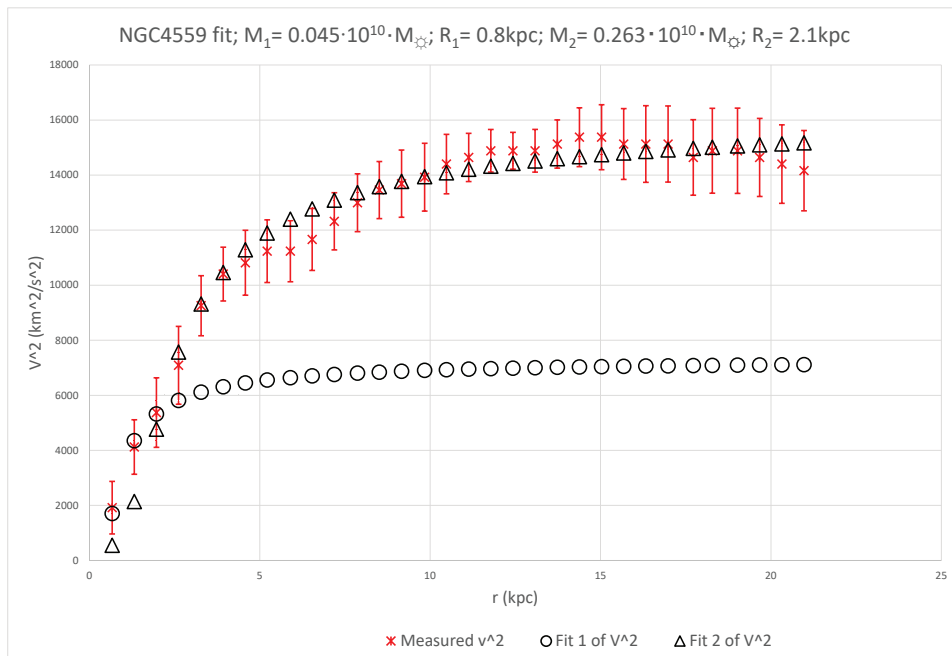


FIG. 157. NGC4559

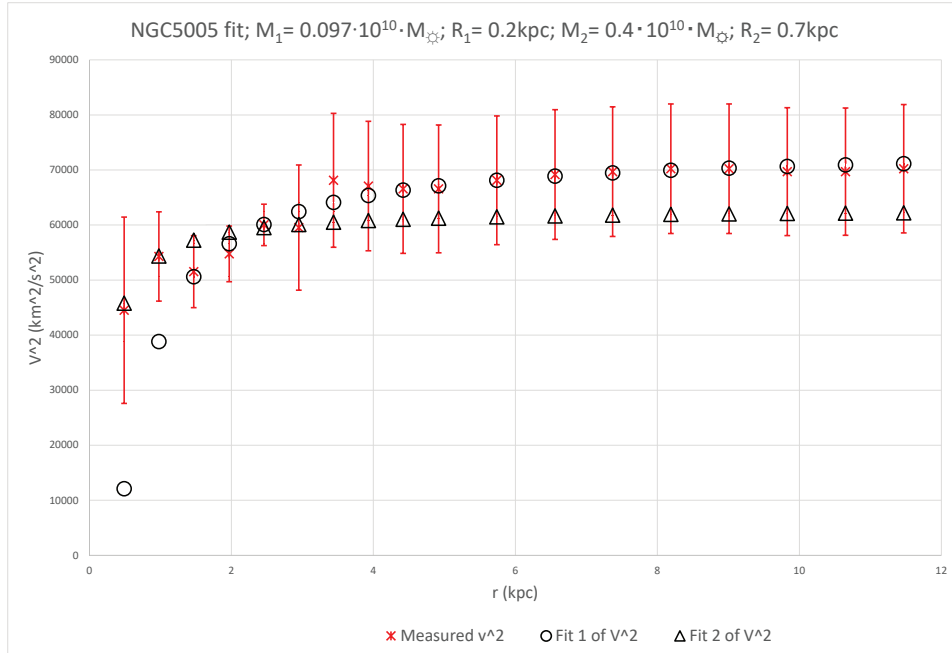


FIG. 158. NGC5005

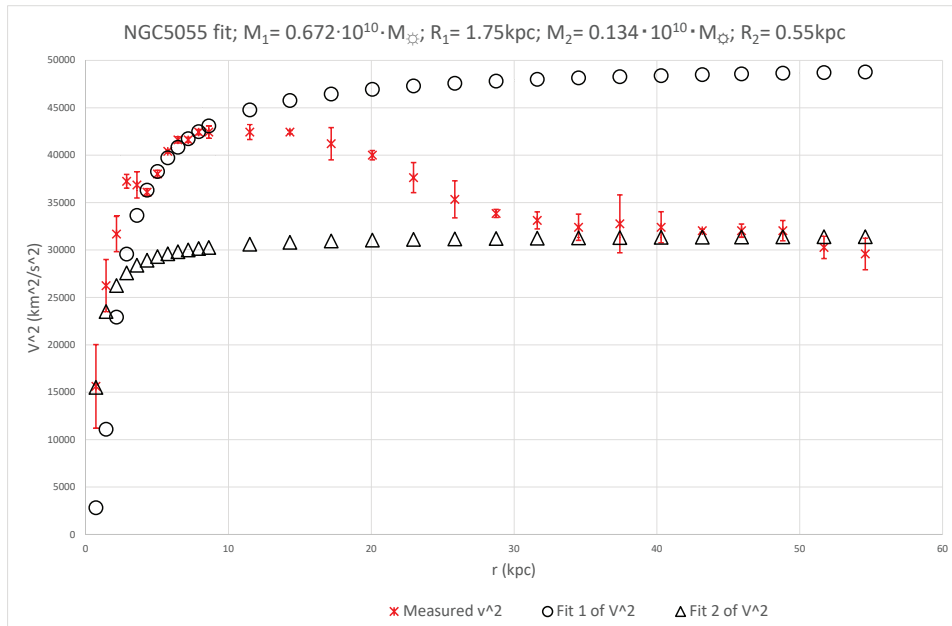


FIG. 159. NGC5055

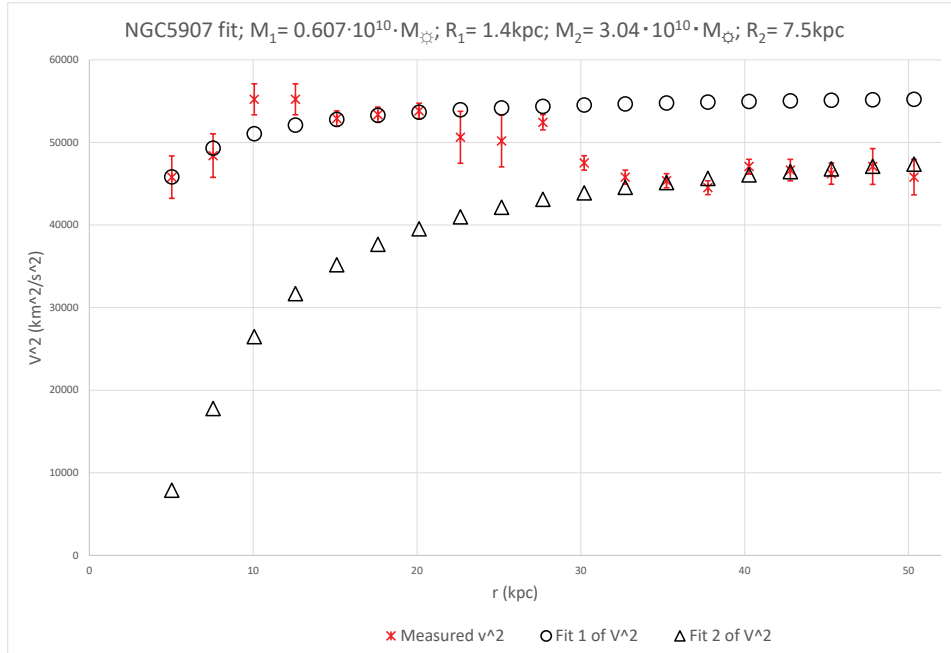


FIG. 160. NGC5907

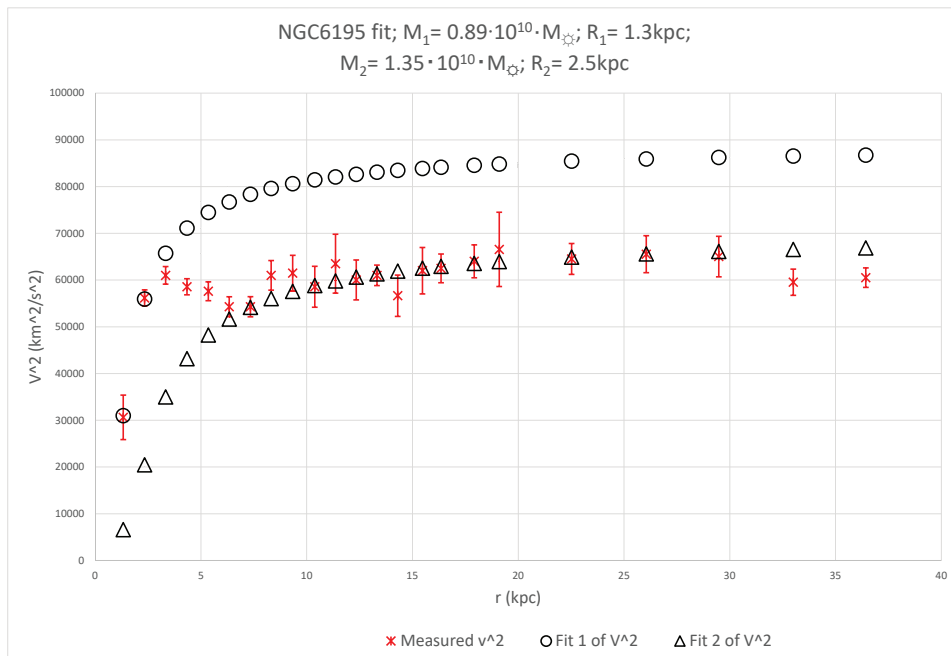


FIG. 161. NGC6195

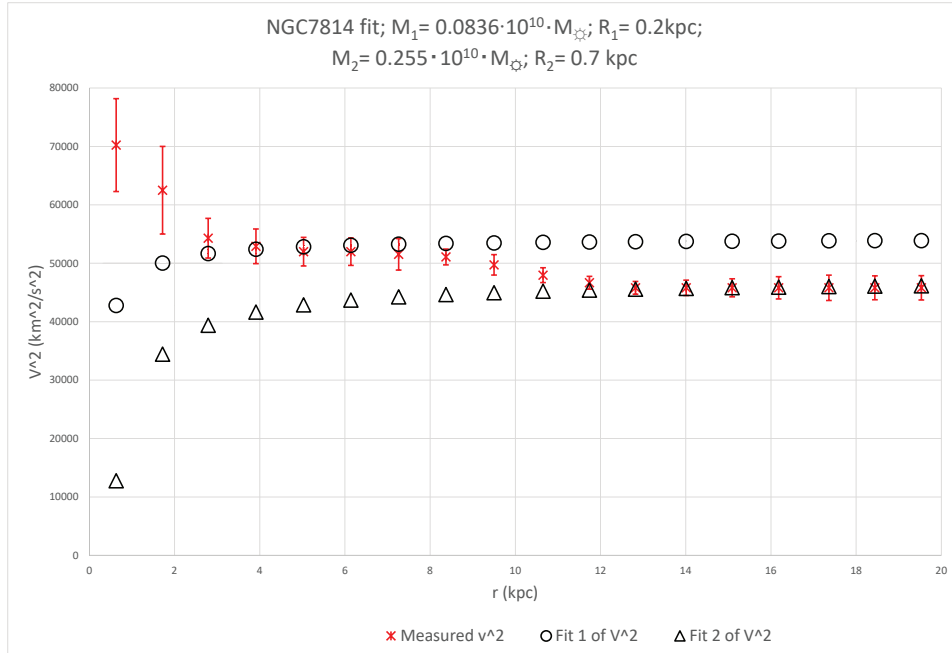


FIG. 162. NGC7814

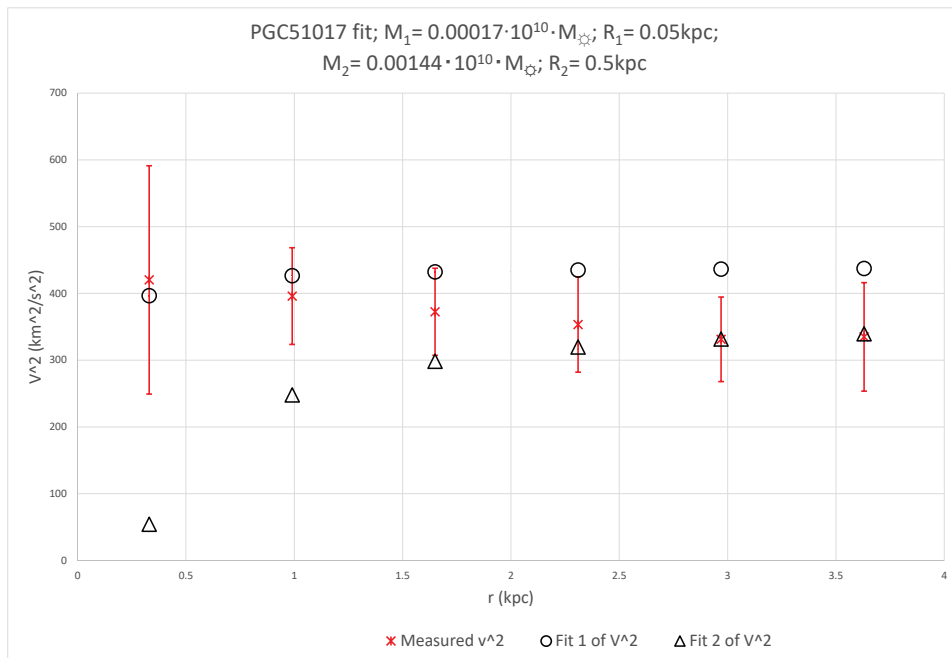


FIG. 163. PGC51017

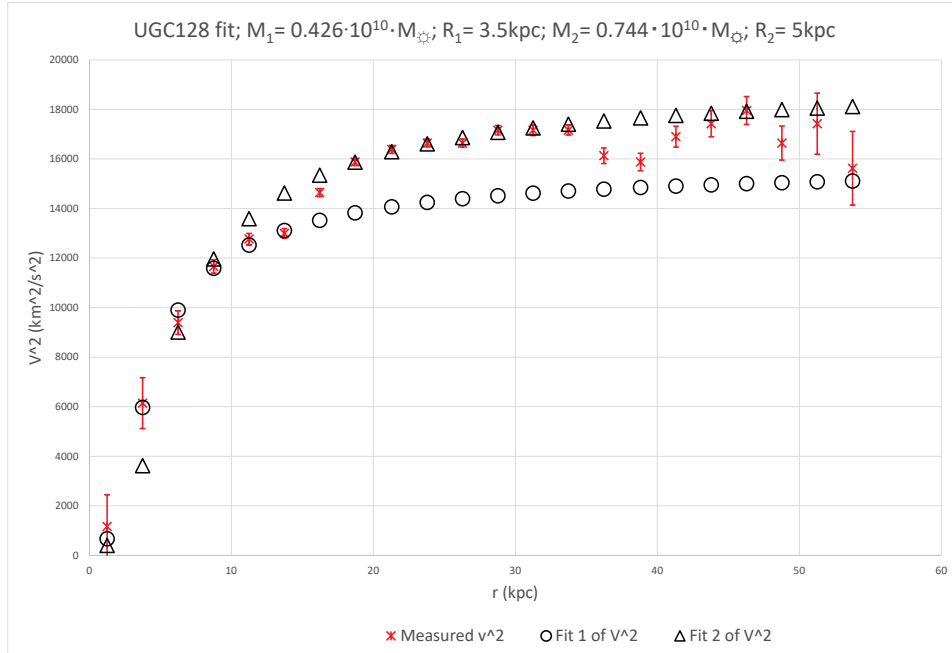


FIG. 164. UGC128

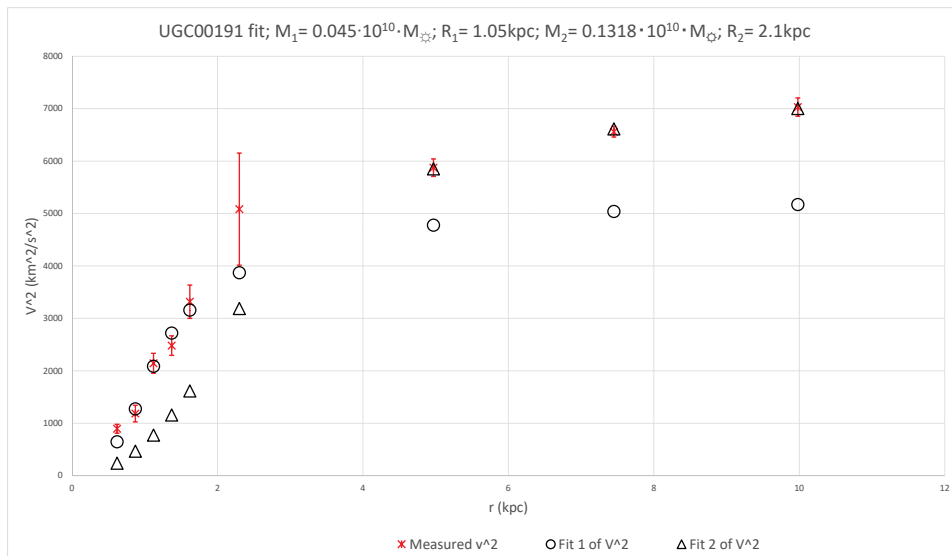


FIG. 165. UGC00191

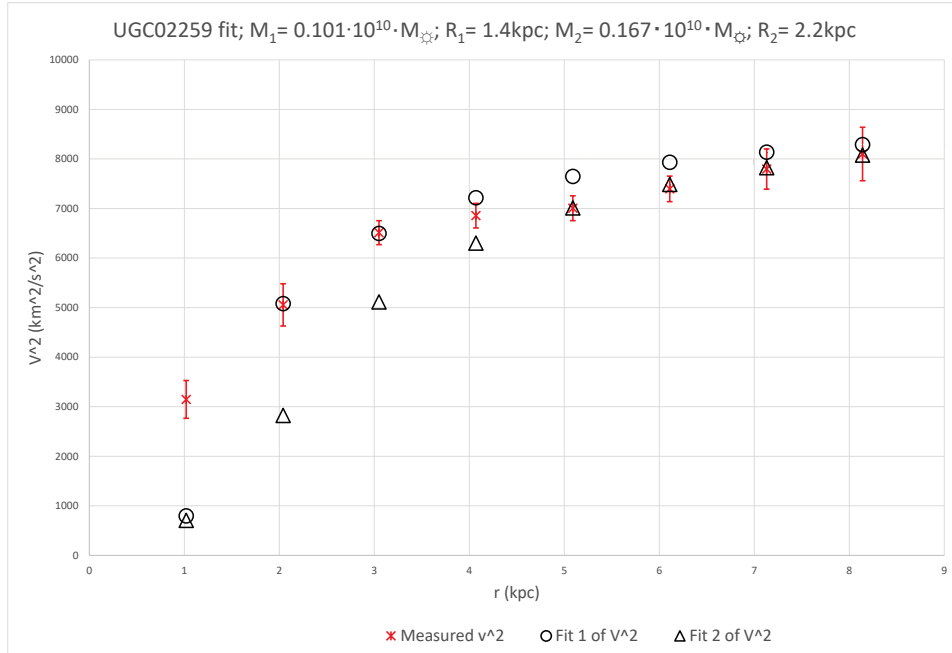


FIG. 166. UGC02259

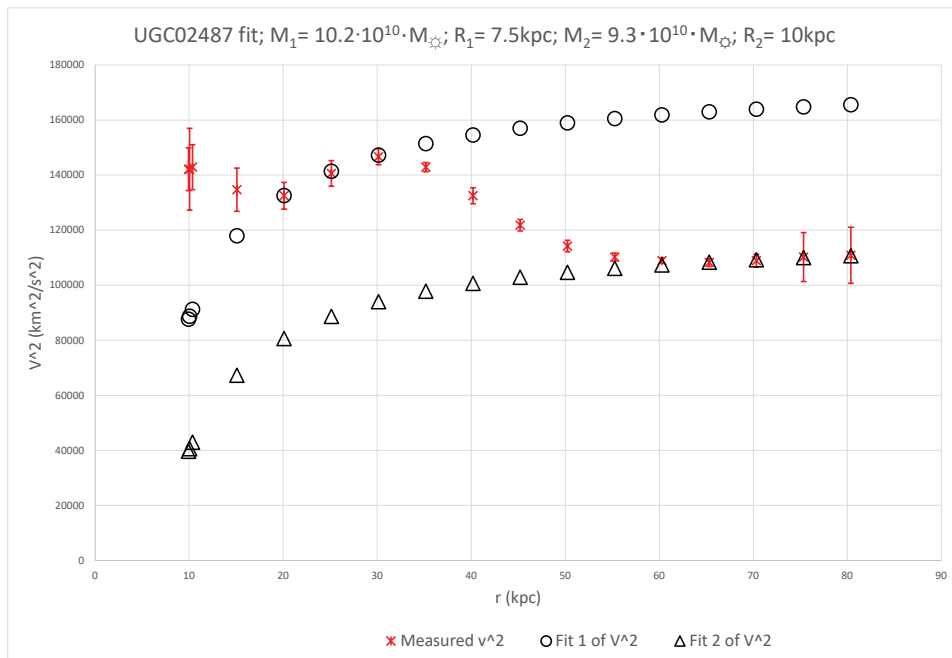


FIG. 167. UGC02487

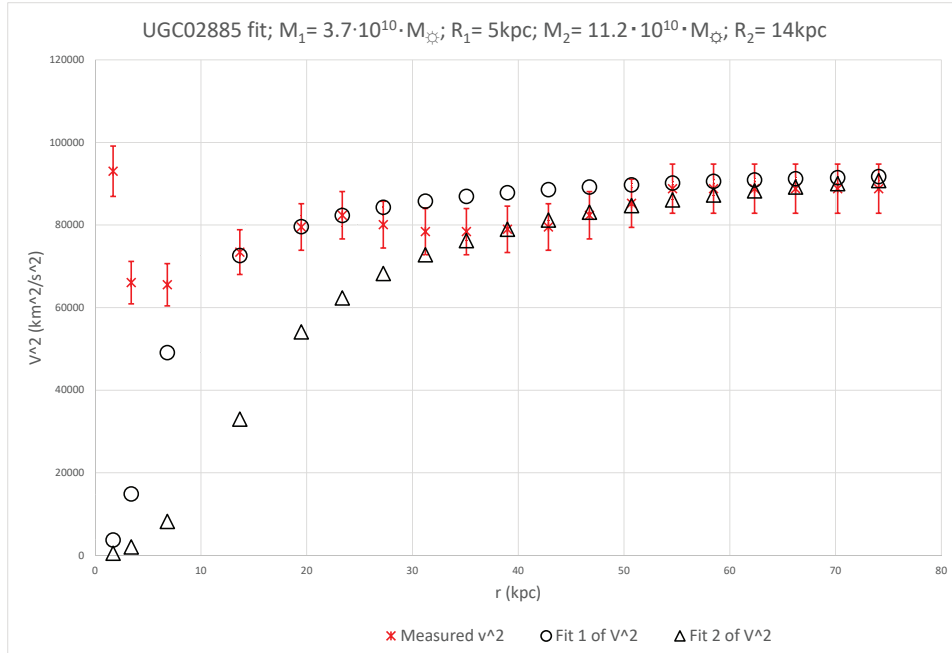


FIG. 168. UGC02885

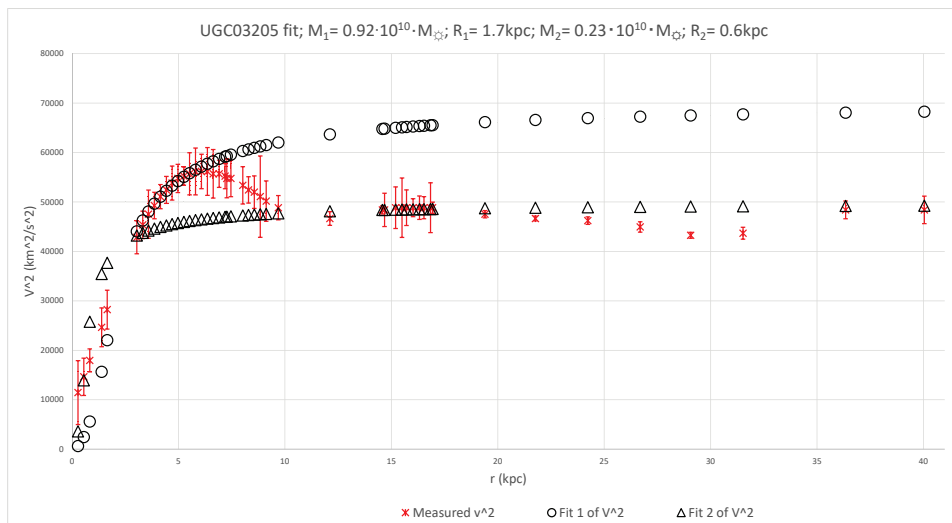


FIG. 169. UGC03205

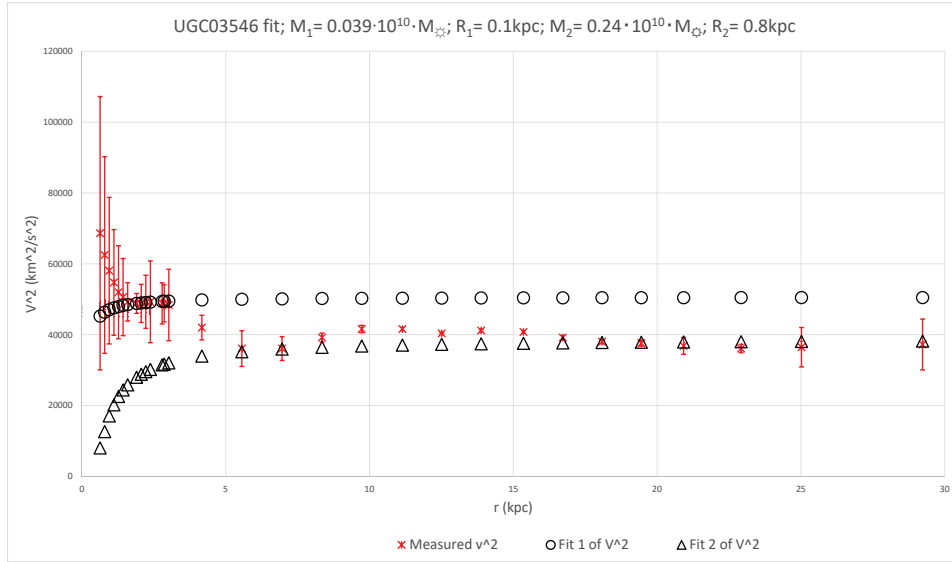


FIG. 170. UGC03546

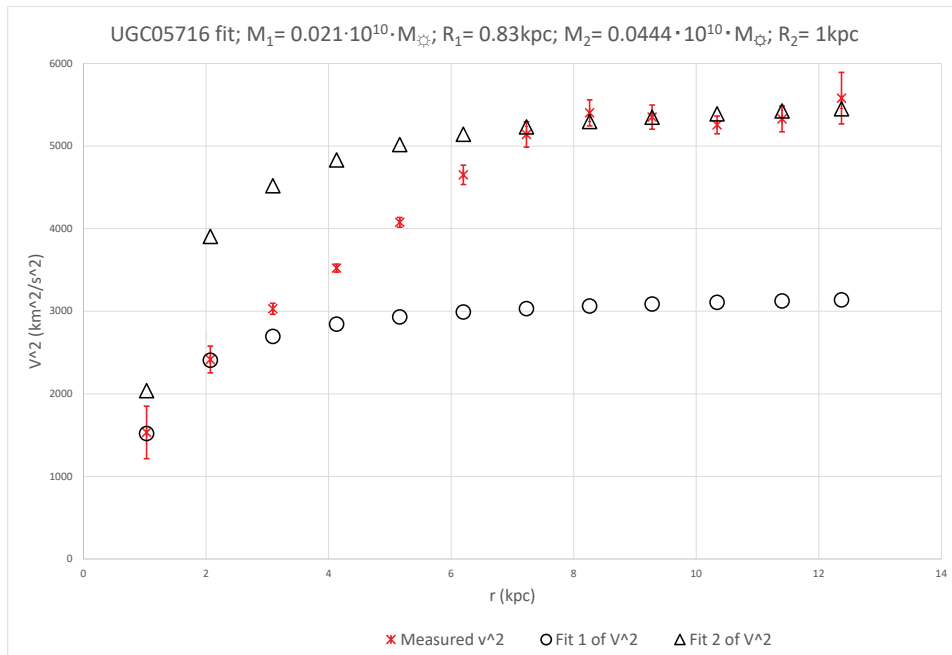


FIG. 171. UGC05716

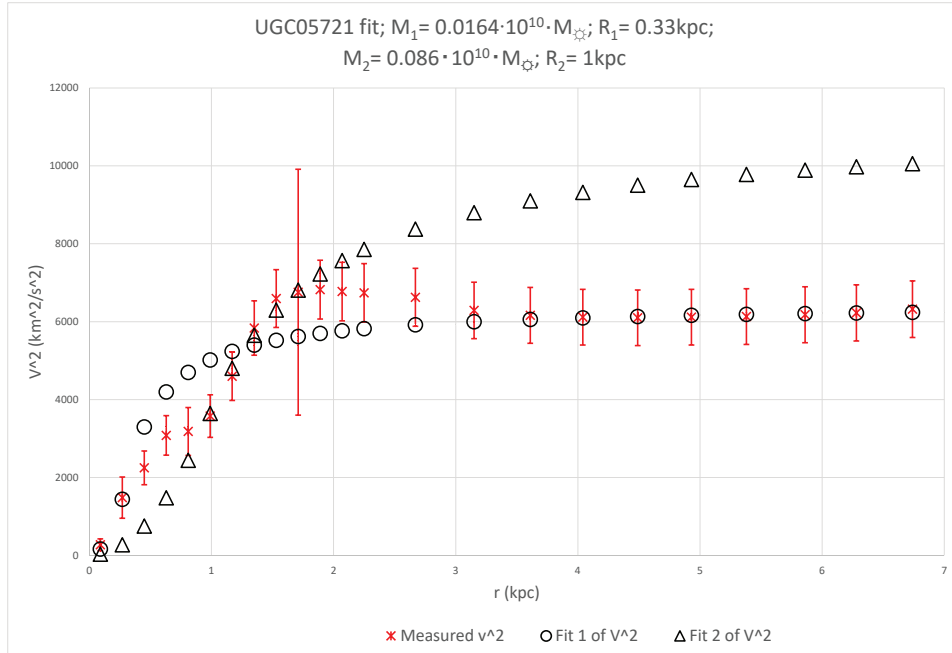


FIG. 172. UGC05721

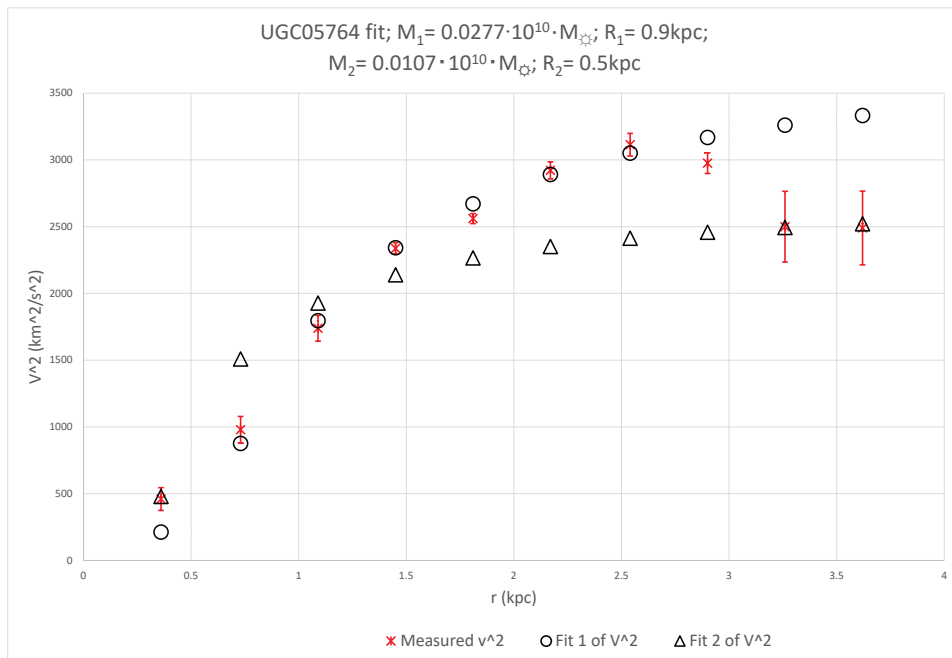


FIG. 173. UGC05764

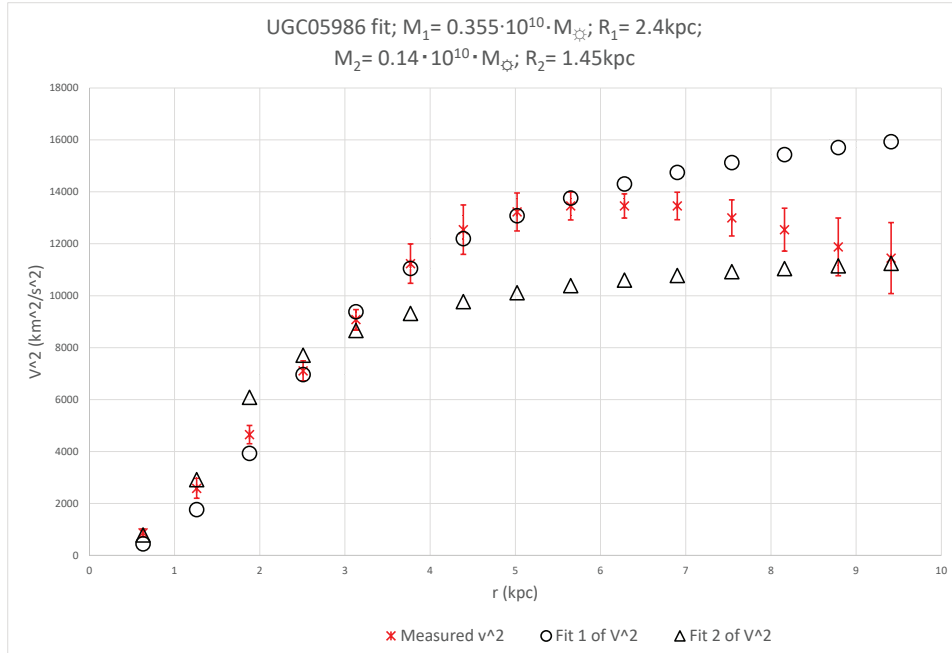


FIG. 174. UGC05986

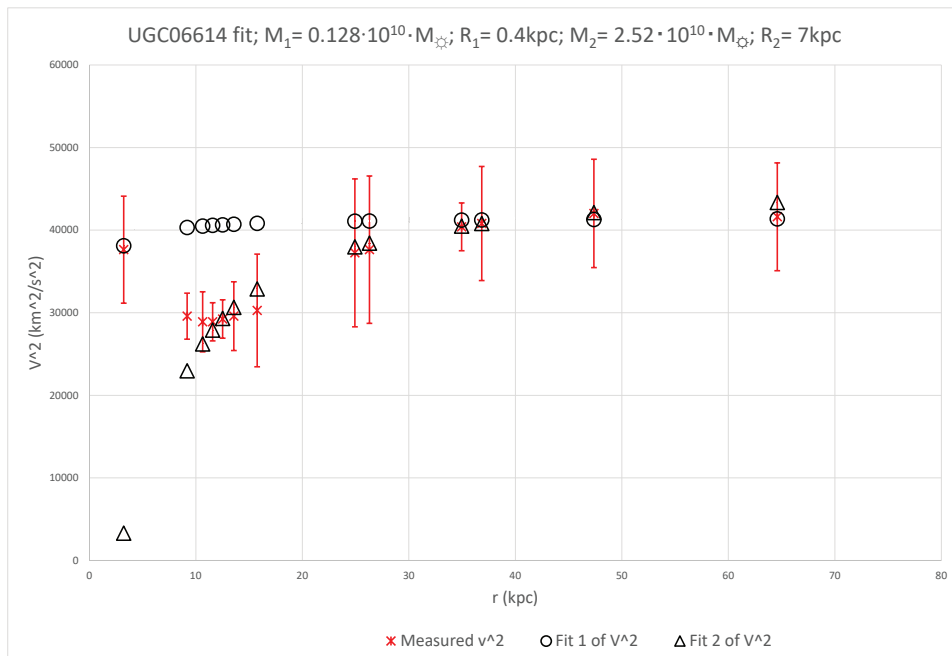


FIG. 175. UGC06614

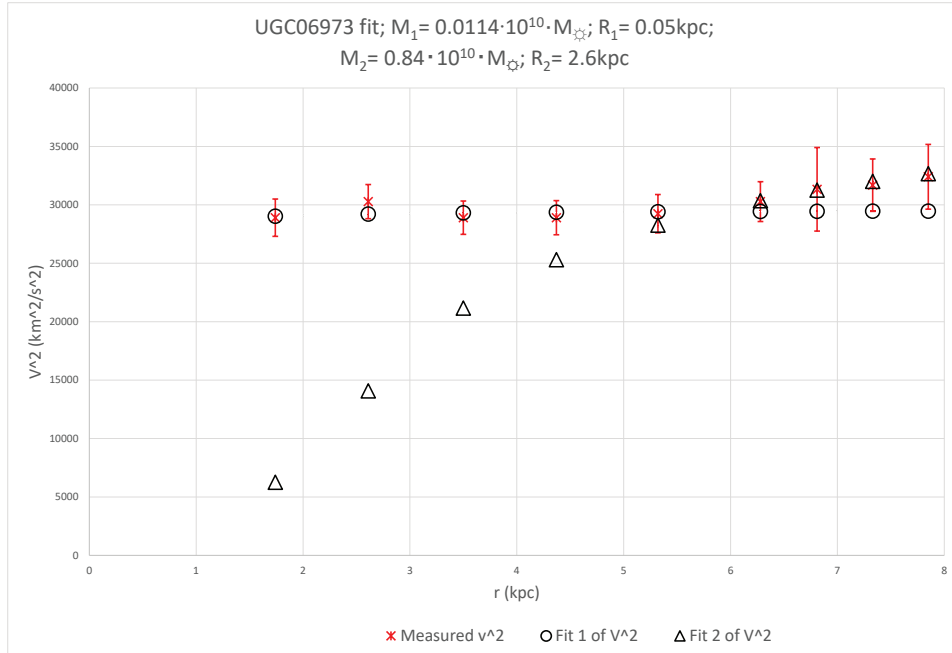


FIG. 176. UGC06973

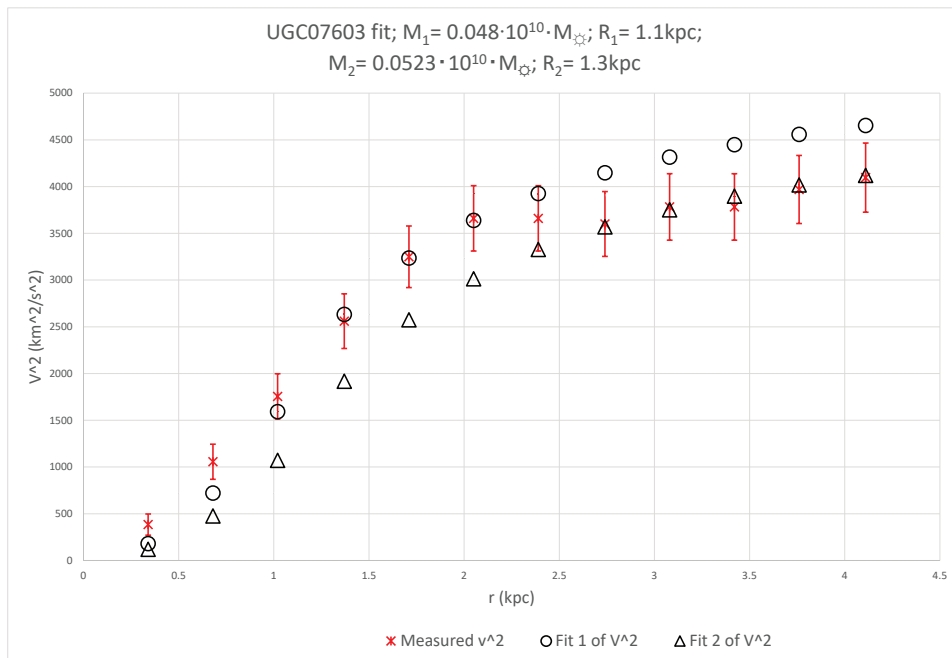


FIG. 177. UGC07603

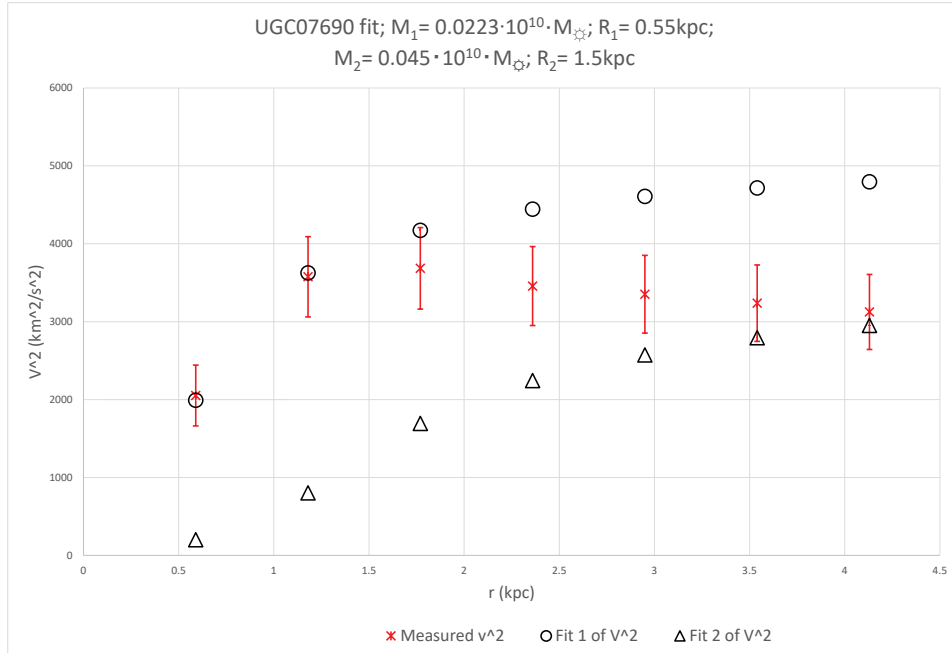


FIG. 178. UGC07690

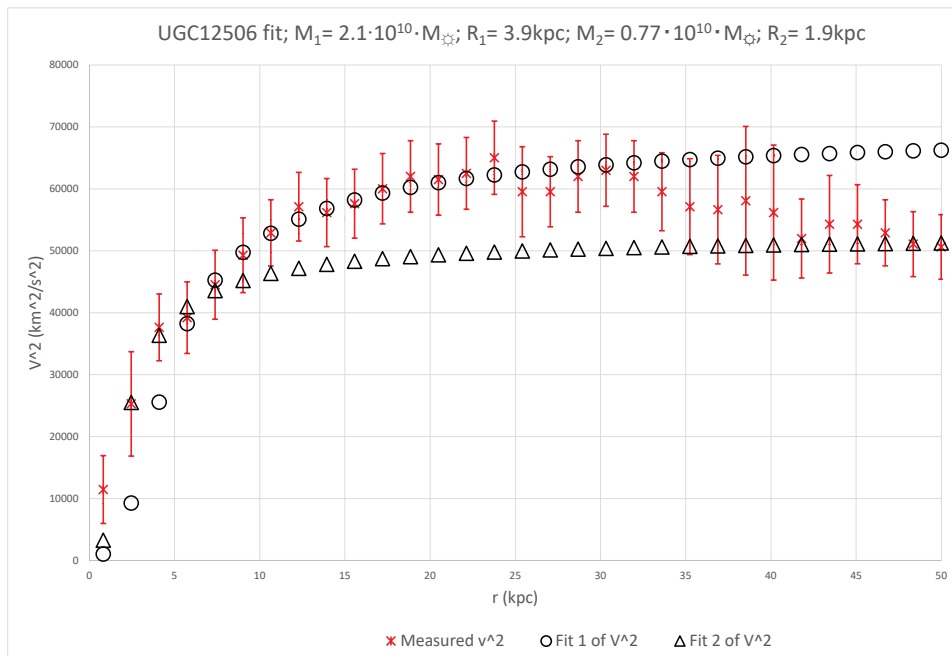


FIG. 179. UGC12506